Design assessment of rehabilitated corroded plates with composite patches through FEA

Nikos Kallitsis

School of Naval Architecture and Marine Engineering

Shipbuilding Technology Laboratory

<u>Supervising professor</u>

Konstantinos N. Anyfantis

National Technical University of Athens February 2022

Περίληψη

Οι ναυπηγικές κατασκευές, όπως τα πλοία και οι πλωτές πλατφόρμες, λειτουργούν σε ένα διαβρωτικό περιβάλλον που επιταχύνει την απώλεια υλικού στις εξωτερικές επιφάνειες. Αντίστοιχα αποτελέσματα προκύπτουν εσωτερικά στα void spaces και τους χώρους εμπορεύματος λόγω της συνδυαστικής δράσης παραγόντων όπως η υγρασία και οι υψηλές θερμοκρασίες κατά τις συνθήκες λειτουργίας. Αυτό οδηγεί σε συσσωρευμένη απώλεια πάχους στα ελάσματα της κατασκευής, ελαττώνοντας τη δυνατότητά τους να αντέξουν τα φορτία σχεδίασης και οδηγόντας στην έναρξη ρωγμών σε περιοχές υψηλής τάσης ή σε αστάθεια λυγισμού. Στην τελευταία περίπτωση, συνήθης τρόπος επιδιόρθωσης είναι η αφαίρεση και αντικατάσταση του ελάσματος (ολική ή μερική) ή κατάλληλη ενίσχυση με χρήση ενισχυτικών και διπλών ελασμάτων.

Σε αυτήν την εργασία εξετάζεται μια εναλλακτική μέθοδος επισκευής για την αποκατάσταση της αντίστασης λυγισμού ενός διαβρωμένου χαλύβδινου ελάσματος με τη χρήση ενός Carbon Fiber Reinforced Polymer (CFRP) patch. Παρ' όλο που μια επίπτωση μπορεί να είναι η αβεβαιότητα για τη κόλληση δύο διαφορετικών υλικών, ένα μεγάλο πλεονέκτημα είναι η ασφάλεια της εγκατάστασης αποφεύγοντας εργασίες φλόγας που μπορεί να είναι επικίνδυνη σε εύφλεκτα περιβάλλοντα (FPSOs / LNGs / δεξαμενές που δεν έχουν εξαεριστεί σωστά). Επομένως, πραγματοποιήθηκε μια εκτίμηση της μεθοδολογίας για τη χρήση CFRP patch για την αποκατάσταση της ελαστικής λυγισμικής ικανότητας ενός διαβρωμένου χαλύβδινου ελάσματος υπό θλιπτικές / διατμητικές τάσεις. Αυτή η μεθοδολογία είναι καινοτόμα, αφού χρησιμοποιεί ένα συνδυασμό τεχνικών από τα Design of Experiments (DoE), που έχουν αποδειχτεί αποτελεσματικά στον σχεδιαστικό χώρο υπολογισμών και μοντέλων.

Η μέθοδος των πεπερασμένων στοιχείων χρησιμοποιήθηκε για την εκτίμηση του μοντέλου της ελαστικής λυγισμικής ικανότητας, διορθωμένη κατά Johnson. Ένα ακριβές πρόγραμμα αριθμητικών πειραμάτων δημιουργήθηκε λόγω της παραμετρικής φύσης του μοντέλου: μήκος, πλάτος και πάχος της χαλύβδινης πλάκας, καθώς και το μήκος, πλάτος, αριθμός στρώσεων και σχήμα του CFRP patch. Όσον αφορά το σχήμα, καψουλοειδές, οκταγωνοειδές και τετράγωνο patch χρησιμοποιήθηκε για σύγκριση. Επιπλέον, CFRP στρώσεις ύφανσης (plain-weave) σε προδιευθετημένη ακολουθία στρώσεων χρησιμοποιήθηκαν για να περιοριστεί ο αριθμός παραμέτρων του προβλήματος και να δοθεί προσοχή στις μεταβλητές σχεδίασης της μεθόδου επισκευής. Τα αποτελέσματα των προσομοιώσεων χρησιμοποιήθηκαν σε Central Composite Design (CCD) δύο παραγόντων καθώς και σε Response Surface Methodology (RSM), έχοντας τη λυγισμική αντίσταση της επισκευασμένης πλάκας ως τη βασική απόκριση. Τέλος, τα σχέδια επισκευής αξιολογήθηκαν και με βάση την θραύση του CFRP και την αποτυχία σύνδεσης υλικών με βάση υπάρχουσα έρευνα στον τομέα. Έπειτα από εκτίμηση της ορθότητας της μεθόδου μέσω στατιστικών μεθόδων, γίνεται εφαρμογή της για κάποιες περιπτώσεις διαβρωμένων πλακών απλής έδρασης που συναντάται σε ναυπηγικές κατασκευές για λόγους επίδειξης της μεθόδου.

Abstract

Marine structures, i.e., ships and offshore, operate in a corrosive environment which accelerates material wastage to external surfaces. Analogous results occur internally in void spaces and cargo compartments due to the combinative action of factors such as humidity and high temperatures in service conditions. This leads to accumulated thickness reductions of the structure's platings, decreasing their ability to bear their design loads and resulting in crack initiation at highly stressed areas or local buckling instabilities. In the latter case, common repair practice is cropping and renewal of the plate (full or partial) or appropriate reinforcement through steel stiffeners or plate doublers.

This paper undertakes an alternative repair technique for restoring a corroded steel plate's buckling strength with the application of a Carbon Fiber Reinforced Polymer (CFRP) patch. Although a downside may be the uncertainty behind the adhesively bonded bi-material joint, a major upside is the installation process's safety by avoiding hotwork which can be life-threatening in flammable environments (FPSOs / LNGs / improperly degassed tanks). Therefore, an assessment for the design methodology of a CFRP patch for the rehabilitation of a corroded steel plate's elastic buckling capacity under compressive / shear stress has been developed. This method is innovative in essence, since it employs a cooperative framework of techniques sourcing from Design of Experiments (DoE), which have proven to be highly efficient in computational design space exploration and surrogate modeling.

Finite Element Methodology (FEM) was used for the evaluation of the model's elastic buckling capacity, corrected according to Johnson's parabola. A precise numerical experimentation program was then developed for tackling the parametric nature of the model; the steel plate's length, width and thickness, as well as the CFRP patch's length, width, number of plies and shape. Regarding the shape, capsular, octagonal and rectangular patches were tested and compared. Additionally, plain weave CFRP plies in a predefined stacking sequence were used in order to lessen the problem's unknown parameters and focus on the rehabilitation method's main design variables. The results of these simulations were utilized through a two factor Central Composite Design (CCD) in conjunction with the Response Surface Methodology (RSM), having the rehabilitated plate's buckling strength as the main response. Finally, the obtained repair designs were assessed with respect to CFRP fracture and bondline failure according to existing research in the field. After assessing the robustness of this method through statistical techniques, it is ultimately applied over a range of simply supported corroded plates found in marine structures for demonstration purposes.

Acknowledgements

First and foremost, I would like to thank my supervising professor Konstantinos Anyfantis for his guidance and patience throughout the duration of this study. Not only did he assist me with his knowledge and experience, but he also supported me and challenged me to go one step further. Through our conversations, I gained new perspectives on subjects of interest and saw the importance of scientific research for technological advancements.

Additionally, I would like to thank my friends and colleagues for supporting me during this time and helping get the best out of me.

Finally, I would like to express my deepest gratitude to my family for their love and support on every decision.

Nikos Kallitsis

Contents

Figures

Tables

1 Introduction

1.1 Scope of work

Various structures are used in the maritime industry, with different forms, load-bearing capabilities, travelling speeds, etc., depending on the structure's purpose. For example, passenger ships are faster and have higher restrictions for water tightness between compartments than cargo ships. Nonetheless, all marine structures are designed to withstand extreme weather and/or seagoing conditions while maintaining a structural strength reserve. Their design life is 25 years minimum, with the majority of this timeframe being spent in the sea.

According to centuries-old experience in the industry, the structures mentioned above are designed and built to withstand their in-service conditions. Nevertheless, this does not guarantee constant structural integrity throughout their design life. For this reason, during a marine structure's lifetime, multiple surveys are conducted by Classification Societies to approve their good seaworthiness (seakeeping ability), ensuring their safe and smooth operation. During these surveys, the marine surveyor, the crew and/or the superintendent check for faults according to each Classification Society's list of checkmarks. Most classes are members of the International Association of Classification Societies (IACS) and follow the same Common Structural Rules (CSR) when a vessel is IACS-CSR certified. According to IACS, one common form of damage that should be investigated during surveys is material wastage due to corrosion.

According to IACS [1], there are three different types of corrosion:

- General: Occurs uniformly on the surface of the metal plate.
- Grooving: Is found near welds caused by galvanic current.
- Pitting: Occurs randomly in areas with local coating breakdown.

The factors that initiate and/or accelerate material wastage at the structure's exterior are saline water (seawater) and heavy scale accumulation. However, corrosion is not solely found externally but also internally in flooded with seawater areas, such as ballast tanks, and often in cargo areas due to the hazardous chemical composition the cargo might have or water remaining. The main factors for corrosion initiation/magnification are:

- Water, dirt, or oil remainings due to drainage or design flaws.
- Scale buildup at the vessel's external wetted surfaces.
- High stresses.
- High-temperature areas, such as heated fuel tanks.
- Coating breakdown due to poor maintenance.

The resultant corrosion, or material wastage, leads to the reduction of the structural member's effective thickness, i.e., the thickness (material) that contributes to the structural response of the member when it is subjected to external loads. Hence, the requirement for the surveyor to be able to identify possible material wastage in structural items. This can be performed in two ways, either visually or by thickness measurements. According to IACS [1], thickness measurements are performed at areas known to be susceptible to corrosion in order to identify/verify the existence of material wastage or to measure the defect's magnitude.

As aforementioned, material wastage leads to the reduction of a structural member's effective thickness, thus also reducing its load-bearing capabilities. In other words, the member's structural response to loads below their design values could be endangering a structure's safe operation. This phenomenon could lead to unwanted results such as crack initiation/propagation, buckling or even the material succumbing to the applied load. For instance, a double bottom plate could buckle during hogging loading conditions that would otherwise not affect it. Other examples of suspect areas are the transverse bulkheads (Figure 1), the tank top, and spaces adjacent to the hot engine room.

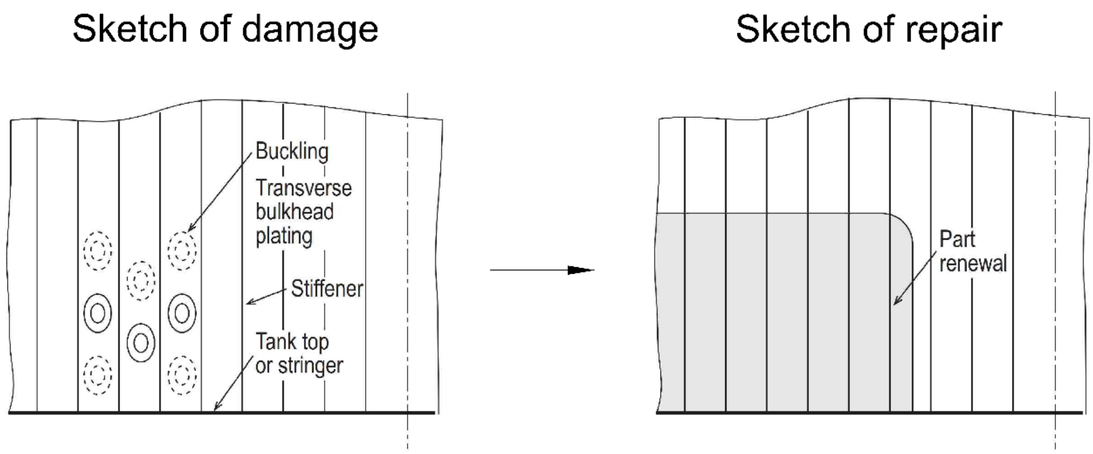

Figure 1. IACS [1] recommended repair practice for buckling caused to a part of a transverse bulkhead (in cargo hold region) possibly caused by heavy general corrosion.

Due to the corrosion's risks mentioned above, IACS [1] has created guidelines for inspection of suspect areas and a standard repair practice if material wastage above a given limit is identified. Therefore, during a standard survey, if a plate's thickness measurement is below its renewal's value with a buckling risk, standard practice is cropping and renewal of the plate with a thickness equal to or greater than the original. In other cases, additional stiffeners may be installed in the area, or a plate doubler could be applied. These practices require hot-work operations, posing a safety threat where such actions are prohibited. Therefore, proper preparation of the area and adjacent compartments shall be performed beforehand, e.g., scrubbing/degassing. These areas of interest are, for example, inside or adjacent to a ship's flammable compartments, such as its cargo tanks or its fuel oil tank. In offshore platforms, the operation might need to halt for the preparation and repair to be conducted.

Although common repair practices exist, it is evident that they are limited by factors that could pose a safety risk for hot-work operations. Hence the growing interest over the past years for alternative repair practices that utilize cold-work operations for reinforcing the damaged area with fiber-reinforced composites. Furthermore, in order to temporarily (or permanently) prevent unwanted results, such as those mentioned above, fiber-reinforced composites can be installed in the area.

1.2 State of the art

Fiber-reinforced composite patches (e.g., GFRP, CFRP) can be used for repairing or preventing damage caused by several factors, including corrosion. These composites can be in the form of stiffeners (Anyfantis [2]) or doublers (Karatzas [3]) and can, for example, prevent buckling from occurring or propagating further. However, this repair technique is not only limited to the case of material wastage but can also be used for repairing cracks in metallic plates (Karatzas [4]).

Apart from the scientific community (Hashim et al. [5], Aabid et al. [6], Turan [7], and those mentioned above), the subject matter has also gained traction in the maritime industry. Notably, several Classification Societies, such as Bureau Veritas (BV [8]) and Det Norske Veritas (DNV [9]), have issued guidelines proposing composite patches as a means to rehabilitate the structural integrity of a corroded metallic structure. In addition, the American Society of Mechanical Engineers (ASME [10]) has also issued guidelines for repairing pipelines using the techniques mentioned earlier. Finally, EU projects such as Marstruct, Copatch and Ramses have examined the case of fiber-reinforced composite patches as a repair method.

Despite the interest of both the scientific community and the maritime industry, the novel repair methodology of composite patches has not yet been approved by the International Maritime Organization (IMO) as a common repair practice for primary supporting members. However, this method has been approved and is widely used in other industries, such as the aeronautical. This delay is caused by the lack of in-service reports, limited applications and several factors concerning the rehabilitation of the composite (e.g., design life, debonding). However, the method can be used in a case-by-case scenario with the approval of the Classification Society after having examined the problem and usually for non-primary supporting members.

This study serves as a preliminary investigation of a methodology for rehabilitating corroded marine plates using fiber-reinforced composite patches to prevent premature buckling. The repair is meant to serve as a short-term means of temporarily restoring a uniformly corroded metallic plate's initial elastic compressive and shear buckling strength. The proposed design is set up using computational and statistical mechanics, arising from finite element analysis (FEA) and design of experiments (DoE), respectively. The employment of these tools subtracts the need for laboratory experimentation or extensive computation work. The main objective is to set up a methodology for choosing the optimal design solution against the investigated defect.

1.3 Design basis

Marine structures, such as ship hulls and offshore platforms, consist of plated geometries forming structural members such as decks, platforms, bulkheads, and stiffeners (e.g., bulb profiles, L, T profiles, and flat bars). The most commonly used material is marine structural steel, found in various grades. Namely, grade 'A' mild steel (LR [11]) is the most common, while grade 'AH32' or 'AH36' higher tensile steel can also be used in areas where greater strength is required (e.g., hull's main deck). The main difference between the different material grades is their yield stress, which is 235 MPa, 315 MPa and 355 MPa, respectively. Higher tensile steel grades are used for members with a high possibility of developing high stresses during their design loading conditions, and plasticity is not desirable. Other materials such as aluminium and composites can also be used in military marine structures (e.g. submarines) where their unique properties, e.g. their weight-to-strength ratio, are beneficial.

A structural member's scantlings, e.g., thickness, length, width, cross-section, are calculated using design load scenarios and (primarily) empirical formulas. Since corrosion is a known phenomenon, the IACS-CSR [12] has guidelines for a corrosion addition, in terms of additional thickness, that should be added to the net calculated scantlings. Thus, the final gross scantlings include a safety margin in cases of unexpected events, e.g., a ship cannot attend repairs in time or is travelling through highly corrosive environments.

Corrosion leads to a percentage of the member's cross-sectional material being wasted, thus reducing its effective properties. For example, its effect on a plate is the reduction of its effective thickness and, thus, lowered load-bearing capabilities. Material addition to the damaged cross-section could be used as a treatment method, e.g., by installing a fiber-reinforced composite patch to the weakened area. However, this solution includes a plethora of design parameters, some of which affect each other. The most important ones are the fiber's material, the matrix's material, the laminate's stacking sequence, the number of plies used, the patch's basic dimensions, the repair's configuration (one or two-sided), and the shape. In the case of composites, the environmental and installation conditions are also factors that dictate their structural behavior. For example:

- Materials’ handling: Proper handling of the materials’ transportation and storage is essential, as they may negatively affect the repair technique’s result.
- Galvanic corrosion: Attention shall be given to galvanic corrosion between conductive fibers (e.g. carbon fiber) and the metallic substrate. This can be avoided with a thicker bondline or glass fiber insulation layers between the substrate and the patch.
- Flammability: Due to the nature of the composite materials, it is assumed that the patch is exposed to flammable environments as it can burn fast.
- Installation environment: The installation environment shall be controlled to avoid environmental loads that threaten curing (humidity, high temperature). Additionally, the surface shall be cleaned with blasting methods and removal of coating remainings and prepared with primer.
- Installation process: The adhesive used and the application method (hand lay-up, pre-preg, or vacuum infusion) are also crucial factors to the resultant structural response of the component.

It is evident that the problem being assessed has a multi-parametrical nature. Therefore, several assumptions are made to lessen its complexity and, thus, minimize its total processing time (setup and calculations). First, let the installation and environmental conditions be optimal for the application and curing of the composite patch. Thus, all risks considering the materials’ handling, galvanic corrosion, flammability, and installation environment can be neglected for the current assessment, although such idealizations cannot be obtained on ship. Additionally, let the adhesive bonding between the composite patch and the metal substrate be perfect. Although this connection is crucial to the repaired structure’s operation, it can be disregarded since the study aims to develop guidelines for the proposed repair method.

As aforementioned, the composite’s patch properties are essential to its obtained structural properties. A plain weave (cross-ply) fiber-reinforced polymer patch with a stacking sequence of $[0/90]_n$ is proposed. The fibers’ orientation within the matrix is in two perpendicular directions (bi-directional); thus, the composite can be characterized as orthotropic (Kollar [13]). Concerning the material of the patches, the most commonly used are carbon fiber reinforced polymers (CFRP) or glass fiber reinforced polymers (GFRP), whose mechanical properties are listed in **Table 1**.

Table 1. Material properties for steel, CFRP, and GFRP.

Property	Steel Grade ‘AH32′ [1]	CFRP [2,3]	GFRP [3]
Young’s modulus of elasticity	206 GPa	42.95 GPa	213.4 GPa
Poisson’s ratio	0.3	0.3	0.3
Yield/Fracture Stress	315 MPa	352 MPa	549 MPa

[1] LR [11], [2] Karatzas [3], [3] Kollar [13]. The composites’ application method is assumed to be vacuum infusion and the matrix is epoxy-resin based.

Moreover, the repair’s design parameters are also important, i.e., principal dimensions, shape, and configuration. The patch’s main dimensions, i.e., its length, width, and thickness, are the most influential to the resultant structural response of the assembly since material addition and obtained stiffness are analogous. Its thickness is dependent on the number of plies since it is a product of the ply’s thickness and the number of plies used. However, these parameters are constrained by the problem’s associated factors. For example, its length and width cannot surpass the applied area’s boundaries, while its thickness should be appropriate, not interfering with surrounding items.

Additionally, the patch's shape can have various geometrical forms, such as rectangle, ellipsoid, and octagonal (**Figure 2**). Similar to the case of the main dimensions, the design should ensure correct design practice and safe operation. For example, some shapes are more challenging to manufacture than others, leading to higher repair costs. They also affect the resultant stress distribution on the patch's surrounding structure and itself. Although this study is focused on buckling restoration, it should be noted that the problem mentioned above could lead to unwanted stress localizations and adhesion problems.

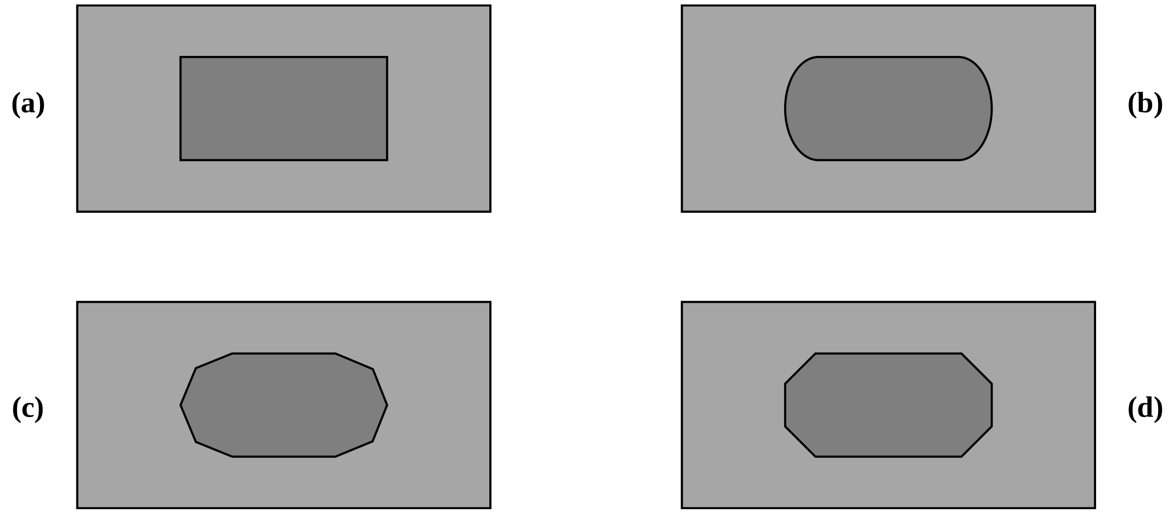

Figure 2. Possible shape forms that the repair patch can have: (a) rectangular, (b) ellipsoid, (c) octagonal horizontal, (d) octagonal vertical.

Finally, another design parameter is the patch's configuration since it could be applied to one side of the metal plate or on both sides (**Figure 3**). This parameter is dependent on the surrounding equipment, environmental conditions and accessibility. For example, one side might have equipment installed that is not easily moved, high humidity, or installation difficulties due to space restrictions. It should be noted that in the case of a one-sided patch, a secondary bending moment occurs, which should be taken into account since it asymmetrically loads the structure.

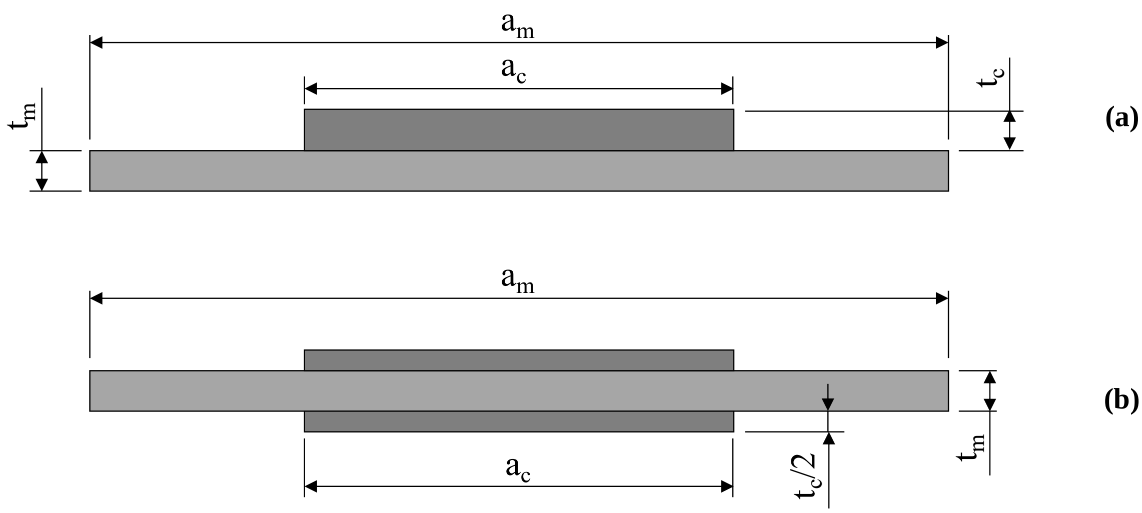

Figure 3. Possible patch configurations: (a) one-sided application (single strap joint) and (b) two-sided application (double strap joint).

In summarizing, the study's main design parameters are:

- Material:
    - For metallic marine plates, the most common materials are various grades of marine steel or aluminum.
    - For composite patches, the most common materials are CFRP and GFRP.
- Composite patch's design parameters:
    - Principal dimensions: length, width, corroded thickness. The latter is dependent on its initial thickness and the corrosion's extent.
- Composite patch's design parameters:
    - Principal dimensions: length, width, thickness. The latter can be replaced by the individual ply's thickness and the number of plies used.
    - Shape: rectangular, ellipsoid, octagonal.
    - Configuration: one-sided, double-sided.

Common to other engineering problems, the ship can be examined in a macroscopic/general view or more microscopic/specific views if better results in a specific area are required. For example, the ship can be assumed as a prismatic beam when studying a three cargo holds problem. However, in the case of connecting a chock to the transom area, a more detailed structural analysis of the specific area (component and surrounding structure) is required. It should be noted that during these assumptions, one may gain better visualization of the results while sacrificing resources (computation time, design) and validity of the transferred loads. In all cases, the design engineer shall examine the problem thoroughly and apply the boundary and load conditions appropriately.

As mentioned above, a marine structure consists of plates and stiffeners, i.e., stiffened panels. During operation, loads are distributed across the assembly and are undertaken by the combined action of beams and plates. When examining a stiffened panel's plate area between stiffeners, the plate could be isolated by assuming it to be simply supported across its edges. At the same time, the active load is transferred through these same edges, i.e., in place of the boundary stiffeners. Using this hypothesis, all external loads can be analyzed as tensile, compressive and shear forces acting on a plate. A schematic of a bulk carrier's cargo hold compartmentation and some supporting members is shown in Figure 4.

It should be noted that part of this study has been published in the international journal Applied Mechanics of MDPI in a paper titled "Buckling Strength Assessment of Composite Patch Repair Used for the Rehabilitation of Corroded Marine Plates". The paper is attached at the appendix of the thesis for reference, in its published form (its page numbers are unrelated to the thesis' numbers).

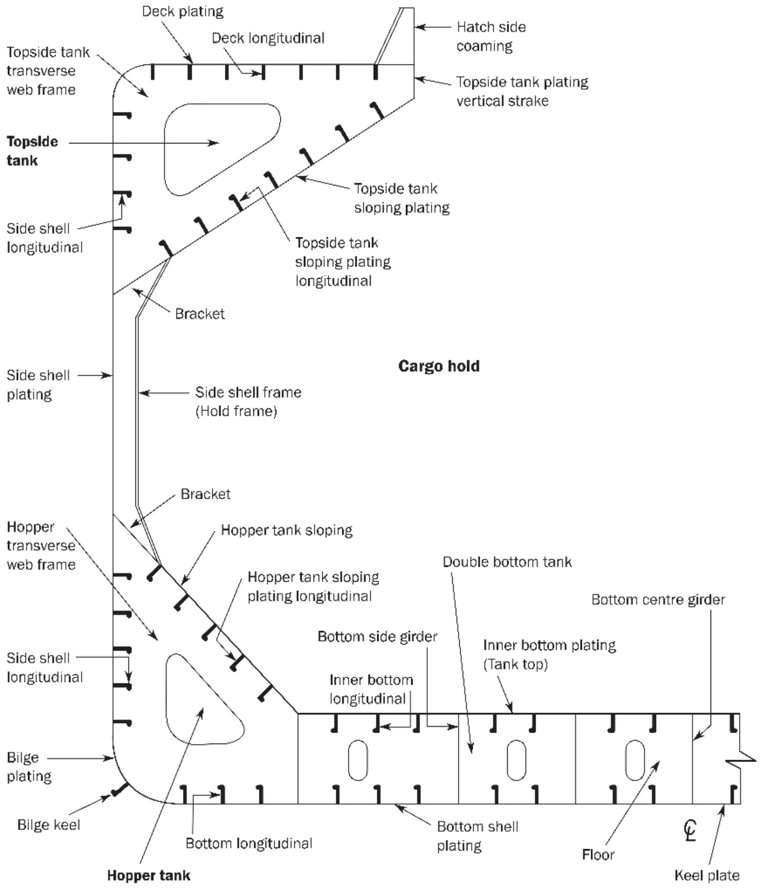

Figure 4. Schematic of a cargo hold's compartments and supporting members (Common Structural Rules for Bulk Carriers and Oil Tankers, Jan 2019).

2 Design Methodology

2.1 Design of the repair

While some defects are "normal" and predictable during a marine structure's lifetime, others occur from unexpected events. For example, severe weather conditions for a prolonged time might cause the conditions for an existing light defect to propagate to severe damage. Another example is the installation of equipment that might not exist in the vessel's as-built design, such as a scrubber casing with the associated equipment inside the casing and the engine room. Additionally, modifications are common to be made to the existing mooring equipment (bollards, chocks and mooring winches) due to changes established by a Canal through which the ship passes (e.g., Panama Canal). Thus, while a marine structure is built according to some design scenarios, additional modifications might be performed during its lifetime by adding or subtracting structural items and equipment in certain areas. These modifications are examined according to design scenarios indicated by the IACS-CSR [12] and approved by the appointed Classification Society before being built and installed. However, these changes might cause a combined action during loading that could lead to unexpected defects, e.g., stress concentrations.

In order to minimize the risk of defects occurring or propagating, several surveys are conducted within the framework of preventive maintenance. During these surveys, suspect areas are examined according to the Classification Society's guidelines to verify their good condition and safe operation until the following planned survey. If a defect that could cause an unwanted risk exists on the ship or platform, repair action is required. Depending on the case, the repair could be performed while travelling, harbouring, or dry-dock. Usually, small-scale operations in a secure and easily accessible area can be conducted at sea (e.g., tank top, ballast tank), assuming that the necessary equipment is stored on the ship. On the other hand, large-scale operations that require intrusive installations necessitate the need for the ship to be on lang (e.g., a large composite patch on the upper deck or transverse bulkhead).

For the subject being studied, assume that corrosion is detected on a plate during a ship's survey through thickness measurements. Let these measurements indicate that the magnitude of material lost or the position of the defective plate sets the structural member at buckling risk if left untreated. Based on existing recommended practices currently applied in the shipbuilding industry (DNV [9]), if the structural member serves as primary support, then traditional repair methods are used (e.g., cropping and renewal). Similar repair techniques are applied in case the defect's extent is significant since it is assumed that a composite patch would not adequately rehabilitate its initial structural strength. However, if the structural member is not a primary component and the defect has a smaller extent, a composite patch could be installed. These decision-making points are illustrated in the flowchart in **Figure 5**.

The purpose of this study is to introduce guidelines for repairing a plate at risk of buckling due to corrosion. However, these novel guidelines should also acknowledge the current design and repair methods being applied. Thus, for the decision-making process, from the defect's identification to the verification that the composite patch repair method could be used, the current repair guidelines proposed by BV [8] and shown at **Figure 5** are used.

Having verified the suitability of a composite patch for rehabilitating the defective corroded plate's initial buckling strength, the patch's material, shape and configuration shall be decided. The designer could decide these parameters through experience or statistical tools. Specifically, the appointed designer might find it troublesome to use a shape with abrupt edges since they might develop unwanted stress concentrations during loading. Another example is the inability to access both sides of the metal plate to apply the double-sided configuration. However, in all cases, the proposed design must be examined to verify assumptions made and ensure that alarming stresses or deformations are not developed.

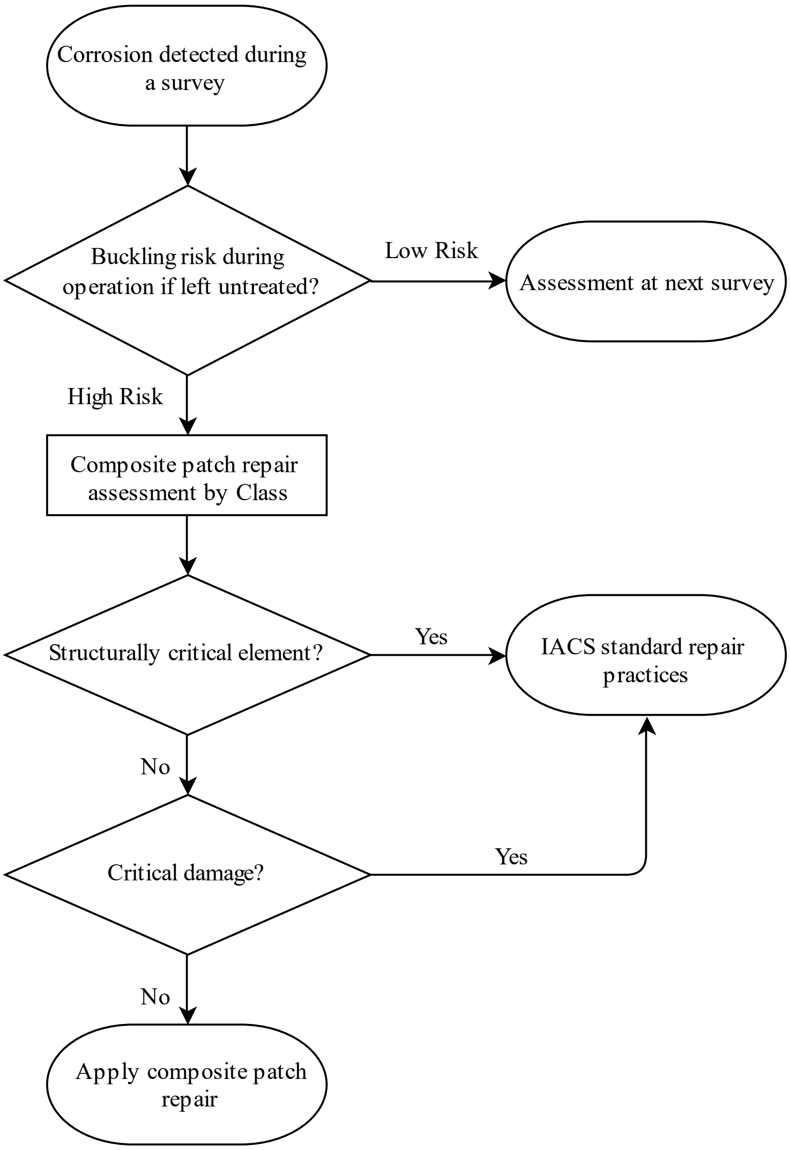

Figure 5. Flowchart illustrating the decision points from the defect detection to the approved repair method.

The other option includes using statistical tools, specifically one-factor-at-a-time (OFAT) analyses. This methodology examines one design parameter while all other factors that affect the result remain fixed. Furthermore, this analysis technique is followed due to the discrete nature of these parameters – e.g., the patch's material and configuration is a binary decision – while the shape has four options, as shown in **Figure 2**. Therefore, the patch's material, shape and configuration could either be decided by the design engineer's preference or statistical tools.

After setting the parameters mentioned earlier, the patch's main dimensions must be assigned, i.e., its design parameters. In order to minimize the problem's complexity, the patch is assumed to have an aspect ratio α_c equal to that of the metal substrate α_m. Thus, the composite's length α_c and width b_c are a product of the plate's respective values – i.e., a_m and b_m – and its aspect ratio – i.e., $a_c/b_c = \alpha_c = \alpha_m = a_m/b_m$. Hence, let these two parameters be replaced by a percentage coverage of the substrate, denoted by c. As a result, the following expressions are obtained: $c = a_c/a_m = b_c/b_m$.

The final design parameter that must be set is the patch's thickness. As mentioned in a previous paragraph, this value is dependent on each ply's thickness and the total number of plies used, denoted by t_{ply} and N_{plies}, respectively. Then, a DoE statistical analysis is performed to obtain a resultant field of acceptable solutions for the design parameters. In order to execute the analysis, the allowable range of values that the design parameters can have must be defined by the designer, i.e., a minimum and maximum value for the percentage coverage c and the number of plies N_{plies}. It should be noted that the ply's thickness t_{ply} is irrelevant for the analysis since it is constant and set at the initial stages along with other constants (e.g., shape).

The DoE analysis is used to generate a response surface, through response surface methodology (RSM), with the addition of another parameter, the attainable factor of safety (FoS). The latter is calculated using elastic buckling analyses on the data points set by the DoE in order to construct the response surface. The final product is a fitted surface (points) that indicates the FoS obtained for various combinations of the patch's coverage and the number of plies.

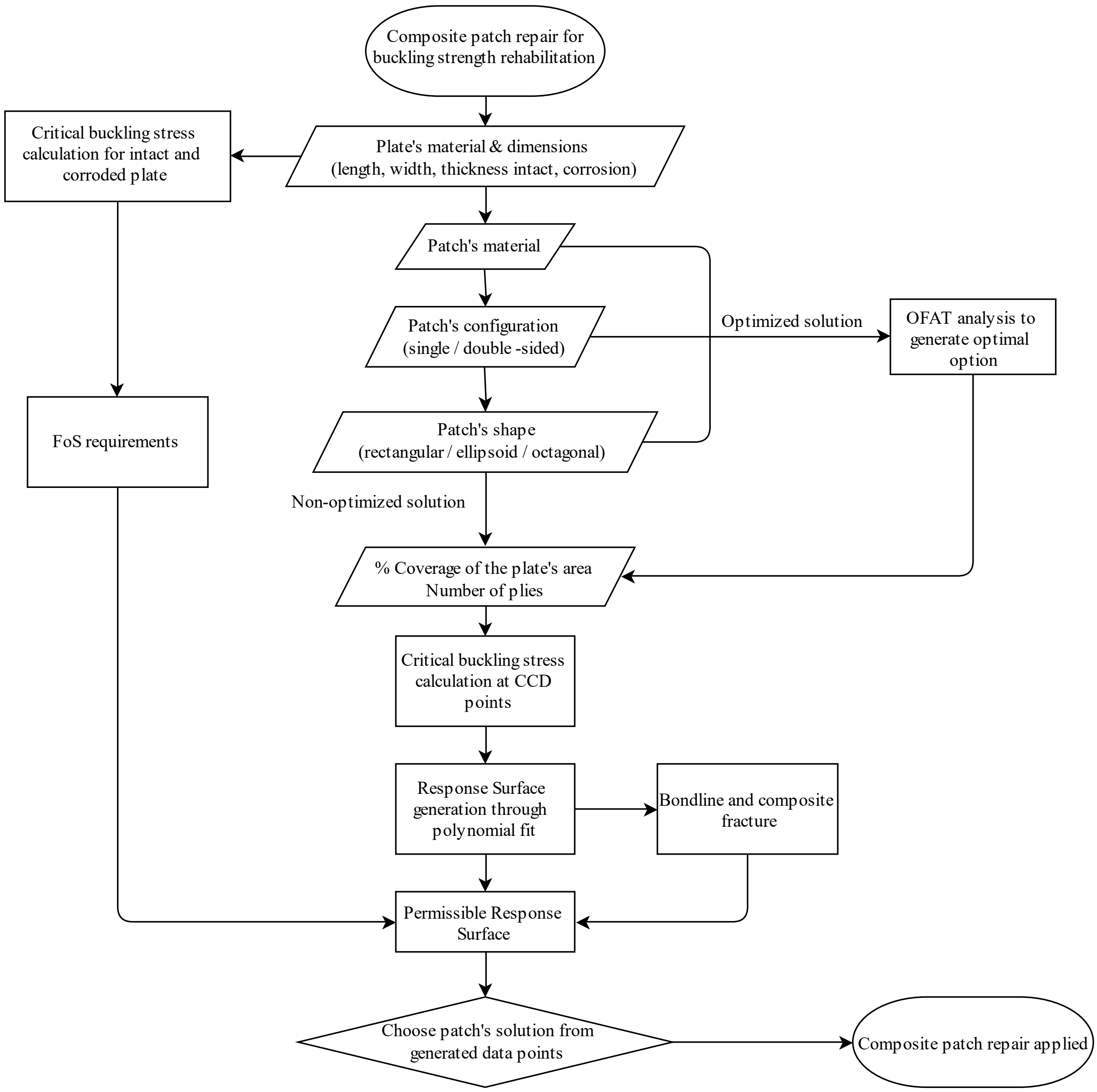

Figure 6. Flowchart of the proposed preliminary design methodology.

In order to differentiate the acceptable solutions of the response surface, specific parameters are used:

- Factor of Safety:

  The attainable FoS must be at least 1, which translates to complete rehabilitation of the plate's initial elastic buckling strength. The designer could further restrict the acceptable solutions with higher FoS according to the design preferences.

- Composite's fracture:

  The obtained solutions must ensure that the suggested patch design fulfils its purpose but does not fracture under the applied loads.

- Bondline:

  The response surface shall be restricted, if necessary, to ensure the safety of the bondline between the composite patch and the metal substrate.

The design methodology proposed is visualized in the flowchart shown in **Figure 6**. The flowchart essentially depicts the suggested novel design guidelines examined in this study. Thus, having established a composite patch repair for rehabilitating the buckling strength of a metal plate (**Figure 5**), the above steps could be used to design said patch.

2.2 Thin plate theory

2.2.1 Bending theory

Following Timoshenko's [14] thin plate theory, assume a plate of length a, width b and thickness t, which is considered small compared to the other two dimensions (thus the expression "thin plate"). Additionally, let the plane xy be the middle plane of the plate, i.e., the plane midway between the two faces of the plate. In this manner, x and y axes are directed along the edges of the length and width, respectively, as shown in **Figure 7**, while z is the perpendicular axis and positive downwards.

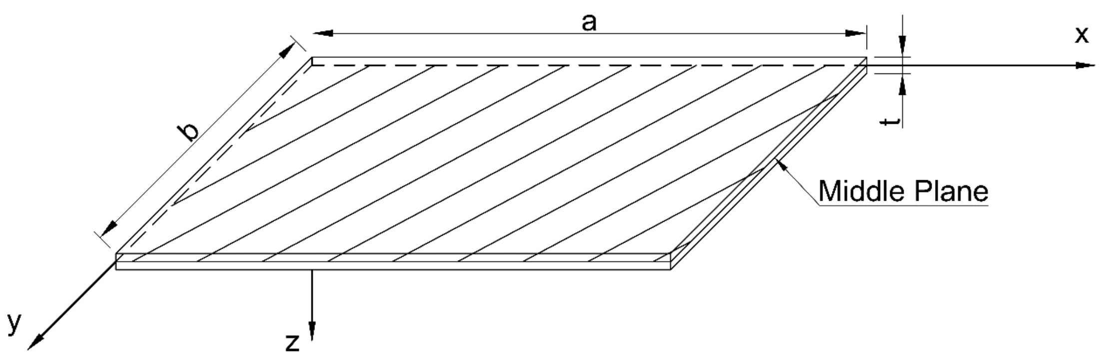

Figure 7. Bending/buckling model.

Bending can occur in three ways that are summarized in the following paragraphs. In each case, the structure's expressions for its mechanical properties are derived from an analysis of an element cut out of the plate by two planes parallel to xz and yz planes. This element's dimensions are dx, dy, dz, as shown in **Figure 8**. The following assumptions are made in each bending case:

- The plate is level before the application of any load.

- The deflections are small relative to the thickness.

- The middle plate acts as a neutral surface (it does not undergo any deformation).
- All perpendicular lines at the middle plane remain perpendicular throughout the plate's bending.

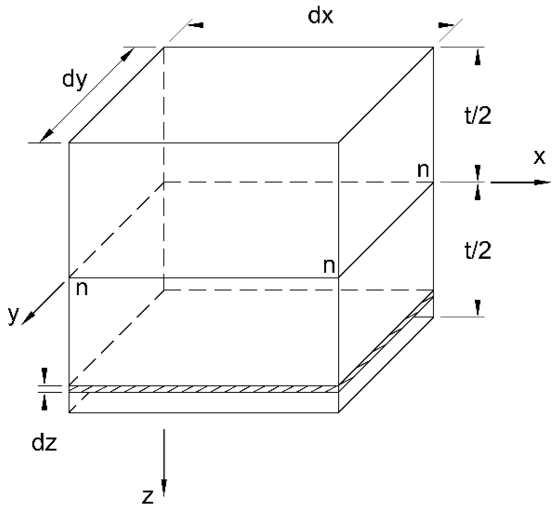

Figure 8. Pure bending element.

2.2.1.1 Pure Bending

In a pure bending state, a thin plate is bent by uniformly distributed bending moments (per unit length) M_x and M_y across the edges and parallel to the y and x-axis, respectively (as shown in **Figure 9**). Both values are positive when compression is produced at the plate's upper part and, therefore, tension at the lower. These moments can be calculated using the expressions:

$$M_x=-D\left(\frac{\partial^2 w}{\partial x^2}+\nu\frac{\partial^2 w}{\partial y^2}\right) \tag{2.1}$$

$$M_y=-D\left(\frac{\partial^2 w}{\partial y^2}+\nu\frac{\partial^2 w}{\partial x^2}\right) \tag{2.2}$$

where:

- $D=\frac{E}{1-\nu^2}\int_{-t/2}^{t/2} z^2 dz=\frac{Et^3}{12(1-\nu^2)}$: Flexural rigidity of the plate
- w: Deflection of the plate
- v: Poisson's ratio, dependent on the plate's material
- E: Young's modulus of elasticity, dependent on the plate's material

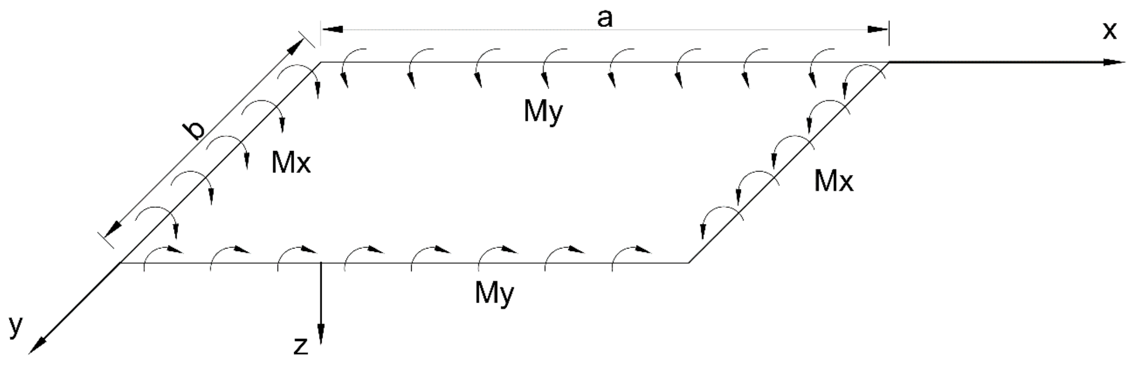

Figure 9. Pure bending plate's loads.

The moments developed inside the bent plate can be examined using an element cut out, as mentioned previously. This element is cut using the primary planes xz and yz, as well as a plane inclined to the primary axes x and y in an angle of value a (**Figure 10**). At this element, both normal stresses and shear stresses develop, allowing for the action of bending and twisting moments. These moments, which are denoted as M_n and $M_{nn'}$, can be calculated using the formulas:

$$M_n=-D\left(\frac{\partial^2 w}{\partial n^2}+\nu\frac{\partial^2 w}{\partial n'^2}\right) \qquad 2.3$$

$$M_{nn'}=D(1-\nu)\frac{\partial^2 w}{\partial n \partial n'} \qquad 2.4$$

These are generalized expressions for the moments developed inside the bent plate. When a = 0 or π then $M_n = M_x$, while when a = $\pi/2$ or $3\pi/2$ then $M_n = M_y$. In both cases, the torsional moment is zero, while the expressions for M_x and M_y are identical to 2.1 and 2.2.

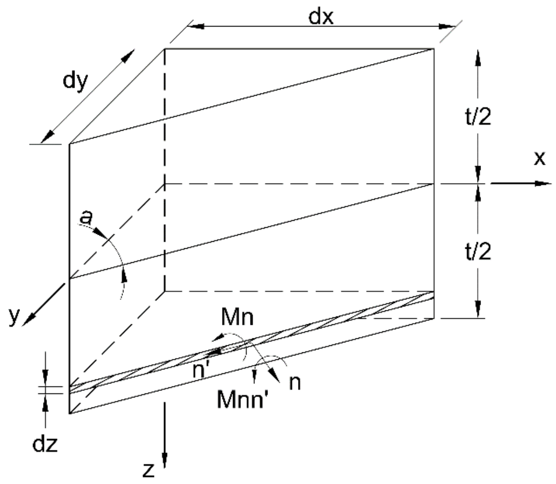

Figure 10. Pure bending element's loads.

The total potential energy in the plate's element results from the work done by the applied loads. In pure bending, the only loads applied are the edges' bending moments. Thus, the energy can be calculated as:

$$dU=-\frac{1}{2}\left(M_x\frac{\partial^2 w}{\partial x^2}+M_y\frac{\partial^2 w}{\partial y^2}\right)\partial x \partial y \qquad 2.5$$

By substituting the bending moments with their expressions 2.1 and 2.2, the total strain energy of the plate can be obtained using the formula (for the plate's entire surface):

$$U=\frac{1}{2}D\iint\left[\left(\frac{\partial^2 w}{\partial x^2}\right)^2+\left(\frac{\partial^2 w}{\partial y^2}\right)^2+2\nu\frac{\partial^2 w}{\partial x^2}\frac{\partial^2 w}{\partial y^2}\right]dxdy \tag{2.6}$$

2.2.1.2 Bending by Distributed Lateral Load

Another loading condition that can cause a plate's bending is a distributed load acting perpendicular to the middle plane. Let this load can be denoted by q. If an element is cut out of the plate, similar to pure bending, not only bending and twisting moments develop on it but also vertical shearing forces due to the perpendicular load q (**Figure 11**). The expression for the values of M_x and M_y are the same as those in 2.1 and 2.2 of pure bending. The twisting moments M_{xy} and M_{yx} can be calculated with the help of 2.4 as:

$$M_{xy}=-M_{yx}=D(1-\nu)\frac{\partial^2 w}{\partial x\partial y} \tag{2.7}$$

The shearing forces Q_x and Q_y can be obtained using the equations:

$$Q_x=-D\frac{\partial}{\partial x}\left(\frac{\partial^2 w}{\partial x^2}+\frac{\partial^2 w}{\partial y^2}\right) \tag{2.8}$$

$$Q_y=-D\frac{\partial}{\partial y}\left(\frac{\partial^2 w}{\partial x^2}+\frac{\partial^2 w}{\partial y^2}\right) \tag{2.9}$$

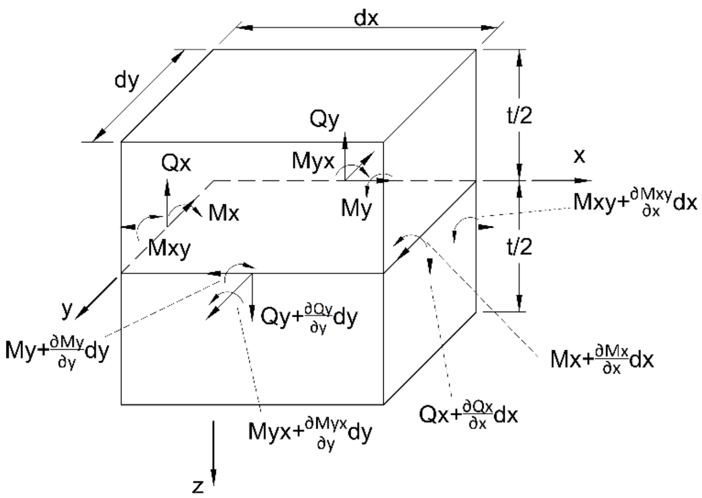

Figure 11. Distributed lateral load bending element's loads.

Considering only the work done by the bending and twisting moments and neglecting the shearing forces, the total potential energy in the plate's element can be calculated as:

$$dU=\frac{1}{2}D\left[\left(\frac{\partial^2 w}{\partial x^2}\right)^2+\left(\frac{\partial^2 w}{\partial y^2}\right)^2+2\nu\frac{\partial^2 w}{\partial x^2}\frac{\partial^2 w}{\partial y^2}\right]dxdy+D(1-\nu)\left(\frac{\partial^2 w}{\partial x\partial y}\right)^2dxdy \tag{2.10}$$

The strain energy of the entire plate can be calculated using the equation:

$$U=\frac{1}{2}D\iint\left\{\left(\frac{\partial^2 w}{\partial x^2}^2+\frac{\partial^2 w}{\partial y^2}\right)^2-2(1-\nu)\left[\frac{\partial^2 w}{\partial x^2}\frac{\partial^2 w}{\partial y^2}-\left(\frac{\partial^2 w}{\partial x \partial y}\right)^2\right]\right\}dxdy \qquad 2.11$$

2.2.2 Combined bending and tension/compression

Assume a plate with a lateral load on its middle plane, as described in 2.2.1.2. In addition, there are now forces acting in the same plane, stretching or compressing it. If a small element of the plate is cut, as in previous cases, then the forces that develop due to the new loads are N_x, N_y, N_{xy} and $N_{yz,}$ depending on the direction they act in (**Figure 12**). These loads achieve an equilibrium with the following equations:

$$\begin{aligned}\frac{\partial N_x}{\partial x}+\frac{\partial N_{yx}}{\partial y}=0\\ \frac{\partial N_y}{\partial y}+\frac{\partial N_{xy}}{\partial x}=0\end{aligned} \qquad 2.12$$

By neglecting any stretching in the middle plane, the work done by the forces acting in it is given by the equation:

$$T_1=-\frac{1}{2}\iint\left[N_x\left(\frac{\partial w}{\partial x}\right)^2+N_y\left(\frac{\partial w}{\partial y}\right)^2+2N_{xy}\frac{\partial w}{\partial x}\frac{\partial w}{\partial y}\right]dx\,dy \qquad 2.13$$

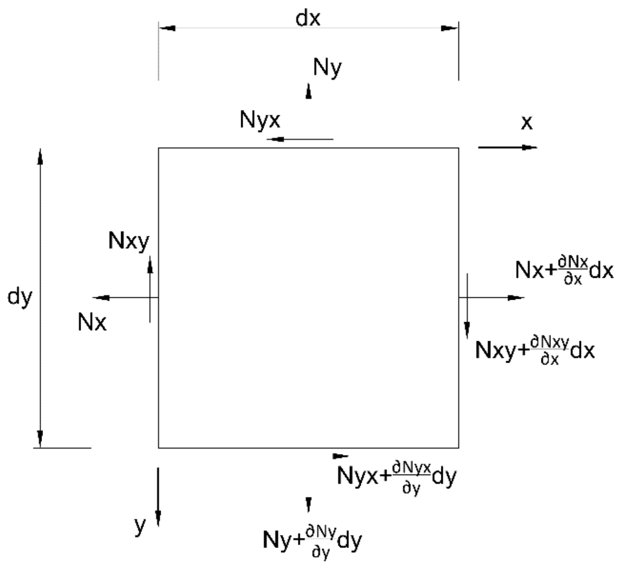

Figure 12. Combined bending and tension element's loads.

The work produced by the load normal to the plate is given by:

$$\begin{aligned}T_2=\frac{1}{2}\iint\left[N_x\left(\frac{\partial w}{\partial x}\right)^2+N_y\left(\frac{\partial w}{\partial y}\right)^2+2N_{xy}\frac{\partial w}{\partial x}\frac{\partial w}{\partial y}\right]dx\,dy\\ +\frac{1}{2}D\iint\left\{\left(\frac{\partial^2 w}{\partial x^2}^2+\frac{\partial^2 w}{\partial y^2}\right)^2-2(1-\nu)\left[\frac{\partial^2 w}{\partial x^2}\frac{\partial^2 w}{\partial y^2}-\left(\frac{\partial^2 w}{\partial x \partial y}\right)^2\right]\right\}dxdy\end{aligned} \qquad 2.14$$

Thus, the total strain energy of the plate can be calculated by adding all work done to the plate by the applied loads:

$$U=T_1+T_2$$

$$U=\frac{1}{2}D\iint\left\{\left(\frac{\partial^2 w}{\partial x^2}^2+\frac{\partial^2 w}{\partial y^2}\right)^2-2(1-\nu)\left[\frac{\partial^2 w}{\partial x^2}\frac{\partial^2 w}{\partial y^2}-\left(\frac{\partial^2 w}{\partial x\partial y}\right)^2\right]\right\}dxdy \qquad 2.15$$

2.2.2.1 Deflection of a Simply Supported Rectangular Plate

In order to determine the deflection of a plate, the boundary conditions must be known. Therefore, let the plate be simply supported across its edges. However, the equations that surround this type of restraint must be acknowledged.

In the following example, the plate's edge along the y axis is simply supported. This condition restricts the displacement of the edge normally to the xy plane. Additionally, the edge can rotate freely with respect to the y axis; therefore, no bending moments M_x can develop. Thus, in the case of a simply supported plate at the x = 0 edge, the following boundary conditions are in effect:

$$(w)_{x=0}=0 \quad \& \quad M_x=-D\left(\frac{\partial^2 w}{\partial x^2}+\nu\frac{\partial^2 w}{\partial y^2}\right)=0 \qquad 2.16$$

In the case of a simply supported plate, all edges are restrained. Therefore, by applying the above equations to all edges, the following boundary conditions are formed for a simply supported plate:

$$\begin{array}{ll} (w)_{y=0}=0 & (w)_{y=b}=0 \\ (w)_{x=0}=0 & (w)_{x=a}=0 \\ \left(M_y\right)_{y=0}=0 & \left(M_y\right)_{y=b}=0 \\ (M_x)_{x=0}=0 & (M_x)_{x=a}=0 \end{array} \qquad 2.17$$

With the above conditions in effect, the deflection of the surface can be expressed by a double trigonometric series:

$$w=\sum_{m=1}^{\infty}\sum_{n=1}^{\infty}a_{mn}\sin\left(\frac{m\pi x}{a}\right)\sin\left(\frac{n\pi y}{b}\right) \qquad 2.18$$

The boundary conditions are supported by this expression, i.e., the deflection w and bending moments M are zero along the plate's edges. By substituting the deflection w in equation 2.11, the total potential energy of bending is:

$$U=\frac{1}{2}D\int_0^a\int_0^b\left\{\sum_{m=1}^{\infty}\sum_{n=1}^{\infty}a_{mn}\left(\frac{m^2\pi^2}{a^2}+\frac{n^2\pi^2}{b^2}\right)\sin\left(\frac{m\pi x}{a}\right)\sin\left(\frac{n\pi y}{b}\right)\right\}^2 dx\,dy$$

$$U=\frac{ab}{8}D\sum_{m=1}^{\infty}\sum_{n=1}^{\infty}a_{mn}^2\left(\frac{m^2\pi^2}{a^2}+\frac{n^2\pi^2}{b^2}\right)^2 \qquad 2.19$$

Similarly, in the case of a uniformly compressed plate in the x-direction with a compressive force per unit length at the edges x = 0 and x = a equal to N_x, the work done by this load can be calculated using 2.13:

$$T_1=\frac{1}{2}\int_0^a\int_0^b N_x\left(\frac{\partial w}{\partial x}\right)^2 dx\,dy \tag{2.20}$$

By substituting the deflection's equation 2.18:

$$T_1=\frac{ab}{8}N_x\sum_{m=1}^{\infty}\sum_{n=1}^{\infty}a_{mn}^2\frac{m^2\pi^2}{a^2} \tag{2.21}$$

2.2.3 Buckling theory

Following Timoshenko's [14] buckling theory of thin plates, when gradually applying an external load to the plate's middle plane, i.e., compressive or shear forces, the plate is initially in a state of flatform equilibrium. However, when the load reaches its critical value, the middle plane becomes unstable, and the plate begins to buckle. The energy method can be used to determine the load's critical value.

In the previous chapter, several cases of plate bending were examined. The strain energy was calculated using the work produced by the loads applied to the plate. If the work done by the loads is denoted as ΔT and the potential energy as ΔU, then the system is stable if:

$$\Delta U>\Delta T$$

By removing the load, the plate reverts to its initial undeformed shape (e.g., if the plate is subjected to compressive forces, then the plate returns to its uncompressed form). The system is unstable if:

$$\Delta U<\Delta T$$

Thus, the critical value for the load is obtained from the equation:

$$\Delta U=\Delta T \tag{2.22}$$

which is the point where the equilibrium changes from stable to unstable, and buckling occurs.

2.2.3.1 Elastic Buckling of Simply Supported Rectangular Plate Uniformly Compressed in One Direction

Assume a rectangular plate simply supported along all its edges and compressed by uniformly distributed forces acting on its sides at x = 0 and x = a (**Figure 13**). Let this force per unit length of the edge be denoted by N_x. Then, as shown in paragraph 2.2.2.1, the deflection of the plate, when the plate becomes unstable by gradually increasing the value of N_x, can be calculated using equation 2.18:

$$w=\sum_{m=1}^{\infty}\sum_{n=1}^{\infty}a_{mn}\sin\left(\frac{m\pi x}{a}\right)\sin\left(\frac{n\pi y}{b}\right)$$

In the above expression, m is the number of half-waves across the x-axis, while n is the number of half-waves in the perpendicular direction y-axis.

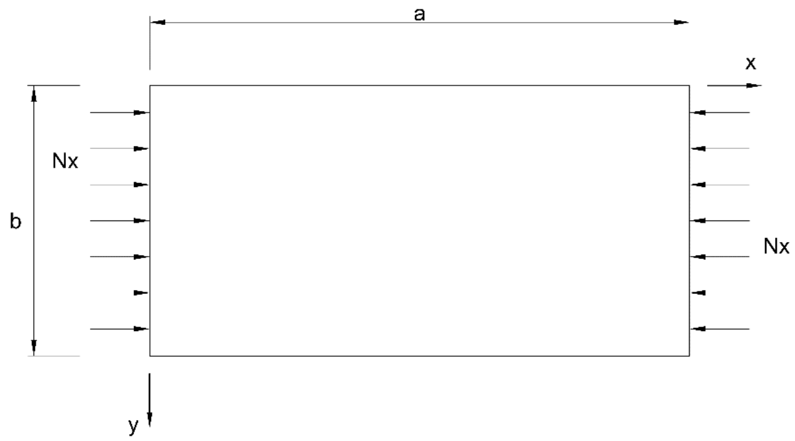

Figure 13. Buckling with uniform compression loading condition.

The strain energy of the system can be obtained using equation 2.19:

$$\Delta U = \frac{\pi^4 ab}{8} D \sum_{m=1}^{\infty} \sum_{n=1}^{\infty} a_{mn}^2 \left(\frac{m^2}{a^2} + \frac{n^2}{b^2} \right)^2$$

The work done by the compressive forces can be expressed with equation 2.20 and by substituting the deflection with its expression 2.18:

$$\Delta T_1 = \frac{\pi^2 b}{8a} N_x \sum_{m=1}^{\infty} \sum_{n=1}^{\infty} m^2 a_{mn}^2$$

The compressive force's critical value can be obtained by solving equation 2.22 using the above expressions. The following occurs:

$$N_x = \frac{\pi^2 a^2 D \sum_{m=1}^{\infty} \sum_{n=1}^{\infty} a_{mn}^2 \left(\frac{m^2}{a^2} + \frac{n^2}{b^2} \right)^2}{\sum_{m=1}^{\infty} \sum_{n=1}^{\infty} m^2 a_{mn}^2}$$

In order to find the critical value, the above expression must become a minimum. To obtain this result, all parameters a_{11}, a_{12}, a_{21}, …, except one, must be taken equal to zero. As m and n increase, so do the coefficients in front of a_{mn}. Hence, a_{11} is taken as the parameter not equal to zero since it has the smallest coefficient.

$$N_x = \frac{\pi^2 a^2 D}{m^2} \left(\frac{m^2}{a^2} + \frac{n^2}{b^2} \right)^2 = \frac{\pi^2 D}{a^2} \left(m + \frac{a^2}{b^2} \frac{n^2}{m} \right)^2 \qquad 2.23$$

At this point, the similarity between the critical buckling values of the compressive forces acting on a plate and a prismatic bar should be observed. In the equation above, the first factor represents the Euler load for a strip of unit width and length a. The second factor shows the proportion of the continuous plate's stability being greater than an isolated strip's stability. It can be seen that this magnitude depends on the plate's ratio a⁄b and the number of half-waves across the xy plane. In the case of a prismatic bar, buckling occurs for the force's value:

$$P_{cr} = \frac{\pi^2 EI}{l^2}$$

where I is the section's moment of inertia and l the bar's length. In the case of a square plate, for example, the respective critical value is:

$$N_{x,cr} = \frac{4\,\pi^2 D}{a^2}$$

It should be noted that the number of half-waves in both directions was assumed equal to one to minimize the force’s value. By comparing the above, D is analogous to EI since both represent the flexural rigidity of each structure, and a is equivalent to l. Therefore, the statement above stands true since it can be concluded that a square plate requires four times the compressive force of a prismatic bar’s critical value to buckle. Hence, the plate is four times more stable.

Equation 2.23 can also be written as:

$$N_x = \frac{\pi^2 D}{b^2}\left(\frac{b}{a}m + \frac{a}{b}\frac{n^2}{m}\right)^2 \qquad 2.24$$

By denoting:

$\alpha = a/b$ as the plate’s aspect ratio

$K = \left(\frac{1}{\alpha}m + a\frac{n^2}{m}\right)^2$ as the plate’s buckling coefficient

the above expression for the compressive force becomes:

$$N_x = K\frac{\pi^2 D}{b^2} \qquad 2.25$$

The critical value of the load can be calculated as:

$$N_{x,cr} = K_{cr}\frac{\pi^2 D}{b^2} \qquad 2.26$$

where:

$$K_{cr} = \min\left(\frac{1}{\alpha}m + a\frac{n^2}{m}\right)^2 \qquad 2.27$$

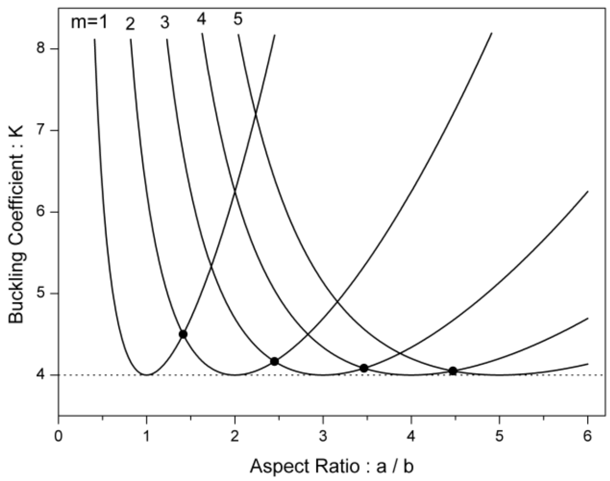

Figure 14. Compression buckling coefficient.

In the diagram above (**Figure 14**), the relation between the buckling coefficient K and the plate’s aspect ratio α has been plotted for subsequent cases of half-waves m (from 1 to 5) and assuming n = 1. The curves m and m+1 intersect at one point, as shown with the black dots in the diagram. This point's abscissa can be calculated as:

$$x_{\text{inter}}=\frac{\sqrt{m(m+1)}}{n} \tag{2.28}$$

In **Figure 14**, for a specific aspect ratio, several buckling coefficient values correspond to it (perpendicular intersection with more than one curve). This means that the plate can buckle with more than one eigenforms. However, only one corresponds to the minimum value for the buckling coefficient (critical value). Therefore, this eigenform, and therefore the curve whose perpendicular intersection gives the lowest coefficient value, seems to change after each intersection point. Thus, the same diagram can be replotted to show the critical buckling coefficient with respect to the plate's aspect ratio by using equation 2.27 and breaking the curves at their intersection points.

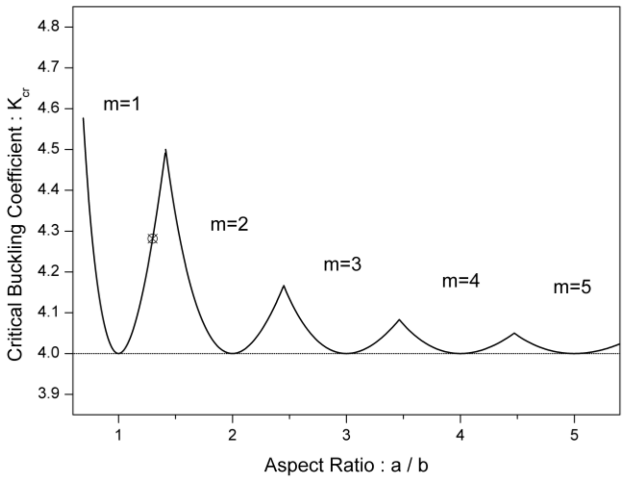

Figure 15. Compression critical buckling coefficient.

The above diagram (**Figure 15**) can be used for a plate of specific dimensions to find the critical buckling coefficient K_{cr}, as well as the number of half-waves that develop across its longitudinal direction. For example, for a plate with an aspect ratio a⁄b = 1.3, the critical buckling coefficient is K_{cr} = 4.2817. This point can be seen in the same diagram with a marked circle. The graph shows that the number of half-waves that develop across its length direction is one (m = 1).

From both diagrams, it is also visible that the curves' minimum is at the value of K = 4, and their curvature tends to open as m increases. This means that as the aspect ratio increases, each successorial wave-form curve is closer to the value of 4 than its predecessor. The divergence of two subsequent curves' intersection points from the minimum value of 4 is shown in the diagram below (**Figure 16**).

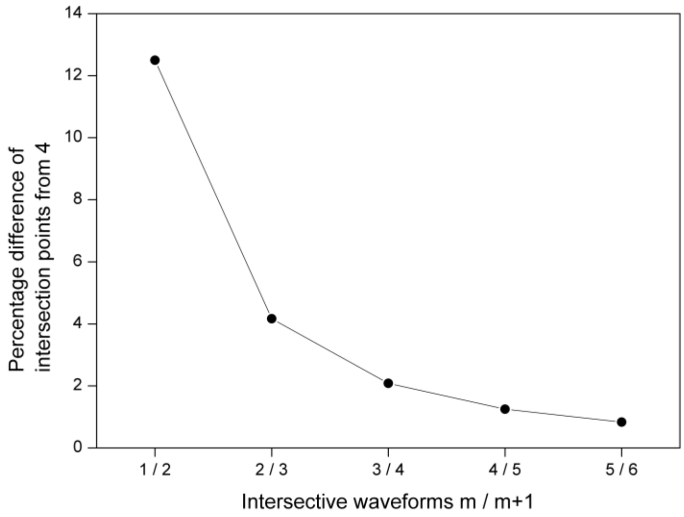

Figure 16. Buckling coefficient divergence.

The intersection point between the first and second wave-form diverges from the value of 4 by more than 12%. However, four intersection points after, i.e., between the fifth and sixth wave-form, the percentage is below 1%. Thus, an approximation would be that for long plates, the critical buckling coefficient can be considered equal to 4. As shown in a previous example, K_{cr} = 4 for a square plate with one half-wave across both directions of the plate. Thus, as the ratio a/b increases (long plates), the number of half-waves across the x-direction increases in a way that the rectangle tends to subdivide into buckled squares.

This statement can also be supported mathematically. In equation 2.28, the abscissa is identical to the ratio a/b, therefore:

$$\frac{a}{b}=\frac{\sqrt{m(m+1)}}{n}$$

In the case currently examined, n = 1. For a large number of half-waves across x-direction, i.e., for a long plate, the above expression can be transformed to:

$$\frac{a}{b}\approx m$$

Thus, long plates buckle in half-waves with a length equal to the plate's width, i.e., the plate is subdivided into buckled square plates. This is a phenomenon caused due to the lower energy state of such deformation. An example of this case is given in **Figure 17**, which illustrates the first eigenform of a long plate with an aspect ratio equal to 5.

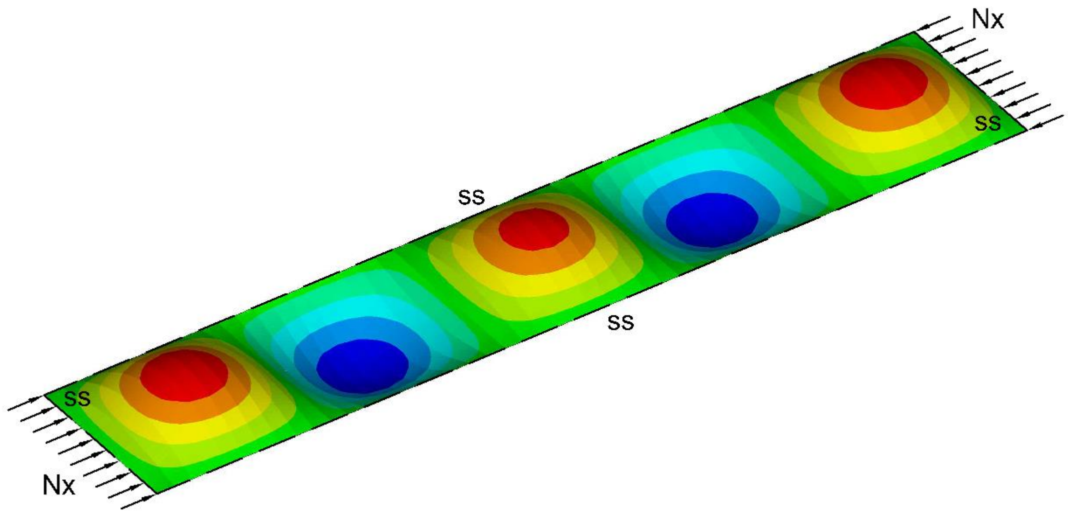

Figure 17. First eigenform of a long plate with an aspect ratio equal to 5.

This study focuses on buckling with one half-wave across the transverse direction since it is the most possible due to the lower critical buckling coefficient value (achieving a minimum compressive force N_x). This can be proved by the following equations:

$$(K_{cr})_{m,n} < (K_{cr})_{m,n+1}$$

$$\left(\frac{1}{\alpha}m + a\frac{n^2}{m}\right)^2 < \left(\frac{1}{\alpha}m + a\frac{(n+1)^2}{m}\right)^2$$

$$\frac{1}{\alpha}m + a\frac{n^2}{m} < \frac{1}{\alpha}m + a\frac{(n+1)^2}{m}$$

$$n^2 < (n+1)^2$$

$$n < n+1$$

$$0 < 1$$

It should be noted that the critical value of the compressive force $N_{x,cr}$ can be referred to as an eigenvalue, whereas the deflection surface w of this value is an eigenform. Ultimately, the elastic buckling of a plate is a problem of eigenvalues-eigenforms.

As proposed by Timoshenko [14], the critical value of the elastic compressive stress is:

$$\sigma_{E,cr} = \frac{N_{x,cr}}{t} = K_{cr}\frac{\pi^2 E}{12(1\text{-}\nu^2)}\left(\frac{t}{b}\right)^2$$

This shows that $\sigma_{E,cr}$ = f (K_{cr}, E, ν, t, b) and from previous equations K_{cr} = f (m, a, b), since it has been established that the critical case occurs assuming n = 1. Additionally, when comparing two plates with identical geometry (equal dimensions), the aspect ratio α (i.e., length a and width b) and thickness t are considered constant. Assuming the same number of half-waves m, then the only parameters the critical stress depends on are E and ν, which essentially is the material. For plates with a material of similar Poisson's ratio ν, as the elastic modulus increases, the plate is more rigid since it requires more significant stresses to buckle.

The following table sums up the results when comparing geometrically identical plates of different materials. It should be noted that the width to thickness ratio was taken equal to $t/b = 0.01$ and Poisson's ratio $\nu = 0.3$.

Table 2. Critical compressive stress comparison between materials.

Property		**a/b**			
		1	**1.5**	**2**	**2.5**
K_{cr}		4	4.34	4	4.13
m		1	2	2	3
High Carbon Steel E=200-215 GPa	$\sigma_{E,cr}$ [MPa]	72-78	78-84	72-78	75-80
Cast Iron E=165-180 GPa	$\sigma_{E,cr}$ [MPa]	60-65	65-71	60-65	62-67
Aluminum Alloy E=68-82 GPa	$\sigma_{E,cr}$ [MPa]	25-30	27-32	25-30	25-31

2.2.3.2 Elastic Buckling of Simply Supported Rectangular Plate under Shear Stress

Similar to paragraph 2.2.3.1, assume a rectangular plate simply supported along all its edges and submitted to shearing forces on all its sides (**Figure 18**). Let this force be denoted by N_{xy}/N_{yx}. For describing the deformation of the plate, equation 2.18 can be used once again:

$$w = \sum_{m=1}^{\infty}\sum_{n=1}^{\infty} a_{mn} \sin\left(\frac{m\pi x}{a}\right) \sin\left(\frac{n\pi y}{b}\right)$$

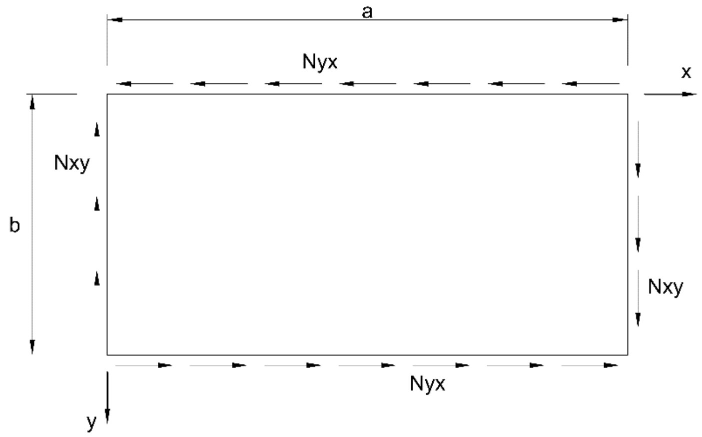

Figure 18. Buckling with shear stress loads.

The strain energy of the system can be obtained by the equation 2.19:

$$\Delta U = \frac{\pi^4 ab}{8} D \sum_{m=1}^{\infty}\sum_{n=1}^{\infty} a_{mn}^2 \left(\frac{m^2}{a^2} + \frac{n^2}{b^2}\right)^2$$

The work done by the shearing forces can be expressed with the equation 2.13, with the only acting forces being the shearing:

$$\Delta T_1 = -N_{xy} \int_0^a \int_0^b \frac{\partial w}{\partial x}\frac{\partial w}{\partial y} dx\, dy$$

The shearing force's critical value can be obtained by solving equation 2.22 using the above expressions. The following occurs:

$$N_{xy} = -\frac{ab}{32} D \frac{\sum_{m=1}^{\infty}\sum_{n=1}^{\infty} a_{mn}^2 \left(\frac{m^2}{a^2}+\frac{n^2}{b^2}\right)^2}{\sum_n \sum_n \sum_p \sum_q a_{mn} a_{pq} \frac{mnpq}{(m^2-p^2)(q^2-n^2)}}$$

where m, n, p, q are such integers that m ± p and n ± q are odd numbers. To minimize this equation, a homogeneous system of linear equations is constructed, and through its solution, the following critical shearing stress equation is obtained (Timoshenko [14]):

$$\tau_{E,cr} = k \frac{\pi^2 D}{b^2 t}$$

, where k = 9.4 approximately. This equation is satisfactory for plates where the ratio $a/b \leq 1.5$, i.e., for plates that do not differ much from a squared shape. The following approximate solution is followed for long narrow plates, i.e., $a \gg b$. The deflection surface is obtained by the equation:

$$w = A\sin\left(\frac{\pi y}{b}\right)\sin\left(\frac{\pi}{s}(x-ay)\right) \qquad 2.29$$

, where s is the length of half-waves and a is the slope of nodal lines. With shearing forces acting on the plate's sides, the buckled shape has nodal lines that are not straight, as shown in **Figure 19**. By substituting the equation for deflection 2.29 to equation 2.11 and the equation for the work done by the load and equating these two using 2.22, the following equations are obtained:

$$\tau_{E,cr} = k_{cr} \frac{\pi^2 D}{b^2 t} \qquad 2.30$$

, where:

$$k_{cr} = 5.35 + 4\left(\frac{b}{a}\right)^2 \qquad 2.31$$

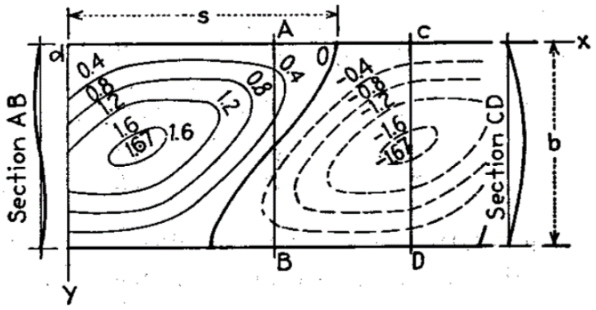

Figure 19. Shear buckling eigenforms.

This equation for k_{cr} is a parabolic curve (**Figure 20**) that gives exact solutions for long narrow plates and a good approximation for square plates (k_{cr} = 9.35 for a square plate, while the exact value is 9.4, as shown previously).

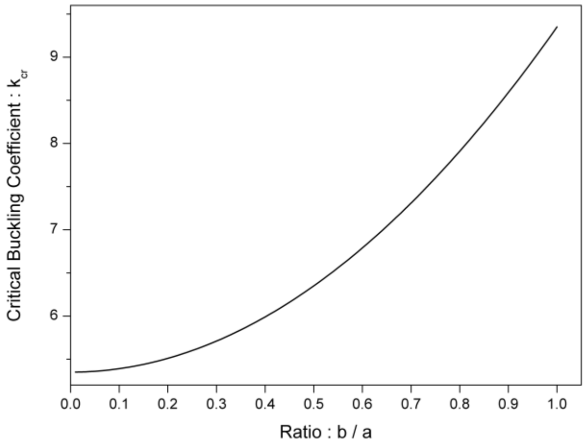

Figure 20. Shear critical buckling coefficient.

2.2.3.3 Anelastic Buckling

The analysis conducted in paragraphs 2.2.3.1 and 2.2.3.2 has assumed that the plate's buckling stress value is within the elastic range, i.e., it does not surpass the materials' yield stress. If, however, the critical stress value exceeds the yield point, a correction for anelastic buckling is carried out. The buckling stress, in this case, is obtained by the Johnson-Ostenfeld parabola equations, taking into account the work of both elastic and plastic action. Therefore, the following corrections should be applied:

- Buckling of simply supported rectangular plate uniformly compressed in one direction:

$$\sigma_{cr}=\sigma_{E,cr} \qquad \text{for} \qquad \sigma_{E,cr}\leq {}^{\sigma_y}/_2$$
$$\sigma_{cr}=\sigma_y\left(1-\frac{\sigma_y}{4\sigma_{E,cr}}\right) \qquad \text{for} \qquad \sigma_{E,cr}> {}^{\sigma_y}/_2 \tag{2.32}$$

- Buckling of simply supported rectangular plate under shear stress:

$$\tau_{cr}=\tau_{E,cr} \qquad \text{for} \qquad \tau_{E,cr}\leq {}^{\tau_y}/_2$$
$$\tau_{cr}=\tau_y\left(1-\frac{\tau_y}{4\tau_{E,cr}}\right) \qquad \text{for} \qquad \tau_{E,cr}> {}^{\tau_y}/_2 \tag{2.33}$$

In the equations above, the material's yield stress is denoted by the subscript 'y'. According to LR [11], the shear yield stress can be calculated from the material's yield stress as $\tau_y = \sigma_y / \sqrt{3}$.

The elastic or anelastic behavior of a plate can be characterized with the help of the plate's slenderness ratio β, which can be calculated as:

$$\beta=\frac{b}{t}\sqrt{\frac{\sigma_0}{E}}$$

A plate's behavior can be visualized by plotting the critical buckling stress with respect to the slenderness ratio, as shown in the diagram below (**Figure 21**). This diagram is the combination of

Euler’s curve for elastic buckling and the Johnson-Ostenfeld parabola for anelastic buckling values. Although only compressive stresses are shown, the same diagram applies to shearing stresses.

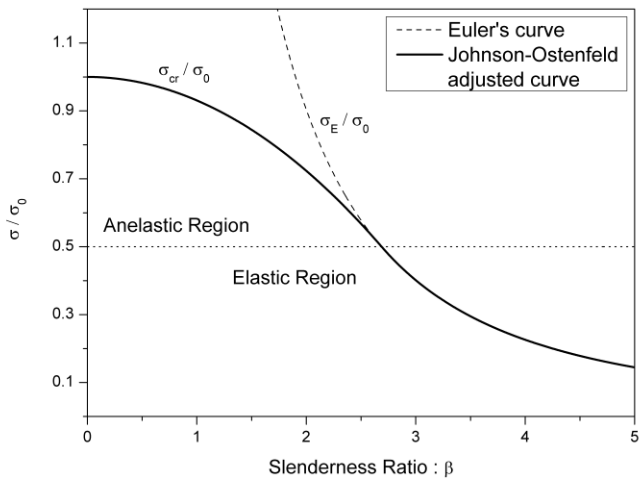

Figure 21. Elastic/anelastic buckling curves with respect to the slenderness ratio (applicable for both compressive and shear buckling).

2.2.3.4 Post-buckling capacity

The proposed method might be criticized for using elastic buckling theory and not introducing non-linearities to make the problem more realistic. However, the former allows for a safe preliminary assessment of the obtained FoS since it underestimates the critical buckling stress. This phenomenon is thoroughly explained by Hughes [15], where it is stated that the stresses do not distribute uniformly internally at a stiffened panel during compression. This occurs because the stiffened edges have higher rigidity than the unsupported center. Thus, the center is the first to buckle, while the former areas buckle at a higher value, demonstrating post-buckling capacity. Hence, by assuming elastic buckling, the proposed method’s real-world application will exhibit a better structural response than the one obtained from numerical calculations.

2.3 Composites theory

2.3.1 Theory fundamentals

This chapter analyses the fundamentals of composites’ theory based on Kollar’s [13] composites theory. The patches used in this study are carbon fiber reinforced polymers, i.e., fiber-reinforced composite.

In a composite, the fibers are within a matrix. From a micromechanics’ point of view, the structure has heterogeneous properties, i.e., the properties differentiate from point to point. Another way to analyze the structure is on a larger scale (macro mechanics). Then, it could be assumed that the structure is homogenous, i.e., the properties are the same between measurement points (quasi-homogeneous). The structure’s properties are a combination of fibers and matrix properties.

A composite is made from thin layers called plies. Each ply is composed of fibers (continuous or discontinuous) embedded in a matrix. These fibers may be aligned in one direction or be misaligned in specified or random directions (angles). The combination of several plies leads to the formulation of a laminate. This laminate equates to the structure whose analysis is to be performed.

Woven fibers (biaxial weave) are used in this study to benefit from the continuous fibers' stiffness and strength in two directions, as well as the matrix's protection and support. A ply such as this is referred to as fabric, i.e., woven fabric. The woven fabric used is a cross-ply laminate, i.e., the fibers are aligned only in the 0 and 90-degree directions. The 0-degree and 90-degree directions are identical to the x-axis and y-axis directions, respectively (as explained and shown below).

When analyzing a structure, a reference point is required. For example, a composite has two coordinate systems:

- Local coordinate system:
  - Aligned with the fibers or axes of symmetry.
  - Axes: x_1, y_1, z_1
  - Displacements: u_1, u_2, u_3
  - Normal stress: σ_1, σ_2, σ_3
  - Shear stress: τ_{23}, τ_{13}, τ_{12}
  - Normal strain: ε_1, ε_2, ε_3
  - Shear strain: γ_{23}, γ_{13}, γ_{12}
- Global coordinate system:
  - Attached to a fixed reference point.
  - Axes: x, y, z
  - Displacements: u, v, w
  - Normal stress: σ_x, σ_y, σ_z
  - Shear stress: τ_{yz}, τ_{xz}, τ_{xy}
  - Normal strain: ε_x, ε_y, ε_z
  - Shear strain: γ_{yz}, γ_{xz}, γ_{xy}

A composite could be generally anisotropic, monoclinic, orthotropic, transversely isotropic, or isotropic. This characterization is based on the composite's behavior, dependent on the fibers' orientation within the matrix. For example, in a cross-ply laminate, the fibers are oriented in two perpendicular directions (bi-directional), parallel to the ply's edges. Thus, the composite is orthotropic since there are three mutually perpendicular symmetry planes with respect to the alignment of the fibers. The reference plane is taken to be the laminate's midplane. If the laminate is symmetrical, the midplane is also a neutral plane.

2.3.2 Stress-strain relationship

The stress-strain relationship can be described using the equation:

$$\begin{Bmatrix}\sigma_x\\ \sigma_y\\ \sigma_z\\ \tau_{yz}\\ \tau_{xz}\\ \tau_{xy}\end{Bmatrix}=[\bar{C}]_{6x6}\begin{Bmatrix}\varepsilon_x\\ \varepsilon_y\\ \varepsilon_z\\ \gamma_{yz}\\ \gamma_{xz}\\ \gamma_{xy}\end{Bmatrix} \qquad 2.34$$

where $[\bar{C}]_{6x6}$ is a 6x6 stiffness matrix in the x, y, z coordinate system. The inversion of the above relationship results in the following:

$$\begin{Bmatrix}\varepsilon_x\\ \varepsilon_y\\ \varepsilon_z\\ \gamma_{yz}\\ \gamma_{xz}\\ \gamma_{xy}\end{Bmatrix}=[\bar{S}]_{6x6}\begin{Bmatrix}\sigma_x\\ \sigma_y\\ \sigma_z\\ \tau_{yz}\\ \tau_{xz}\\ \tau_{xy}\end{Bmatrix} \qquad 2.35$$

where $[\bar{S}]_{6x6}$ is a 6x6 compliance matrix in the x, y, z coordinate system.

The same equations exist in the x_1, y_1, z_1 coordinate system but with the respective notations for the stresses and strains and the matrices being $[C]_{6x6}$ and $[S]_{6x6}$. Thus:

$$[\bar{S}]=[\bar{C}]^{-1} \qquad\qquad [S]=[C]^{-1} \qquad 2.36$$

With CFRP being an elastic material, both stiffness and compliance matrices are symmetrical.

Because the composite is orthotropic, all out-of-plane shear strains are zero, i.e., $\gamma_{13} = \gamma_{23} = \gamma_{12} = 0$. The following engineering constants apply to the structure:

$$E_1=\frac{\sigma_1}{\varepsilon_1} \qquad G_{12}=\frac{\tau_{12}}{\gamma_{12}} \qquad \nu_{12}=-\frac{\varepsilon_2}{\varepsilon_1} \qquad \nu_{23}=-\frac{\varepsilon_3}{\varepsilon_2}$$

$$E_2=\frac{\sigma_2}{\varepsilon_2} \qquad G_{13}=\frac{\tau_{13}}{\gamma_{13}} \qquad \nu_{13}=-\frac{\varepsilon_3}{\varepsilon_1} \qquad \nu_{31}=-\frac{\varepsilon_1}{\varepsilon_3}$$

$$E_3=\frac{\sigma_3}{\varepsilon_3} \qquad G_{23}=\frac{\tau_{23}}{\gamma_{23}} \qquad \nu_{21}=-\frac{\varepsilon_1}{\varepsilon_2} \qquad \nu_{32}=-\frac{\varepsilon_2}{\varepsilon_3}$$

The stiffness matrix is written in the form:

$$[C]=\begin{bmatrix}[L]_{4x4} & [0]_{4x4}\\ [0]_{4x4} & [M]_{4x4}\end{bmatrix} \qquad 2.37$$

By using equation 2.34, it can be seen that the normal stresses in the fibers' directions (parallel to the local coordinate system) do not produce shear deformations. Additionally, there is no extension-shear, bending-twist, and extension-twist coupling in an orthotropic laminate.

In a laminate, the plies are considered to be perfectly bonded together. Thus, the normal stresses, out-of-plane shear stresses, and displacements are equal between adjacent layers:

$$\begin{array}{lll}(\sigma_z)_{ply}=(\sigma_z)_{ply+1} & (u)_{ply}=(u)_{ply+1} & (\varepsilon_x)_{ply}=(\varepsilon_x)_{ply+1}\\ (\tau_{xz})_{ply}=(\tau_{xz})_{ply+1} & (v)_{ply}=(v)_{ply+1} & (\varepsilon_y)_{ply}=(\varepsilon_y)_{ply+1}\\ (\tau_{yz})_{ply}=(\tau_{yz})_{ply+1} & (w)_{ply}=(w)_{ply+1} & (\gamma_{xy})_{ply}=(\gamma_{xy})_{ply+1}\end{array} \qquad 2.38$$

In the relationships above, the subscript ‘ply’ corresponds to the bottom ply under examination, while ply+1 is its adjacent ply above.

In cases where a composite plate with fibers parallel to the x-y plane is subjected to uniformly distributed forces along the edges and parallel to the plate’s plane, plane stress conditions are in effect. Then, one normal stress and the out-of-plane shear stresses are zero. If x-y (or x_1-x_2) is the plane parallel to the plate, then the following assumption for the stresses is made:

$$\sigma_z=0 \qquad \tau_{yz}=0 \qquad \tau_{xz}=0 \tag{2.39}$$

Equation 2.39 is also in effect for the local coordinate system x_1, x_2, x_3. With plane-stress condition in effect, equation 2.34 becomes:

$$\begin{Bmatrix}\sigma_1\\ \sigma_2\\ \sigma_{12}\end{Bmatrix}=\begin{bmatrix}\frac{E_1}{D} & \frac{\nu_{12}E_1}{D} & 0\\ \frac{\nu_{12}E_2}{D} & \frac{E_2}{D} & 0\\ 0 & 0 & G_{12}\end{bmatrix}\begin{Bmatrix}\varepsilon_1\\ \varepsilon_2\\ \gamma_{12}\end{Bmatrix}=[Q]\begin{Bmatrix}\varepsilon_1\\ \varepsilon_2\\ \gamma_{12}\end{Bmatrix} \tag{2.40}$$

where:

$$D=1-\frac{E_2}{E_1}\nu_{12}^2=1-\nu_{12}\nu_{21} \tag{2.41}$$

The same equations apply to the general coordinate system x, y, z with the stiffness matrix $[\bar{Q}]$.

Let f_x, f_y, f_z be the body forces per unit volume and p_x, p_y, p_z the surface forces per unit area. The system’s total potential energy is:

$$\pi_p=U+\Omega \tag{2.42}$$

where:

- U: Strain energy of volume V calculated using the expression:

$$U=\frac{1}{2}\iiint[\varepsilon_x \quad \varepsilon_y \quad \varepsilon_z \quad \gamma_{yz} \quad \gamma_{xz} \quad \gamma_{xy}][C]\begin{Bmatrix}\varepsilon_x\\ \varepsilon_y\\ \varepsilon_z\\ \gamma_{yz}\\ \gamma_{xz}\\ \gamma_{xy}\end{Bmatrix}dV \tag{2.43}$$

- Ω: Potential energy of the external forces calculates as:

$$\Omega=-\iiint\left(f_x u+f_y v+f_z w\right)dV-\iiint\left(p_x u+p_y v+p_z w\right)dA \tag{2.44}$$

Using the Ritz method, the displacements can be expressed as:

$$u=\sum_{i=1}^{I}A_i u_i \qquad v=\sum_{j=1}^{J}B_j v_j \qquad w=\sum_{k=1}^{K}C_k w_k \tag{2.45}$$

where u_i, v_j, w_k are functions that must satisfy the boundary conditions, and A_i, B_j, C_k are constants that are provided by solving the equilibrium equations (2.46).

At equilibrium, the system’s potential energy (2.42) must satisfy the below expressions:

$$\frac{\partial \pi_p}{\partial A_i} = 0 \quad \text{for i=1, ..., I}$$
$$\frac{\partial \pi_p}{\partial B_j} = 0 \quad \text{for i=1, ..., J} \qquad 2.46$$
$$\frac{\partial \pi_p}{\partial C_k} = 0 \quad \text{for i=1, ..., K}$$

2.3.3 Buckling theory

This paragraph examines buckling of a simply supported, symmetrical and orthotropic composite plate.

Assume a plate of length a, width b and thickness t, which is small compared to the rest of the dimensions, i.e., thin plate theory is applicable. Let xy be the middle plane of the plate, which also serves as a neutral plane since the composite is symmetrical. The x and y axes are directed along the plate's length and width, whereas z is perpendicular and positive upwards. Additionally, applying thin plate theory, the following assumptions are made:

- The strains are linear across the plate.
- Out-of-plane shear deformations are negligible.
- Out-of-plane normal stress σ_z and shear stresses τ_{xz}, τ_{yz} are small compared to those in-plane.

The force-strain relationship is:

$$\begin{Bmatrix} N_x \\ N_y \\ N_{xy} \\ N_x \\ M_y \\ M_{xy} \end{Bmatrix} = \begin{bmatrix} [A]_{4x4} & [B]_{4x4} \\ [B]_{4x4} & [D]_{4x4} \end{bmatrix} \begin{Bmatrix} \varepsilon_x^o \\ \varepsilon_y^o \\ \varepsilon_z^o \\ \gamma_{yz}^o \\ \gamma_{xz}^o \\ \gamma_{xy}^o \end{Bmatrix} \qquad 2.47$$

where the superscript *o* refers to the strains in the reference midplane and [A], [B], [D] are the stiffness matrices of the laminate dependent on the stiffness matrix $[\overline{Q}]$ and the vertical distances from the reference plane.

Since the plate is simply supported, all edges are restrained, and the following conditions apply:

$$(w^o)_{x=0} = 0 \qquad (w^o)_{x=a} = 0$$
$$(w^o)_{y=0} = 0 \qquad (w^o)_{y=b} = 0 \qquad 2.48$$

With these conditions in effect, the deflection surface that satisfies the above can be expressed by:

$$w^o = \sum_{i=1}^{I} \sum_{j=1}^{J} w_{ij} \sin\left(\frac{i\pi x}{a}\right) \sin\left(\frac{j\pi y}{b}\right) \qquad 2.49$$

where I and J are the number of terms in the summations chosen arbitrarily. This expression is equivalent to 2.18 from paragraph 2.2.2.1 of thin plate theory, i.e., the following sets are analogous: m with i, n with j and a_{mn} with w_{ij}. Therefore, in the case of a thin composite plate, i is the number of half-waves that develop across its longitudinal x-axis, while j are the half-waves across its transverse y-axis.

The strain energy of the system is:

$$U=\frac{1}{2}\int_0^a\int_0^b\left[D_{11}\left(\frac{\partial^2 w^o}{\partial x^2}\right)^2+D_{22}\left(\frac{\partial^2 w^o}{\partial y^2}\right)^2+D_{66}\left(\frac{2\partial^2 w^o}{\partial x\partial y}\right)^2+2D_{12}\frac{\partial^2 w^o}{\partial x^2}\frac{\partial^2 w^o}{\partial y^2}\right]dydx \qquad 2.50$$

The work done by the in-plane compressive forces can be expressed using the equation:

$$\Omega=\frac{1}{2}\int_0^a\int_0^b\left[N_x\left(\frac{\partial w^o}{\partial x}\right)^2+2N_{xy}\frac{\partial w^o}{\partial x}\frac{\partial w^o}{\partial y}\right]dydx \qquad 2.51$$

In the case of uniform compressive load in the x-direction, $N_{xy} = 0$. On the other hand, if a shear load is applied, then $N_x = 0$. In this paragraph, only the case of uniform compression is examined therefore:

$$\Omega=\frac{1}{2}\int_0^a\int_0^b N_x\left(\frac{\partial w^o}{\partial x}\right)^2 dydx \qquad 2.52$$

According to the principle of stationary potential energy (equations 2.46):

$$\frac{\partial \pi_p}{\partial w_{ij}}=\frac{\partial(U+\Omega)}{\partial w_{ij}}=0 \qquad 2.53$$

By substituting 2.50 and 2.52 to the above equation and solving the eigenvalue problem, the following expression for the critical compressive force occurs:

$$N_{x,cr}=\pi^2\left[D_{11}\left(\frac{i}{a}\right)^2+2(D_{12}+2D_{66})\left(\frac{j}{b}\right)^2+D_{22}\left(\frac{j}{b}\right)^4\left(\frac{a}{i}\right)^2\right] \qquad 2.54$$

Similar to thin plate buckling (equation 2.24), the critical compressive force increases monotonically with j. Thus, the critical (lowest) value is obtained for j = 1, which translates to one half-wave in the direction perpendicular to the load (y-axis direction). Then:

$$N_{x,cr}=\pi^2\left[D_{11}\frac{1}{a^2}i^2+2(D_{12}+2D_{66})\frac{1}{b^2}+D_{22}\frac{a^2}{b^4}\frac{1}{i^2}\right] \qquad 2.55$$

2.4 Bondline fracture

An additional non-linearity is the existence of the adhesive bondline between the composite patch and the metal plate. According to Anyfantis et al. [16], the cohesive zone might be damaged, which could lead to crack initiation and propagation, resulting in debonding propagation. The latter may develop between the composite and the adhesive, the metal plate and the adhesive, or through a failure of the adhesive itself. In order to avoid non-linear solutions, the following method was proposed for developing an assessment method of the bondline fracture.

During loading, the stresses that develop on the bonded structure's cross-sections are transferred between the two substrates through the bondline. The latter's failure conditions can be evaluated using its fracture toughness G_C, which is its resistance to a defect's propagation. In order to evaluate if the bondline fails under a specific load, the acting strain energy release rate G must be known. This strain energy increases as the applied load also increases. According to the energy method, a bondline defect propagates if:

$$G\geq G_C \qquad 2.56$$

The acting strain energy release rate G can be calculated using the steady state's re-lease rate (SERR) debonding propagation formula:

$$G = G_{SS} = \frac{1}{2\overline{E}_m}\left(\frac{P^2}{t_m} + \frac{P^2}{At_c} - \frac{M_b^2}{It_c^3}\right) \qquad 2.57$$

where:

- P is the axial acting force.
- $M_b = P(\delta - t_m/2)$ is the balance moment, with $\delta = \frac{1+2\Sigma\eta+\Sigma\eta^2}{2\eta(1+\Sigma\eta)} t_c$, $\Sigma = \overline{E}_c/\overline{E}_m$ and $\eta = t_c/t_m$.
- $A = 1/\eta + \Sigma$ and $I = \Sigma\left[\left(\Delta - \frac{1}{\eta}\right)^2 - \left(\Delta - \frac{1}{\eta}\right) + \frac{1}{3}\right] + \frac{\Delta}{\eta}\left(\Delta - \frac{1}{\eta}\right) + \frac{1}{3\eta^2}$.
- $\overline{E}_c = \frac{E_c}{1-\nu_c^2}$ and $\overline{E}_m = \frac{E_m}{1-\nu_m^2}$ are the effective plane stress Young's moduli of the composite and the plate, respectively, while E_c and E_m are their Young's moduli of elasticity, and ν_c and ν_m their Poisson's ratio.

For the case being studied, P is replaced by $N_{x,cr}$ in order to determine whether the proposed patch repair could suffer from bondline fracture. Finally, the maximum stress developed within the metal plate and the composite patch must not exceed the respective material's yielding/fracture value.

3 Physics and data-based models

3.1 FEA model

3.1.1 Theoretical background

During a components loading, internal stresses develop within the body to maintain equilibrium over the volume of the body. Stresses, stains and displacements can be calculated using the principle of equilibrium over the body, e.g., calculating a body's normal forces at a cross-section to obtain its normal stress at the same position. The problem of equilibrium increases in difficulty as the structure becomes more complex. For instance, although the calculations are simple for a cantilever beam, they are more complicated for a 3D hook. This problem is approached by the finite element method (FEM), which splits a body into smaller elements (discretisation) connected at nodes. Thus, the equilibrium problem for an initially infinite number of elements across a body is now reduced to a problem of finite discrete elements' equilibrium.

These discrete elements could be a line, surface or solid, which is a one, two, and three-dimensional object, respectively (**Table 3**). The surface elements could be triangular, usually used for awkward shapes or quadrilateral, which perform better overall. The option of the element type depends on the case being examined. For example, a truss is usually solved using line elements, but solid elements can also be used. It should be noted that the simpler the element, the less computational time is required. Hence, the truss problem using line elements is solved at a fraction of the time required for solid elements. However, for shape anomalies or where more detail is required, more complex elements produce higher accuracy of results.

Table 3. Element types used in FEA

Line element	**Surface elements**		**Solid elements**	
Line	Triangular	Quadrilateral	Tetrahedral	Hexahedron
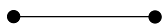	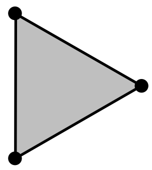	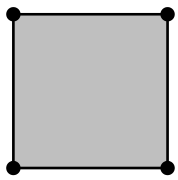	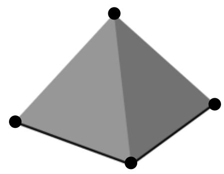	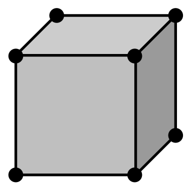

The elements interact at points called nodes. The collection of nodes and elements is called a mesh. As mentioned in the previous paragraph, complex elements such as solids produce more accurate results than simpler elements such as surfaces. However, the former requires more computing time than the latter. Similarly, a body's mesh can be coarse or fine, which is essentially fewer or more elements used to generate the results: the higher the number of elements, the better the accuracy (**Figure 22**). Nonetheless, this comes with a cost, which is the computational time required for the solution to be completed. The statements concerning the calculation times are summarized in **Table 4**.

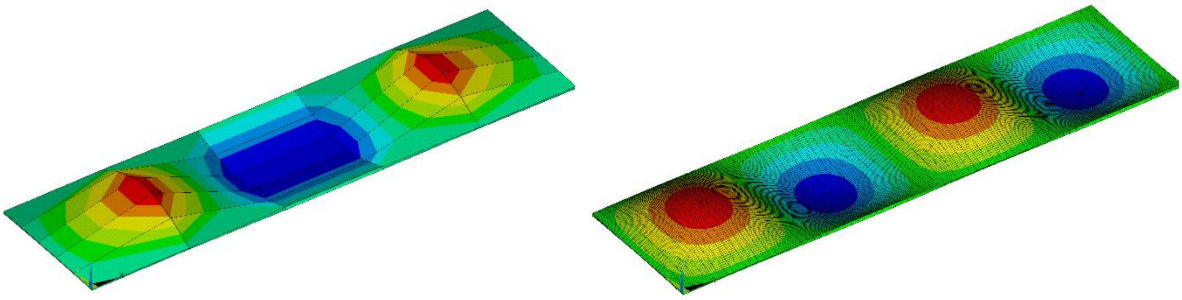

(a) **(b)**

Figure 22. Examples of (a) coarse and (b) fine mesh.

Table 4. Dependency of the calculation time on the element types and mesh.

Element type	**Mesh**	**Calculation time**
Line	Coarse	Less
Surface	↓	↓
Solid	Fine	More

The engineer must examine the problem and approximate according to the needs of the analysis in each case. Some cases can be simplified using uncomplicated geometries but acquiring a high and acceptable level of accuracy. For example, a stiffened panel can be modelled using surface elements for the plate and line elements for the stiffeners or solid elements for both. Depending on the result that needs to be extracted, the engineer should choose the more suitable option. If, for instance, the goal is to obtain the deflection at the centre of the stiffened panel, then the former option can be used since it would require less computational time for very similar results. If, however, the object being studied is the stress concentration developed at the corners of a bracket that connects two perpendicular stiffened panels, then solid elements are a better option since the alternative might not capture some connections between the components.

For stress analysis problems, the variable that is essential to be calculated is the displacement in each node. Through FEM, if the displacements are known for a loading condition, then the stresses and strain can also be extracted. In order to do this, assume that a mesh's elements have a certain amount of stiffness that resists deformation. Then similar to Hooke's law for a spring:

$$\{f\}=[k]\{u\} \tag{3.1}$$

where {f} is the nodal forces and moments, {u} is the nodal displacements and [k] is the element stiffness matrix. Therefore, the element stiffness matrix shows the amount of displacement a node has for specific applied forces. The matrix [k] is dependent on the number of nodes the element has and its degrees of freedom. Specifically, a node has 3 degrees of freedom in a 2D analysis and 6 degrees of freedom in a 3D analysis. For example, a line element, which has two nodes, can have a total of 6 degrees of freedom (DoF) for a 2D analysis and 6 DoF for a 3D analysis.

When analysing a structure, several elements interfere with each other, which results in the local stiffness matrices [k] of each element combining into a global stiffness matrix [K]. As a result, the local matrices are assembled in a way that serves the mesh's continuity, depending on the position of the nodes. Hence, the global stiffness matrix is obtained by a superposition of the element stiffness matrices as:

$$\{K\} = \sum_e \{k\}^e$$

where e represents the element number. Thus, the following equation can be used for the general assembly:

$$\{F\}=[K]\{U\} \tag{3.2}$$

The applied loads and boundary conditions must be set in order to find the displacements at the mesh's nodes. The loads and boundaries affect the load vector {F} and the displacement vector {U} respectively. At the same time, the stiffness matrix [K] is dependent on the elements' connectivity, the structure's geometry, and material properties. Knowing all parameters, the displacements can be obtained by inverting the stiffness matrix:

$$\{U\}=[K]^{-1}\{F\} \tag{3.3}$$

The above formula is the first way of solving equation 3.2 with respect to the displacement vector. Alternative techniques to this direct method exist by using approximations. For example, the potential energy approach can be used to derive the element equations using the formula $\pi_p = U + \Omega$, where π_p is the total potential energy, U is the internal strain energy, and Ω is the potential energy of the external forces. The displacement configuration is obtained by minimizing the total potential energy.

Namely another example is the Galerkin method of weighted residuals, which uses trial functions to approximate the displacement. Since the function does not initially satisfy the equation, it leaves residuals over the region of the problem. The method aims to keep the residuals minimum across the whole region, thus approximating the displacement better.

The result of solving equation 3.2 is the displacement vector {U}, which includes the respective values at each nodal point of the mesh. Next, the displacement at the region between nodal points is calculated using the shape functions of the closest nodal points of each element. Finally, the strains and stresses of a point can be calculated using the now known displacement at the requested position. In summarizing, the steps for solving an FEA problem are:

1. Definition of the problem

   The structure's geometry, loading conditions and boundaries are defined. Additionally, an assessment of the modelling methodology that should be followed is made – e.g., element type, materials, assumptions.

2. Discretisation

   The geometry's mesh is defined according to desired extracted results. A mesh can have a coarse mesh, a finer mesh, or even both in different areas – e.g., two perpendicular walls with coarse mesh but a more refined mesh at their point of intersection to capture local stresses.

3. Solution

   Either by hand calculations or computer software, the problem is solved according to the equations and methodology mentioned previously.

4. Post-processing

   The desired results are obtained and plotted, e.g., stresses, strains, displacements. In this stage, a validation of the results shall be performed in order to verify good design practices.

As mentioned above, the FEM calculations can be performed either by hand or with commercial computer software. The latter has the advantage of performing complex calculations in a fraction of the time needed for a team of engineers to do them by hand. Thus, for the last decades, most of the calculations have been performed using these FEA programs available for commercial use. One of these tools is ANSYS, widely used in the engineering industry.

For this study, ANSYS is used to solve the eigen-buckling problem of the plate. In order to reduce modelling and calculation times, the proposed method for setting up and solving the problem is a parametric design using APDL. APDL, which stands for ANSYS Parametric Design Language, is a code-based version with restricted UI (user interface), allowing easier parametrization. Hence, the problem's constants and parameters are input in constructed script forms. Then, multiple simulations can be solved as a batch. The purpose of these analyses is to obtain the critical elastic buckling stress of a thin plate structure.

In paragraph 3.1.1, the steps for solving a structural problem using FEM was mentioned. Similarly, when solving a problem with a FEA software, the following steps are followed:

- Preprocessing
  - Analysis preference:

    Structural, thermal, CFD, etc.
  - Element Type:

    Line, surface or solid elements.
  - Material Properties:

    Isotropic/Orthotropic material, Young's modulus of elasticity, Poisson's ratio, etc.
  - Sections:

    Beam, Shell, Pipe, etc., if applicable.
  - Modelling:

    Setting up the model's geometry with keypoints, lines, areas, volumes, nodes.
  - Meshing

    Mesh attributes, fine/coarse mesh, triangles/quadrilaterals elements, etc.
- Solution
  - Analysis Type:

    Static, modal, eigen-buckling, etc.
  - Loads:

    Assigning structural loads such as displacement, force/moment, pressure, etc.
  - Constraints:

    Defining the model's boundary constraints by fixing displacements in one or more nodes.
  - Solving:

    Running the simulation.

- Postprocessing

  Processing and assessing the results, such as nodal displacements, elemental forces, deflection plots, stress diagrams etc.

Assessing the results is a critical point of a FE analysis as it could exploit weaknesses in the model, and proper correction would need to be applied. Therefore, enough time to thoroughly plan and execute the first versions of the analysis could reduce the back-and-forth required to adjust the model's parameters.

3.1.2 Modeling methodology

3.1.2.1 Analysis preference

This paragraph analyses the methodology followed for modeling the rectangular plate under examination. As mentioned in the first paragraphs, the study is based on the critical elastic buckling stresses of a plate. Specifically, in order to create the response surface using DoE techniques, the eigen-buckling problem for the uncorroded, the corroded and the repaired (with composite patch) metallic plate is solved multiple times. For the rest of the study, subscript 'm' denotes the metallic plate and 'c' the composite patch.

3.1.2.2 Element type

According to the above, the analyses are structural, while both static and eigen-buckling analyses are conducted to obtain the desired values. The problem being examined is a thin plate since $a_m/t_m >> 20$ is common in tankers and bulk carriers (Zhang [17]); hence, surface elements can be used for representing them in the numerical model. It should be noted that surface elements are also referred to as shell elements. There are two types of shell elements in ANSYS that can be used in this case:

- SHELL181:

  4-node structural shell with six DOFs at each node: translations in the x, y and z directions and rotations about the x, y and z axes.

- SHELL281:

  8-node structural shell with six DOFs at each node: translations in the x, y and z directions and rotations about the x, y and z axes.

Thus, the difference between the two elements is the number of nodes where the FEA calculations are performed. In **Figure 23**, SHELL181's nodes are denoted by I, J, K, L at its four corners, while SHELL281's nodes are I, J, K, L at its four corners and M, N, O, P mid-distance of the former nodes.

Both elements are suitable for thin to moderately thick shell structures such as a ship's lamina. Furthermore, they can be used for linear and non-linear applications, although only the former is of interest for this study. Finally, in addition to their applications, both are suitable for layered models such as composite shells, which will be used for the representation of the repaired plate.

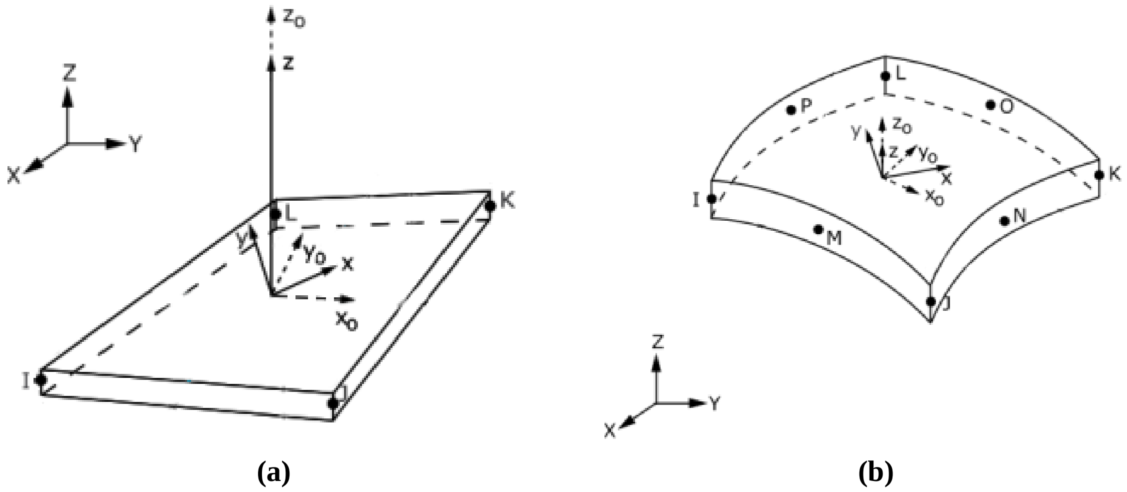

Figure 23. (a) SHELL181 4-node and (b) SHELL 281 8-node shell elements.

The shell elements are appointed to a defined geometrical area and assigned a cross-section, which could have multiple layers. Properties such as thickness, material, orientation, and a number of integration points throughout the thickness are set to each layer.

The Gauss integration theory defines the points where calculations for stress/strain are performed. Their position and weighing factor depend on the section's geometry and the number of integration points. For instance, in the case of quadrilaterals, a 2x2 or 3x3 point integration could be used, as shown in **Figure 24**.

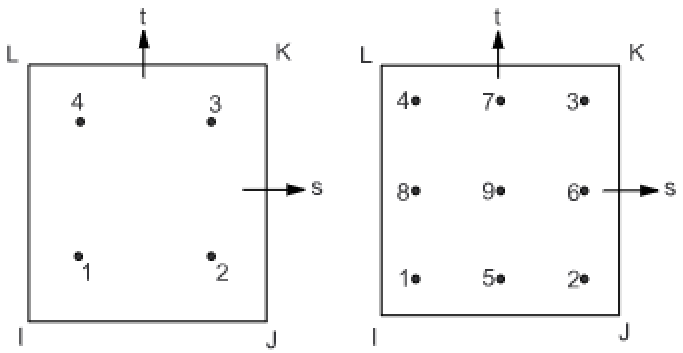

Figure 24. Integration point locations for quadrilaterals.

The element's loads can be either applied to nodes as nodal loading, areas as surface loads (per-unit-area), or lines as line pressure (per-unit-length). Positive pressures act into the element.

In order to assess the effectiveness of each shell element for the problem being examined, a mesh convergence test can be performed. The structure's mesh changes from coarse to fine during this process, while all other parameters remain constant – i.e., an OFAT (one-factor-at-a-time) analysis. The best option is the one that converges faster to the solution with a slight deviation. This technique is examined in paragraph 3.2.2.

Both uniform uni-axial compression and shear elastic buckling of the plate are studied. As mentioned above, the plate can be modelled using shell elements. However, although the former buckling case's boundary conditions can be applied directly, the latter's case requires large beams to approximate some boundary condition effects that are later explained. Thus, beam elements are also used in addition to the shell elements. The two available options for beam elements are BEAM188 and BEAM 189:

- BEAM188:

  2-node beam (linear, quadratic or cubic) with six or seven (optional) DOFs at each node: translations in the x, y and z directions, rotations about the x, y and z axes, and warping magnitude.

- BEAM189:

  3-node beam (quadratic) with six or seven (optional) DOFs at each node: translations in the x, y and z directions, rotations about the x, y and z axes, and warping magnitude.

The difference between the two elements is the number of nodes. In **Figure 25**, BEAM188 has its nodes denoted by I and J at the ends of the beam's line, while SHELL281's nodes are I and J at the endpoints and K mid-distance of the former nodes. In both cases, a node represented by K for BEAM188 and L for BEAM189, is used to define the element's orientation.

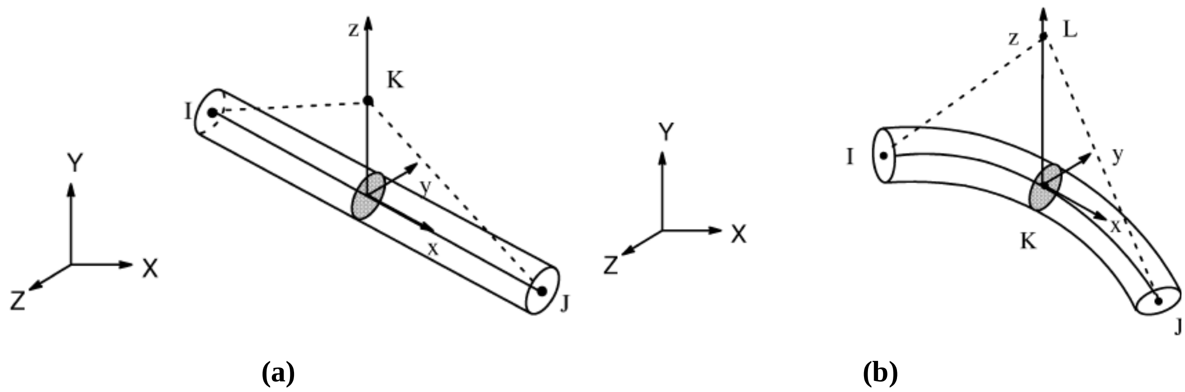

Figure 25. (a) BEAM188 2-node and (b) BEAM189 3-node beam elements.

Both elements are based on Timoshenko's beam theory which includes shear-deformation effects (cross-sections remain plane and undistorted after deformation). Therefore, they are suitable for analyzing slender to moderately thick beam structures. Similar to the case of the beams, a study is carried out where both the element type and mesh division are considered.

The BEAM elements are generated by appointing them to a defined line and assigning to them a section. The cross-section types can be imported from a standard library of sections from ANSYS, a generalized beam, a tapered beam or a pre-integrated composite beam cross-section. Each section is assumed to be an assembly of a predetermined number of 9 node cells, with each cell having four integration points (**Figure 26**).

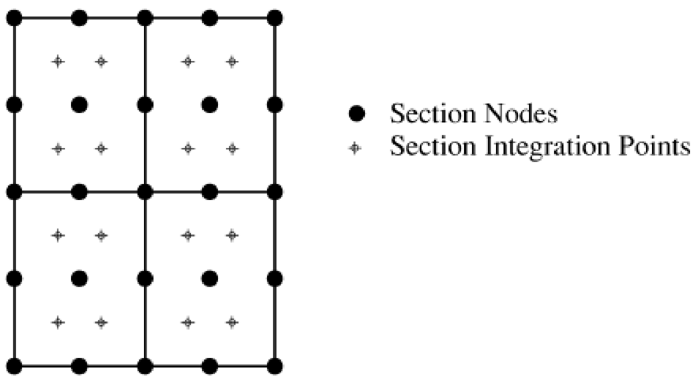

Figure 26. Section Model for BEAM element

The element uses the pre-calculated properties of the section at each element integration point across the length of the line assigned. At these same integration points, the strains and generalized stresses are evaluated and then extrapolated to the nodes of the element.

The element's loads can be either applied to nodes as nodal loading or to lines as lateral pressures (per unit length). Positive pressures act into the element.

3.1.2.3 Material properties

The materials used are marine grade structural steel and a fiber-reinforced composite patch. Regarding the latter, both CFRP and GFRP are under consideration and examined in paragraph 3.2.2 to conclude the most suitable option for the problem. The metal is considered an isotropic material, while the composite is an orthotropic one. The mechanical properties of each material are listed in **Table 1**.

3.1.2.4 Sections

As mentioned previously, two models are to be constructed: a metal plate and a metal plate with a composite patch. The former can be defined using single-layered shell elements. However, the latter is assigned multi-layered shell elements at the region where the composite patch is applied, while all other regions are single-layered. In each section, properties such as thickness, material, orientation and integration points are defined. The structure is modelled so that the local coordinate systems of each element are identical to each other, while the integration points used is 3 (default). The offset of the cross-section is so that the reference line of the local coordinate systems lies on the middle plane of the metallic plate. It should be noted that both local and global coordinate systems are aligned so that the x-axis is parallel to the plate's length, the y-axis to the plate's width and the z-axis to the plate's thickness.

3.1.2.5 Modeling

The problem being examined is a stiffened panel subjected to external loads. The purpose of the study is to investigate the plate's elastic buckling strength initially and after having lost material due to corrosion. Then a composite patch is applied to the center of the metal plate to rehabilitate its lost buckling capabilities.

In order to simplify the problem, the following assumption is made. Since the focus is the buckling strength of the plate positioned between large stiffeners, the plate could be isolated and considered simply supported across its four edges. Thus, the stiffeners are replaced by boundary conditions. Additionally, any external loads can be reduced to axial and shear forces on the plate's plane, assuming out-of-plane forces to be minimal. Hence, the loads transferred to the plate through the stiffeners could be either tensile, compressive or shear. However, only the two latter can cause buckling. The following buckling cases are examined:

- Uniform uniaxial compression buckling
- Shear buckling

In both cases, the geometry of the problem is the same, i.e., a rectangular metal plate with a composite patch installed at its center (**Figure 27**).

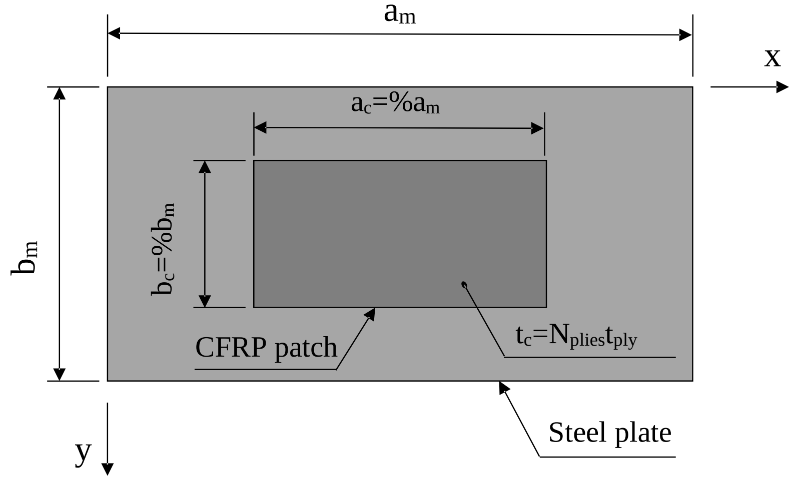

Figure 27. Design schematic of a rectangular composite patch applied to a metal plate.

3.1.2.6 Modeling of uni-compression buckling

As shown in **Figure 27** the geometry is symmetrical to the center of the plate with respect to both the xz plane and yz plane. In order to reduce calculation and modeling time, the quarter model could be used with symmetry conditions applied to its appropriate edges (**Figure 28**). Thus, simply supported conditions, i.e., $U_Z = 0$, are applied to the external edges, while $U_X = ROT_Y = ROT_Z = 0$ and $U_Y = ROT_X = ROT_Z = 0$ are applied to the internal transverse and longitudinal symmetry edges, respectively.

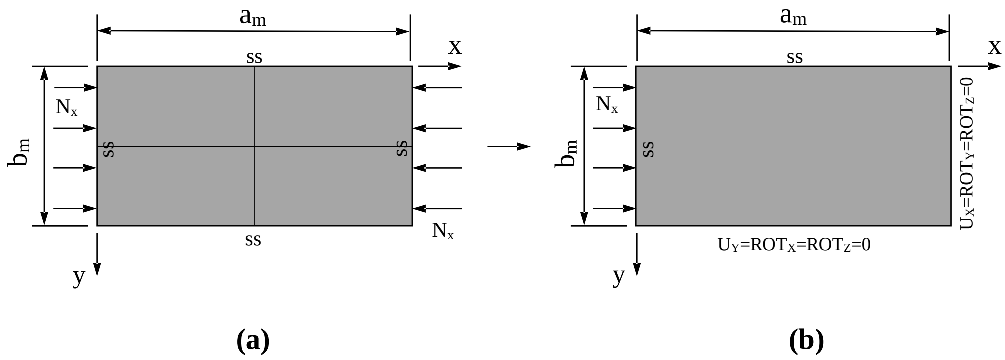

Figure 28. Two-dimensional sketch of the geometry's (a) full and (b) quarter model and its boundary conditions for the case of compressive buckling.

In the initial design, the plate is compressed by distributed forces across its short edges as shown in **Figure 28**. Since the quarter model is used, the distributed force is applied to the short edge it was initially applied to, while the stress distribution is carried out by means of symmetry. The values obtained from the analyses must be corrected according to Johnson-Ostenfeld's parabola for anelastic buckling (Hughes [15]).

3.1.2.7 Modeling of shear buckling

In contrast with the previous paragraph, the same modeling technique cannot be applied to the shear buckling problem. Although the geometry as shown in **Figure 27** is the same, the loading and boundary conditions are different. First of all, in this case the entire geometry is modeled (**Figure 29**a) and symmetry conditions are not utilized. The boundary conditions in effect is the restriction of all degrees of freedom at one of the short edges, i.e., clamping conditions. In the rest of the edges, large beams are modelled with substantial stiffness that allows the geometry to be considered a cantilever, thus having low bending effects (Anyfantis [2]). This way, the shear buckling effect is acquired with a good approximation.

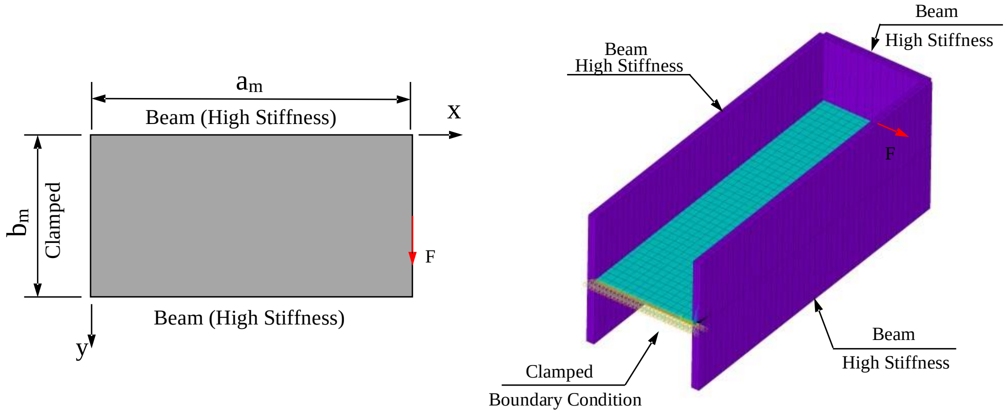

(a) **(b)**

Figure 29. (a) Two-dimensional sketch and (b) three-dimensional representation of the geometry's model and its boundary conditions for the case of shear buckling.

The load is applied to a pilot node at the free short edge's center, with a direction parallel to it. Due to the applied boundaries, a shear load is approximated across all edges of the plate. Thus, the critical buckling force $N_{xy,cr}$ is acquired by dividing the critical buckling force by the plate's thickness. The values obtained from the analyses must be corrected according to Johnson-Ostenfeld's parabola for anelastic buckling (Hughes [15]).

3.1.2.8 Solution

In both compressive and shear buckling, the problem being studied is a linear buckling analysis, while the desired output is the critical buckling stress/load. The former is the critical value of said failure where the structure becomes unstable and a deformation that is associated with a mode shape is produced. In order to obtain these results an eigenvalue buckling analysis that predicts the theoretical buckling strength of an ideal elastic structure (Euler buckling analysis) is performed.

Eigen-buckling analysis is valid solely for structural DOFs and the structure fails suddenly (at the buckling load value) with a horizontal force-deflection curve. Regarding the calculations, it is assumed that is has constant stiffness effects. This method requires a static analysis with prestress to have been conducted in advance, to calculate the stress stiffness matrix.

The eigenvalue and eigenvector extraction procedure follows the block Lanczos method and the first mode is extracted. The eigensolver is based on a block shifted Lanczos algorithm, which is a variation of the classic Lanczos algorithm, where the recursions are performed using a block of vectors instead of a single vector.

Hence, two solutions are performed in each simulation: a static structural with prestress and an eigenvalue buckling analysis.

3.2 DoE analysis

3.2.1 Theoretical background

DoE is the design of an experiment based on input parameters and using statistical tools to approximate the output as best as possible. Assume an experiment where the factors and desired response are determined. The latter is a result that can be measured for various factor combinations, and is the experiment's objective. A model that best represents the parameters and goals of the experiment is then built and run. During each run/simulation, a combination of factors that is predetermined is used and the result is measured. Then the collected data is fit to the assumed model, and a prediction is made for additional factor combinations based on the trends of the acquired data. During this stage, the effects that are most active are also highlighted and a conclusion about the contribution of each factor to the experiment's results can be made.

One basic example of a DoE method is an OFAT analysis, in which the output of an experiment is based on one factor at a time (as indicated by the title itself) without implementing possible interactions between input parameters. Another method used for this study's purposes is an RSM (response surface methodology), which is a two-level design. Specifically, two input design parameters are used to define the design space. A central composite design (CCD) then indicates the data points needed for the method to be performed. According to a face-centered CCD (CCF), three point types are used: factorial (shows two-factor interactions), center (shows curvature), and star (shows quadratic effects). At the points of the design space indicated by the CCD (**Figure 30**), the output is obtained from an experiment. Once these points are specified (known x_1, x_2, and y), a polynomial surface is best fit to them with the help of statistical tools for its lack-of-fit evaluation.

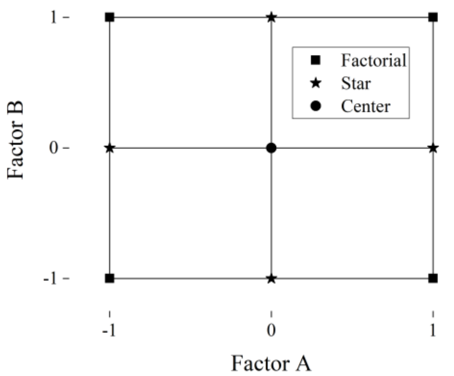

Figure 30. Design points indicated by a CCF.

3.2.2 Modeling methodology

In the case being studied, the design space consists of the patch's percentage coverage (denoted by c) and the number of plies (denoted by N_{plies}). After setting these values' range, their CCD points are configured at the three levels required, i.e., low level (−1), center (0), and high level (+1). Through numerical calculations using FEA, the experimental outputs for the data points are acquired. Then a quadratic polynomial equation of the form

$$y = a_0 + a_1x_1 + a_2x_2 + a_{11}x_1^2 + a_{12}x_1x_2 + a_{22}x_2^2 \qquad 3.4$$

is fit to these points to construct the response surface. In this case, x_1 is the percentage coverage c, x_2 is the number of plies N_{plies}, and y is the obtained FoS. This factor of safety is calculated as

$$\mathrm{FoS} = \frac{\sigma_{\mathrm{repaired}}}{\sigma_{\mathrm{intact}}} \quad \text{or} \quad \mathrm{FoS} = \frac{\tau_{\mathrm{repaired}}}{\tau_{\mathrm{intact}}} \qquad 3.5$$

Using the combination of the above methods (FEA and RSM), a list of acceptable design configurations for the requirements set by FoS, bondline fracture, and material yield is created. A significant advantage of this technique is that it does not require lab experiments for this preliminary design as long as the model is as accurate as possible.

4 Case Study

4.1 Problem setup

Paragraph 2.1 introduced the proposed guidelines for applying a composite patch to a corroded metallic plate as an alternative repair technique for elastic buckling. In order to understand the problem, paragraphs 2.2, 2.3 and 2.4 analyzed the mechanics and necessary theoretical background. The methods used for the simulations and analyses of the study are based on FEM and DoE, which are explained in paragraphs 3.1 and 3.2 respectively. In order to showcase the proposed methodology, a case study is conducted based on the theory and techniques analyzed in the paragraphs mentioned above.

The object of interest is a marine structure, which could be a ship, a submarine, or even an offshore. In order to keep the problem simple, assume a survey is conducted on a commercial ship that is not newly built. During visual inspections corrosion is detected on a girder of the double bottom which requires further examination. Thus, the plate's thickness is measured, indicating that the material wastage equals a 5% reduction of its initial thickness. After further assessing the defect and the damaged area according to the proposed flowchart in **Figure 6**, the Classification Society approves the application of a composite patch to rehabilitate the plate's initial buckling strength capabilities. The plate's dimensions and damage are listed in **Table 5**. After the repair, the plate shall have restored its buckling strength with a FoS equal to 1.0, i.e., its initial value.

Table 5. Metallic damaged plate's properties.

Plate's Property	Symbol	Value	Unit
Material	-	Grade 'AH32' Steel	-
Length	a_m	2250	mm
Width	b_m	900	mm
Intact thickness	$t_{m,intact}$	20	mm
Corrosion	-	5	%
Corroded thickness	$t_{m,corroded}$	19	mm
FoS requirement	FoS_{req}	1.0	-

The patch's properties under consideration are its material, its configuration, and its shape (as shown in the flowchart in **Figure 6**). In order to obtain the optimal combination, OFAT analyses are conducted. The parameters that are listed in **Table 6** are examined against an increasing value of the number of plies and evaluated using the obtained FoS. However, before initiating any analysis, the element properties for the numerical calculations shall be defined. Specifically, mesh convergence tests for four- and eight-node elements were conducted for the compression and shear model containing only the intact metal plate. The results are illustrated in **Figure 31** where the element size is plotted with respect to the percentage deviation of the obtained buckling stress from the one obtained by the minimum allowed size of 20 mm. The graphs indicate that the eight-node elements, combined with a mesh size of 100 mm, provide sufficient accuracy, with less than 0.2% deviation from the converged value.

Table 6. Patch's properties evaluated through OFAT analyses.

Patch's Property	Options	x	y
Material	CFRP/GFRP		
Configuration	One-Sided/Two-Sided	No. Plies	FoS
Shape	Rectangular/Ellipsoid/Octagonal		

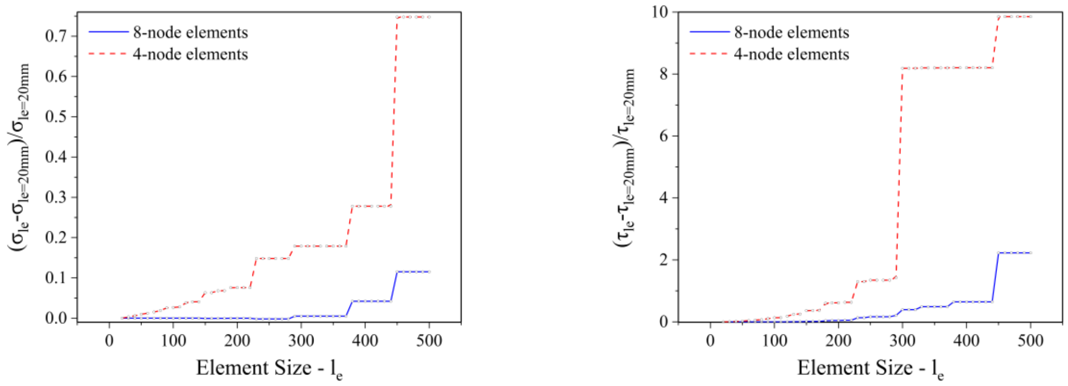

Figure 31. Mesh convergence test for the (a) compression and (b) shear buckling model.

Two OFAT analyses were performed: one for defining the patch's material and configuration and another for the shape. The former analysis uses a rectangular patch as a typical shape, while the coverage percentage is 75%. The results are shown in **Figure 32**, where it can be concluded that the CFRP is a better acting material than the GFRP. Additionally, the one-sided patch has faster buckling restoration capabilities against compression, while the two-sided has a similar effect against shear. However, the one-sided CFRP patch is chosen as the most effective since it restores the buckling capacity for a similar number of plies in both compression and shear.

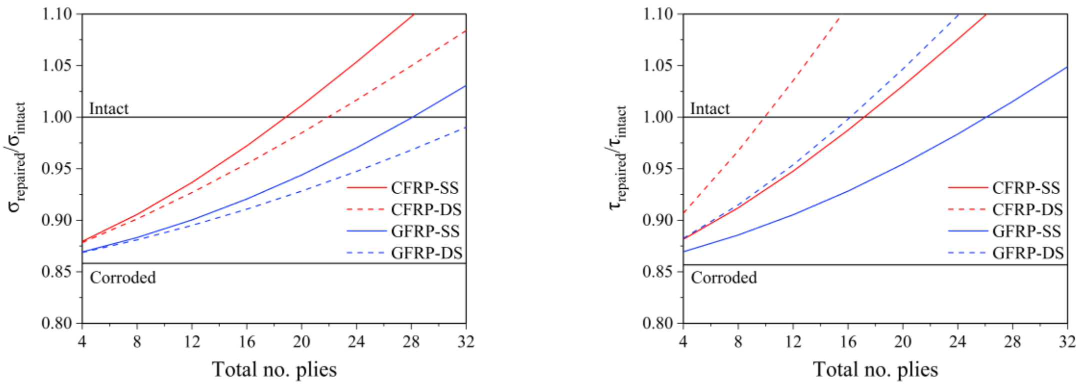

Figure 32. OFAT analysis for determining the repair's optimal combination of material and configuration (SS: single strap, DS: double strap) for the (a) compression and (b) shear buckling model.

Afterward, using these findings, the possible shapes (**Figure 2**) were tested against each other. These analyses were carried out on the compression model, and similar results were assumed for the shear equivalent. The shape with the better rehabilitation performance is the rectangular patch (**Figure 33**).

Thus, the optimal option for restoring the corroded plate's buckling capabilities is a one-sided CFRP rectangular patch.

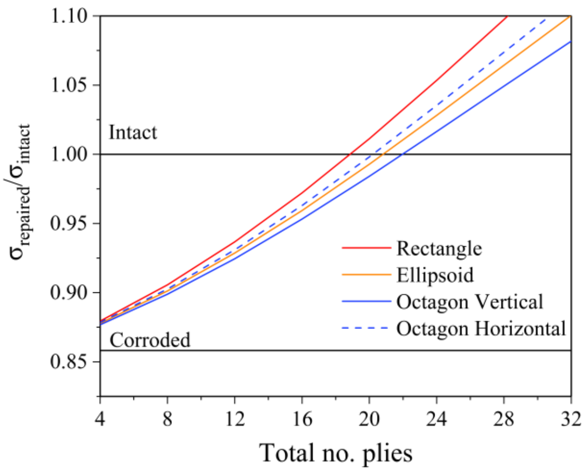

Figure 33. OFAT analysis for determining the repair's optimal shape (compression model).

4.2 Analysis results

In order to perform the RSM, the CCD points, and consequently the design space, must be defined. The two design parameters, i.e., the patch's coverage c and the number of plies N_{plies}, are allowed to take values inside the range specified in **Table 7** between the low and high-level indications. The same table specifies the design points using the CCD design space (**Figure 30**). It should be noted that each ply's thickness is equal to 0.33125 mm (Karatzas [3]).

Table 7. CCD design points.

Factor	Name	Low Level (−)	Center (0)	High Level (+)
x_1	Coverage (c)	40%	70%	100%
x_2	No. Plies (N_{plies})	4	18	32

Using the design points, numerical calculations were conducted, and the resultant stresses were corrected for anelastic buckling, if applicable. By fitting a polynomial as expressed in Equation 10, the resultant response surfaces for the compressive (Equation 4.1) and shear (Equation 4.2) buckling problem are defined by:

$$\mathrm{FoS} = 0.97689 - 0.01555c - 0.00138N_{plies} + 0.00752c^2 + 0.00454cN_{plies} + 5.46826e-06\ N_{plies}^{\ 2} \qquad 4.1$$

$$\mathrm{FoS} = 0.99021 + 0.01289c - 3.39234e-4N_{plies} - 0.0098c^2 + 0.00107cN_{plies} - 8.26793e-07\ N_{plies}^{\ 2} \qquad 4.2$$

These response surfaces are illustrated in **Figure 34**a,b, where both the experimental points obtained by the numerical calculations and the predicted points are plotted. Additionally, the FoS requirement is also visible on the surface as a curve. Any design parameters combination with a generated FoS below the indicated requirement curve is not acceptable. In **Figure 35**a,b, the same surfaces are plotted as a 2D contour for better visualizing the acceptable combinations.

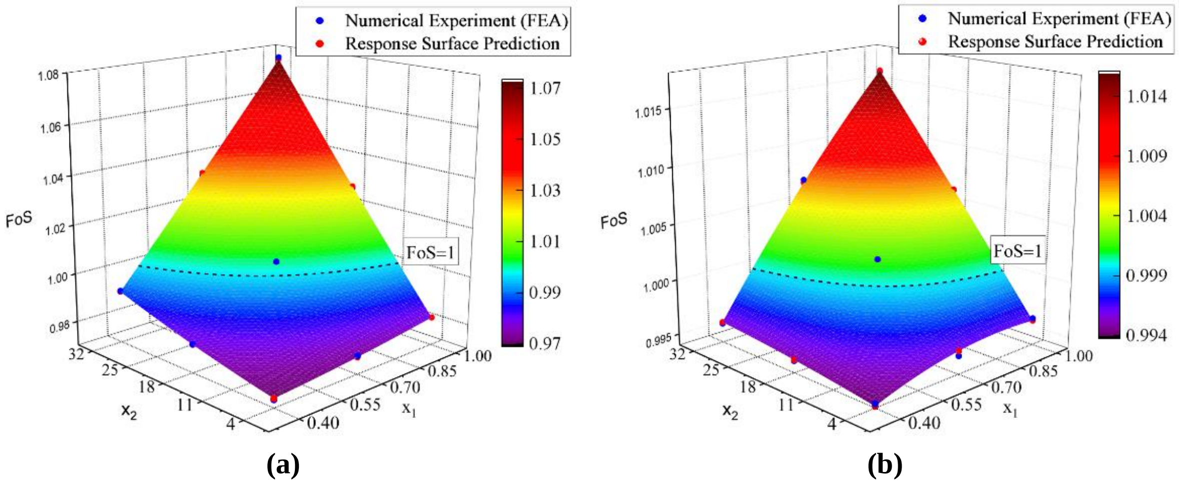

Figure 34. Generated response surface from a polynomial fit to the CCD data points for (a) compressive and (b) shear buckling.

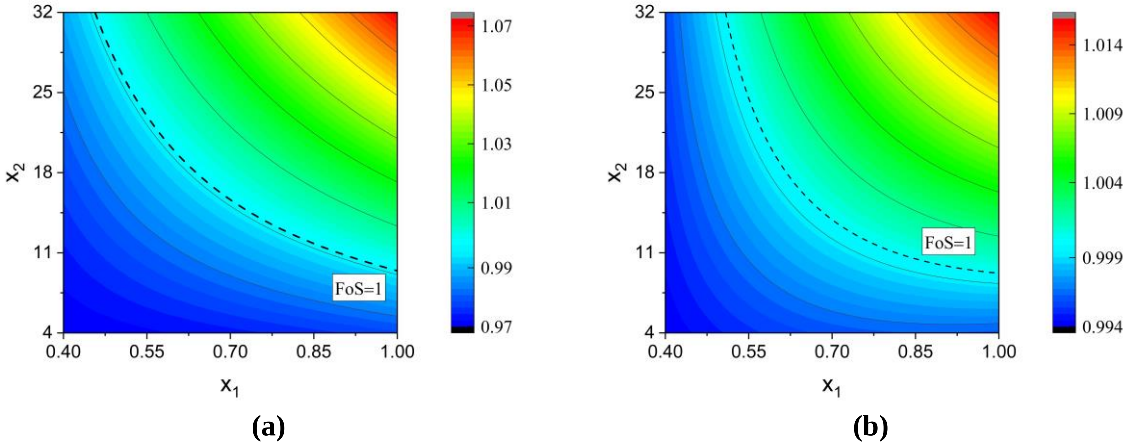

Figure 35. 2D contour plot of the generated response surface for (a) compressive and (b) shear buckling.

The fitted surfaces are evaluated using statistical tools, such as a histogram and a normal probability plot, using the percentage deviation between calculated and predicted values as indicators. The data points used were the CCD design points with the addition of mid-points to further assess the surface's lack of fit (evaluation points). A list of all points used for the method's validation is shown in **Table 8**. The calculated R-squared value for both surfaces is greater than 0.99, which exhibits a 99% fit. The percentage deviations were plotted in histograms (**Figure 36**a,b) and normal probability plots (**Figure 37**a,b), concluding that the prediction model follows a normal distribution and lacks significant statistical noise.

Table 8. Design and evaluation points used in the response surface.

Factor	Name	D + E[1]	E[2]	D + E[1]	E[2]	D + E[1]
x_1	Coverage (c)	40%	55%	70%	85%	100%
x_2	No. Plies (N_{plies})	4	11	18	25	32

[1]Design and evaluation point, [2]Evaluation point

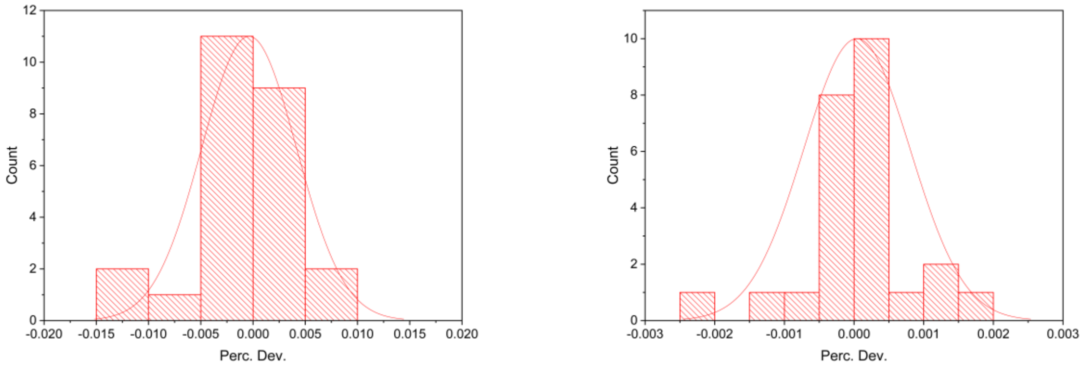

(a) **(b)**

Figure 36. Histogram of the percentage deviation between experimental and predicted values for (a) compressive and (b) shear buckling.

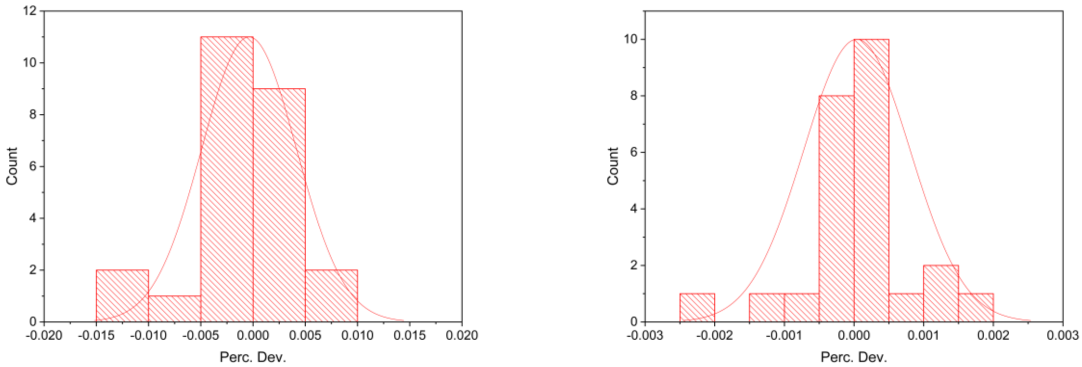

(a) **(b)**

Figure 37. Normal probability plot, with 95% confidence levels, of the percentage deviation between experimental and predicted values for (a) compressive and (b) shear buckling.

The acceptable design combinations are those that satisfy the FoS requirement for both compressive and shear buckling, as shown in Figure 17a,b respectively.

Having restricted the acceptable design combinations using the FoS requirements, the bondline is also checked. The maximum strain energy release rate from the surface's data points is equal to 0.185 N/mm and 0.085 N/mm for the compressive and shear problem respectively. The combination in which these values occur corresponds to [c, Nplies] = [1, 32] for both models, outputting FoS~1.08 and FoS~1.02 respectively. According to Lee [18], the resistance release rate for Mode-1 dominant conditions is equal to approximately 0.33 N/mm. Thus, since the acquired G is less than G_C, the bondline does not fail under Mode-1 failure conditions. It should be noted that Mode-1 dominant fracture was used since it is most probable of occurring than its Mode-2 equivalent, although further mixed-mode requirements could be used if requested.

Finally, the maximum normal stresses developed on the composite patch are equal to 297.6 MPa and 128 MPa for the compression and shear model respectively. Both values are less than the fracture stress and correspond to the combination [c, Nplies] = [0.7, 32] for both models, outputting FoS~1.03 and FoS~1.01 respectively.

It should be noted that partial safety factors for the assessment of the bondline and composite strength can be defined in addition to the primary FoS for the buckling restoration. These safety margins can be respectively defined as

$$\mathrm{FoS}_{\mathrm{bondline}} = \frac{\mathrm{G_C}}{\mathrm{G_{acting,max}}} \tag{4.3}$$

$$\mathrm{FoS}_{\mathrm{fracture}} = \frac{\sigma_{\mathrm{fracture}}}{\sigma_{\mathrm{acting,max}}} \tag{4.4}$$

The safety factors obtained from this case study for the compressive buckling are $FoS_{bondline} = 1.78$ and $FoS_{fracture} = 1.18$, and for the shear buckling $FoS_{bondline} = 3.87$ and $FoS_{fracture} = 2.75$. If additional requirements for $FoS_{bondline} = 2$ or $FoS_{fracture} = 1.4$ were applied, then although the analysis showed adequate buckling restoration, some solutions would not be acceptable under the above evaluation criteria.

5 Concluding Remarks

This study examined the case of material wastage due to corrosion and the risks of buckling it could potentially lead to in the case of a stiffened panel. This is a known problem in marine structures and IACS as well as Classification Societies have issued guidelines to identify the defect at an early stage and treatment techniques depending on the damage's state. In this study, the alternative repair method of composite patches was proposed, which has been acknowledged by entities in the maritime industry such as BV. The objective was to present the theoretical background of the plate's and patch's mechanics that could restore the structure's initial buckling strength, and demonstrate its results through a numerical application. For this reason, tools such as FEM and DoE were introduced to aid in in providing fast and accurate results, as well as developing a design space for the repair. The numerical and statistical analyses proved that such a repair practice is capable of rehabilitating the buckling capacity of a corroded marine plate against compressive and shear loads. The guidelines proposed also show good design practices that could be applied in a real-world scenario.

However, assumptions were made in order to minimize the problem's multiparametric nature. For example the modeling of the structure was simple, possibly disregarding some local imperfections and/or being unable to capture some stress distributions. Thus, the proposed methodology should be further explored, introducing all necessary parameters for the simulations to be as accurate to reality as possible. For instance, the geometry and the adhesive could be modeled with solid elements to examine the components as separate entities from the rest of the assembly. Furthermore, since the linear analysis basis leads to over-engineering of the problem, since the post-buckling effect is ignored, a non-linear analysis should be performed to identify this effect. Thus, the proposed methodology would be enriched, and the model would more accurately represent reality.

Finally, it should be highlighted that the application of the aforementioned improvements does not negate the need for real-world testing. There are several parameters in the problem's environment whose effect would be better understood in laboratory experiments. For example, installation and operating conditions should be accounted for since they also dictate the structural response of the repaired plate under examination. Hence, the next step after developing the analyses should be laboratory testing and employment of the method to existing damages dealt on marine structures. Only after years of monitoring the effects of the repair methodology will the concluding remarks be set, and perhaps will the technique be established as a proposed repair for primary and non-primary supporting members.

References

1. IACS. Guidelines for Surveys, Assessment and Repair of Hull Structures—Container Ships, Rev.1; Witherbys Publishing: Living-stone, UK, 2018.

2. Anyfantis, K.N. Preliminary design assessment of an alternative repair method for corroded shear panels in ship hull structures. Ocean Eng. 2019, 188, 106323.

3. Karatzas, V.A. Assessment and Design of Composite Patch Repairing in Marine Applications. Ph.D. Thesis, National Technical University of Athens, Athens, Greece, 2016.

4. Karatzas, V.A.; Kotsidis, E.A.; Tsouvalis, N.G. Experimental fatigue study of composite patch repaired steel plates with cracks. Appl. Compos. Mater. 2015, 22, 507–523.

5. Hashim, S.; Berggreen, C.; Tsouvalis, N.; McGeorge, D.; Chirica, I.; Moore, P.; Boyd, S.; Nisar, J.; Anyfantis, K.; Misirlis, K.; et al. Fabrication, testing and analysis of steel/composite DLS adhesive joints. Ships Offshore Struct. 2011, 6, 115–126.

6. Aabid, A.; Hrairi, M.; Mohamed Ali, J.S. Optimization of composite patch repair for center-cracked rectangular plate using design of experiments method. Mater. Today Proc. 2020, 27, 1713–1719.

7. Turan, K. Buckling behavior of adhesively patch-repaired composite plates. J. Compos. Mater. 2013, 48, 3253–3261.

8. BV. Adhesive Joints and Patch Repair; Guidance Note NI613DTR00E; BV: Neuilly sur Seine Cedex, France, 2015.

9. DNV. Design, Fabrication, Operation and Qualification of Bonded Repair of Steel Structures; Recommended Practice DNVGL-RP-C301; DNV: Belum, Norwegen, 2015.

10. ASME. Repair of Pressure Equipment and Piping; ASME PCC-2-2011; The American Society of Mechanical Engineers: New York, NY, USA, 2011.

11. Lloyd’s Register. Rules and Regulations for the Classification of Ships; Lloyd’s Register: London, UK, 2016.

12. IACS. Common Structural Rules for Bulk Carriers and Oil Tankers; 2021

13. Kollar, L.; Springer, G. Mechanics of Composite Structures; Cambridge University Press: Cambridge, UK, 2003.

14. Timoshenko, S.; Gere, J. Theory of elastic stability, International Student Edition, 2nd edition; McGraw-Hill: New York, NY, USA, 1985.

15. Hughes, O.; Paik, J. Ship Structural Analysis and Design; SNAME: Jersey City, New Jersey, USA, 2010.

16. Anyfantis, K.; Stavropoulos, P.; Chryssolouris, G. Fracture Mechanics Based Assessment of Manufacturing Defects Laying at the Edge of CFRP-Metal Bondlines; CrossMark: Plano, TX, USA, 2018.

17. Zhang, S. A review and study on ultimate strength of steel plates and stiffened panels in axial compression. Ships Offshore Struct. 2016, 11, 81–91.

18. Lee, M.J.; Kim, W.S.; Jang, C.J.; Kim, K.H.; Cho, T.M.; Lee, B.C.; Lee, J.J. Analysis and Simulation of the Failure Characteristic of a Single Leg Bending Joint with a Micro-Patterned Surface. J. Adhes. 2011, 87, 826–841.

Appendix

applied mechanics

Article

Buckling Strength Assessment of Composite Patch Repair Used for the Rehabilitation of Corroded Marine Plates

Nikos Kallitsis and Konstantinos N. Anyfantis *

Shipbuilding Technology Laboratory, School of Naval Architecture and Marine Engineering, National Technical University of Athens, Zografos, 15780 Athens, Greece; nkallitsis@outlook.com
* Correspondence: kanyf@naval.ntua.gr; Tel.: +30-210-772-1325

Abstract: A common form of damage encountered in marine structures is the accumulation of corrosion in susceptible areas, which leads to material wastage. As a result, the structural strength of the members affected is compromised, endangering their safe operation in design loads. Consequently, structural instabilities may occur, such as buckling due to compressive or/and shear loads. An alternative repair practice for preventing such phenomena, approved for secondary load-carrying members, is the application of composite patches to the damaged area. In this preliminary study, this technique is examined in the scope of developing a framework that can be used to find the optimal solution for restoring the buckling strength of a corroded plate. The methods used to achieve this are based on finite element analysis (FEA) and design of experiments (DoE) to statistically analyze the aforementioned numerical calculations. By introducing the composite patch's percentage coverage of its metal substrate and number of plies as design parameters, a response surface is generated with respect to the obtained factor of safety (regarding its reference uncorroded buckling strength). This list of data points is then evaluated, and an acceptable surface/list of design parameters' combinations is generated.

Keywords: finite element analysis; composite; patch repair; buckling; corrosion; design of experiments; marine; structural analysis; response surface methodology

Citation: Kallitsis, N.; Anyfantis, K.N. Buckling Strength Assessment of Composite Patch Repair Used for the Rehabilitation of Corroded Marine Plates. *Appl. Mech.* **2021**, *2*, 482–500. https://doi.org/10.3390/applmech2030027

Received: 1 July 2021
Accepted: 17 July 2021
Published: 20 July 2021

1. Introduction

When designing a structure, adequate strength reserves against probable loads are provided, considering the operating environmental conditions. Regarding marine structures, offshore platforms and ships are designed to function predominantly in the sea for the majority of their intended life, which is a minimum of 25 years. In this timeline, multiple surveys are conducted to ensure smooth and safe operation, with a frequency usually dependent on the structure's age (preventive maintenance). During these surveys, a common form of damage that the International Association of Classification Societies (IACS) has highlighted is material wastage caused by corrosion.

As noted by IACS [1], there are three types of corrosion: general (usually occurs uniformly on uncoated surfaces), grooving (primarily located in the heat-affected zone), and pitting (due to local coating breakdown). In order to protect against such defects from developing, coating, and other protective measures (e.g., sacrificial anodes) are employed. Some areas are known to be susceptible to this phenomenon due to:

- Water, scale, dirt, or oil remainings due to poor drainage or design flaw.
- High stresses applied to the subject area.
- Coating breakdown usually caused by poor maintenance and the ship's age.
- Operation in a corrosive enabling environment, such as near high-temperature regions (e.g., heated fuel tanks).

Material wastage is primarily identified in two ways: visually or from thickness measurements. The latter is performed in areas known to be susceptible to corrosion or to measure the defect's magnitude. Examples of such suspect areas are the double bottom, the transverse bulkheads (Figure 1), the tank top, and spaces adjacent to the hot engine room (IACS [1]).

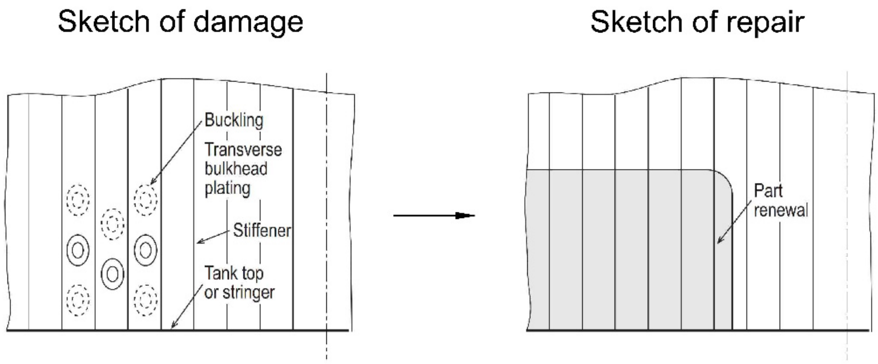

Figure 1. IACS [1] recommended repair practice for buckling caused to a part of a transverse bulkhead (in cargo hold region) possibly caused by heavy general corrosion.

Corrosion leads to material thickness wastage, which can cause underperformance of the load-bearing capabilities of the structural element at hand. For instance, a transverse plating could succumb to shear buckling and a double bottom plating to compressive buckling. Other unwanted results that may occur are crack initiations or material yielding. In order to prevent such structural failures, IACS [1] has developed repair guidelines in which the above concerns are addressed. In case a plate is at buckling risk (or has slightly buckled), common practice is cropping and renewal (with equal or greater thickness than the original), adding an insert plate of increased thickness, or reinforcing the area with additional stiffeners. All these options are hot-working operations, which means that proper preparation of the affected area should be performed, e.g., scrubbing and degassing. This is extremely important in areas inside or adjacent to flammable environments (e.g., repairing a ballast tank's plating neighboring with the cargo tank). In offshore platforms, in addition to the area's preparation, its operation might need to pause during hot work.

Alternative repair techniques have been considered in order to address this problem. A method that has gained attraction over the years is the application of composites to repair or prevent defects that could arise from crack initiation/propagation or material wastage. These fiber-reinforced composites could form stiffeners (Anyfantis [2]) or patches (Karatzas [3]) in order to reinforce the affected area and prevent buckling due to shear or/and compressive loads. Additionally, a similar methodology can be applied to repair cracks in metallic laminates (Karatzas et al. [4]). This topic has also gained the interest of several Classification Societies, such as Bureau Veritas (BV [5]) and Det Norske Veritas (DNV [6]), that propose fiber-reinforced patches to rehabilitate the structural integrity of damaged metallic structures. The American Society of Mechanical Engineers (ASME [7]) has also issued standards for assessing composite patches to repair pipelines. Additionally, the topic of composite patches has also been examined by several EU projects such as Marstruct, Copatch and Ramsses. However, despite interest in the topic (Hashim et al. [8], Aabid et al. [9], Turan [10]), the method has yet to be approved by the International Maritime Organization (IMO) as a valid repair technique for primary supporting members, despite other industries, such as aeronautics, having assessed it as an acceptable practice. The delay in the marine industry is due to the method's limited applications, lack of on-site service reports, and other factors concerning the composite's rehabilitation properties—e.g., repair life, the criticality of the defect. Therefore, composite repairs are usually applicable in a case-by-case scenario approved by the Classification Societies for the repair of (usually) non-primary supporting members.

This preliminary study proposes a methodology for the short- or mid-term rehabilitation of corroded marine plates using composite patches to prevent premature buckling. Specifically, the goal is the restoration of the initial elastic compressive and shear buckling strength of a uniformly corroded plate. In order to achieve this, multiple parameters need to be considered based on design and structural criteria. Additionally, buckling calculations are performed with the assistance of computational and statistical mechanics arising from finite element analysis (FEA) and design of experiments (DoE). These tools allow for a preliminary assessment of the proposed methodology without the need for laboratory experiments or extensive computation work. The study's main purpose is to set up a framework that can be used to choose the optimal design solution for the investigated defect.

2. Design Basis

Marine structures are composed of large metal plates reinforced with stiffeners (most common are bulb profiles, L, T profiles, and flat bars). The material used for both plates and stiffeners is usually marine-grade structural steel and specifically mild steel type "A" or higher tensile steel type "AH32" (LR [11]). The applied loads are undertaken by the combined action of beams and plates (stiffened panels). Thus, each rectangular plate between stiffeners can be assumed as isolated and simply supported (worst case scenario), while its boundary beams transfer active loads to it. A schematic of a bulk carrier's cargo hold compartmentation and some supporting members is shown in Figure 2.

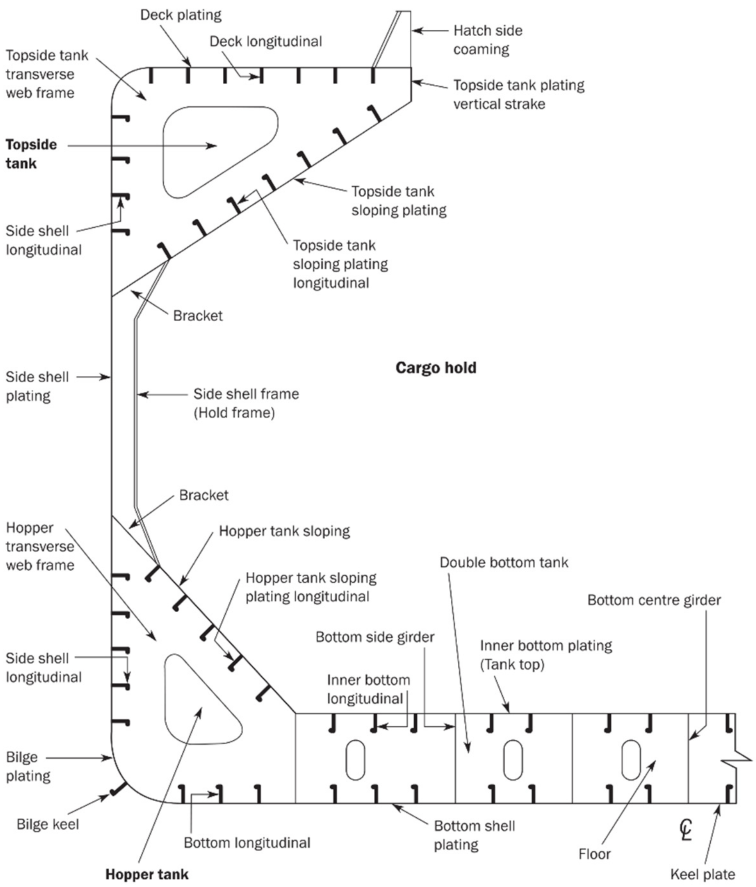

Figure 2. Schematic of a cargo hold's compartments and supporting members (Common Structural Rules for Bulk Carriers and Oil Tankers, January 2019).

As aforementioned, if a plate is corroded, then its effective thickness is reduced. By subtracting material from it, its load-bearing capabilities are lessened due to a weaker cross-section. The structural member's cross-section can be stiffened by adding a fiber-reinforced composite patch, which rehabilitates for the material wastage. However, there are a plethora of configurations for the patch that can be applied due to multiple design parameters. The important ones are the fiber's material, the matrix's material, the laminate's stacking sequence, the number of plies used, the patch's basic dimensions, the repair's configuration (one or two-sided), and the shape. Finally, several other factors affect the final product: humidity, temperature, curing conditions, the adhesive used, and the application method (hand lay-up, pre-preg, or vacuum infusion), the effect of which is out-of-scope.

Some assumptions are made in order to scale down the multi-parametrical nature of the problem. Let the environmental conditions be optimal for the application and curing of the composite patch. This might not be achievable on ship, but satisfactory conditions can be obtained through proper preparations of the working space. Additionally, perfect bonding is assumed for the adhesion of the composite patch with the metal substrate. This can be enforced without significant deviation from the study's main goal, which is to develop guidelines for the repair method proposed.

The patch's properties are also essential since its structural properties are based on its configuration. The proposed patch is a plain weave (cross-ply) fiber-reinforced polymer with a stacking sequence of $[0/90]_n$. Since the fibers' orientation within the matrix is in two perpendicular directions (bi-directional), the composite can be characterized as orthotropic (Kollar [12]). The patches usually used in the industry are carbon fiber reinforced polymers (CFRP), and glass fiber reinforced polymers (GFRP), whose mechanical properties are listed in Table 1.

Table 1. Material properties for steel, CFRP, and GFRP.

Property	Steel Grade 'AH32' [1]	CFRP [2,3]	GFRP [3]
Young's modulus of elasticity	206 GPa	42.95 GPa	213.4 GPa
Poisson's ratio	0.3	0.3	0.3
Yield/Fracture Stress	315 MPa	352 MPa	549 MPa

[1] LR [11], [2] Karatzas [3], [3] Kollar [12]. The composites' application method is assumed to be vacuum infusion and the matrix is epoxy-resin based.

Finally, the repair's configuration is important as well. Specifically, the patch's main dimensions (length, width, thickness) are the most influential to the rehabilitation's effect since the more material is added, the higher the obtained stiffness. The length and width cannot surpass those of the metal substrate's. Its thickness is dependent on the number of plies since it is a product of each ply's thickness and the number of plies used. Additionally, the patch's shape can also have many forms, such as rectangular, ellipsoid, and octagonal (Figure 3), some of which might be more difficult to manufacture than others. The shape's effects are more important for the adhesion problem and the local stresses developed at its boundaries. However, its effect on buckling restoration is examined in this study. Finally, the patch can be applied to one side of the metal plate or on both of its sides (Figure 4). This particular application is dependent on surrounding equipment, and the feasibility of application on both sides since access to an area might not be possible. It should be noted that in the case of the one-sided patch, a secondary bending moment arises, which should also be taken into account when designing the solution as it asymmetrically loads the structure.

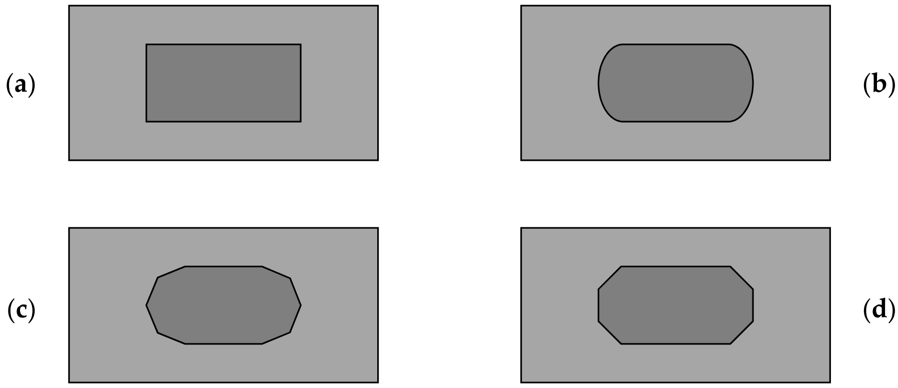

Figure 3. Possible shape forms that the repair patch can have: (**a**) rectangular, (**b**) ellipsoid, (**c**) octagonal horizontal, (**d**) octagonal vertical.

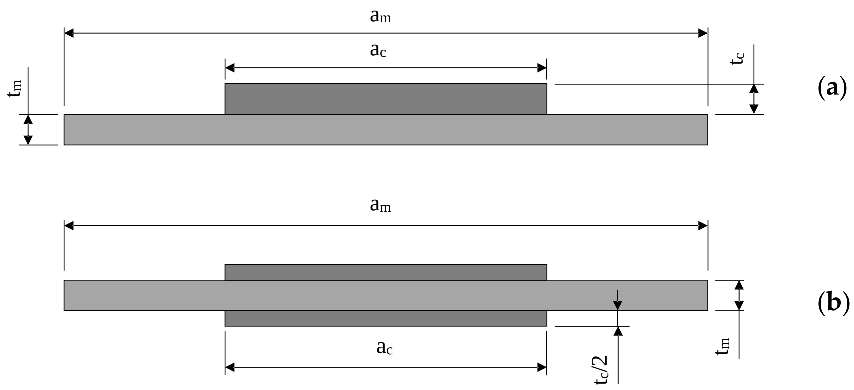

Figure 4. Possible patch configurations: (**a**) one-sided application (single strap joint) and (**b**) two-sided application (double strap joint).

3. Optimal Design Method

3.1. Design of the Repair

As mentioned in the introduction, during a marine structure's lifetime, several surveys are conducted within the framework of preventive maintenance. During these surveys, its members' structural condition is inspected to verify their safe operation until the next planned survey or to notify that repair action is needed otherwise. Depending on a case-by-case basis, a repair might be performed while traveling, harboring, or during dry-dock. Usually, smaller-scale operations in an enclosed and accessible space can be conducted while in sea (e.g., tank top, ballast tank), while larger intrusive installations necessitate the need for the ship to be on land (e.g., large composite patch on the upper deck, transverse bulkhead).

Assume that corrosion is detected during a plate's inspection and the thickness measurements indicate that the magnitude of material lost sets the structural member at buckling risk if left untreated. Based on recommended practices currently applied in the shipbuilding industry (DNV [6]), if the member is structurally critical, traditional repair methods are used. Additionally, the same repair methods are applied if the defect's scale is large, and a composite patch would not provide adequate strength. However, if these previous statements do not apply, a composite patch repair could be installed. The decision-making points from the defect detection to the repair method's application are illustrated in the flowchart in Figure 5.

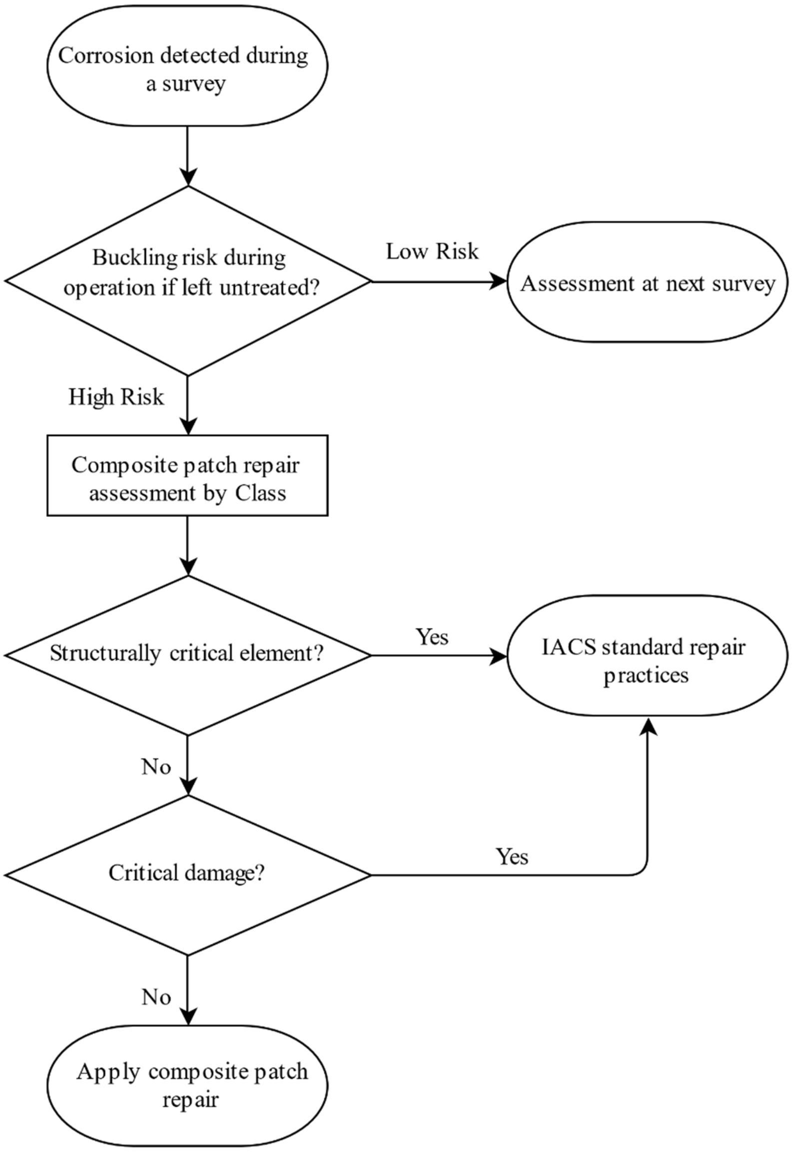

Figure 5. Flowchart illustrating the decision points from the defect detection to the approved repair method.

In case the composite repair technique is possible, the patch's material, configuration (one or double-sided), and shape shall be decided. If there is no preference, then the optimal options can be determined through one-factor-at-a-time (OFAT) analyses. Through these analyses, a design parameter is examined, while all other factors remain fixed. This analysis methodology is followed due to the discrete nature of these parameters—e.g., the patch's material and configuration is a binary decision—while the shape has four choices as shown later in the study. After setting these parameters, the patch's main dimensions must be assigned (design parameters). In order to minimize the problem's complexity, the patch is assumed to have an aspect ratio α_c equal to that of the metal substrate α_m. Thus, the composite's length a_c and width b_c are a product of the plate's respective values (a_m and b_m) and its aspect ratio, i.e., $a_c/b_c = \alpha_c = \alpha_m = a_m/b_m$. Hence, let these two parameters be replaced by a percentage coverage of the substrate (denoted by c). As a result the following expressions are obtained: $c = a_c/a_m = b_c/b_m$.

The final parameter is the patch's thickness, which can also be replaced by its driving magnitude, i.e., the number of plies (N_{plies}). Having set the coverage's and plies' allowable value range, a DoE statistical analysis is conducted with an additional parameter, the attainable factor of safety (FoS). This last value is calculated using elastic buckling analyses on the data points set by DoE in order to construct a response surface through a response surface methodology (RSM). The final product is a fitted surface (points) that indicates the FoS obtained for various combinations of the patch's coverage and the number of plies.

For specified values of FoS, respective to the initial buckling strength, the generated surface indicates the allowable combinations of the patch's design parameters. In order to further validate the method, a fracture check on the patch and the bondline is also conducted. This might result in a possible restriction of the permissible solutions provided by the response surface. This design methodology is visualized in the flowchart shown in Figure 6.

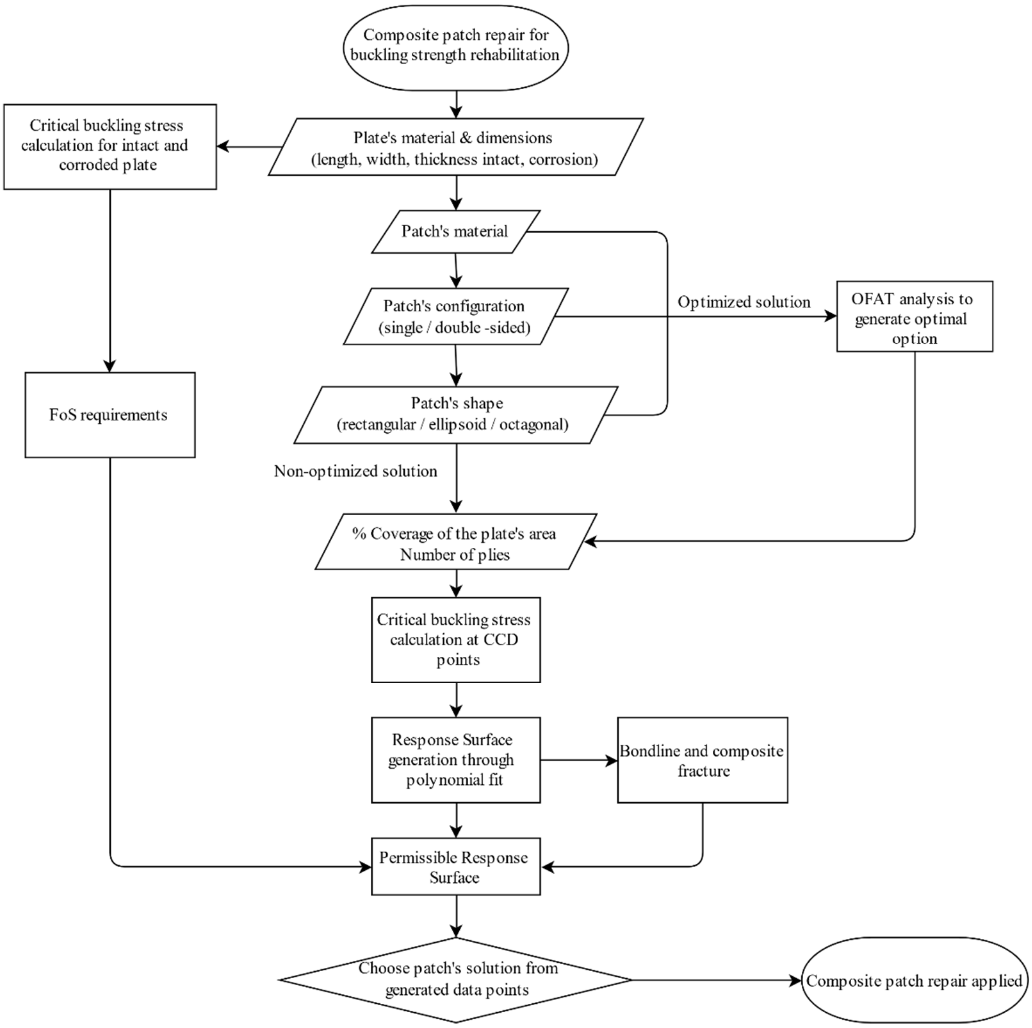

Figure 6. Flowchart of the proposed preliminary design methodology.

3.2. Theoretical Background

Marine stiffened panels are subjected to external loads applied to their middle plane, such as compressive and shear forces. In its initial state, a panel of length a_m, width b_m, and thickness t_m, is in a flatform equilibrium. However, by gradually increasing the applied load, the middle plane becomes unstable and starts to buckle. Moreover, as mentioned in the second section, due to the stiffening system, a plate between stiffeners can be assumed to be simply supported across its edges. By using the energy method, as proposed by Timoshenko [13], the critical elastic buckling stress due to uniform uniaxial compression is calculated as

$$\sigma_{E,cr} = \frac{N_{x,cr}}{t_m} = K_{cr}\frac{\pi^2 E_m}{12(1-\nu_m{}^2)}\left(\frac{t_m}{b_m}\right)^2 \tag{1}$$

where

$$K_{cr} = \min\left(m\frac{b_m}{\alpha_m} + \frac{a_m}{b_m}\frac{n^2}{m}\right)^2 \tag{2}$$

In the above equations, $N_{x,cr}$ is the critical buckling force per unit width, while E_m and ν_m are the plate's Young's modulus of elasticity and Poisson's ratio, respectively (Table 1). Additionally, K_{cr} is defined as the critical buckling coefficient and is dependent on the plate's primary dimensions (length, width) and the values n and m, which are the number of half-waves developed across the plate's longitudinal and transverse directions. A plate's deflection (eigenforms) is most probable to appear with one half-wave across its transverse since the obtained stress (eigenvalue) is lower, indicating a lower stable energy state. Thus, the value of n = 1 can be assumed when calculating critical buckling stresses using Equation (1). It should be noted that by studying Equation (2), as the aspect ratio increases—i.e., long plates—the critical buckling coefficient K_{cr} tends to the value of 4. This effect is visualized in Figure 7a, indicating that a stable energy state is achieved when a long plate buckles forming several half-waves across its length. The number of these half-waves is an integral product of its width (Figure 7b).

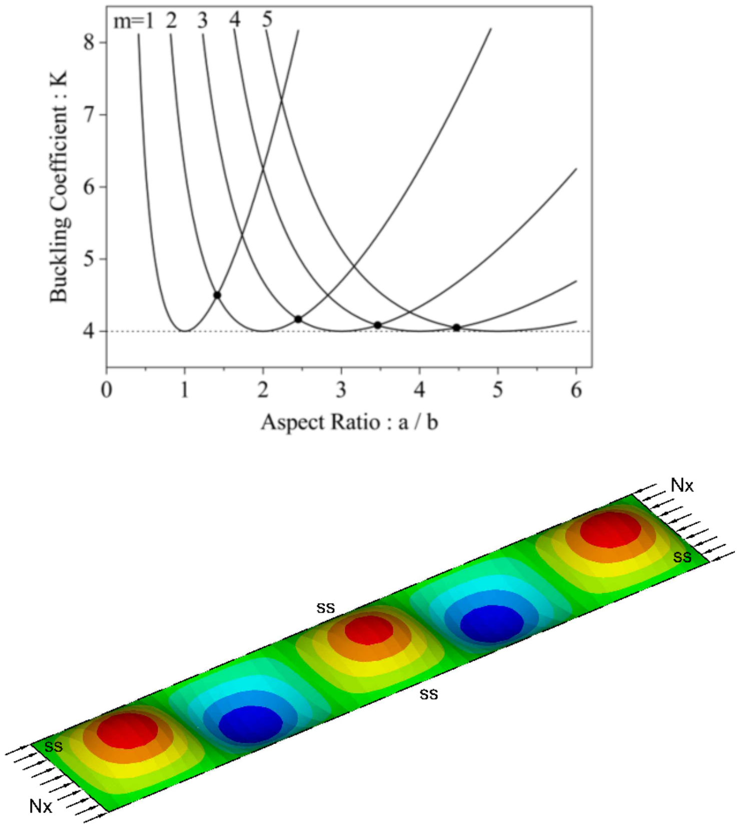

(**a**)

(**b**)

Figure 7. (**a**) Critical compressive buckling coefficient with respect to an increasing aspect ratio and (**b**) the first eigenform of a long plate with aspect ratio equal to 5.

In the case of shear buckling, the critical elastic stress is calculated using the following equation, as proposed by Timoshenko [13]

$$\tau_{E,cr} = k_{cr}\frac{\pi^2 D}{b_m^2 t_m} \tag{3}$$

where

$$k_{cr} = 5.35 + 4\left(\frac{b_m}{a_m}\right)^2 \tag{4}$$

In Equation (3), D denotes the plate's flexural rigidity: $D = E_m t_m^3 / 12\left(1 - \nu_m^2\right)$.

Both Equations (1) and (3) do not limit the obtained stress values, meaning that they could surpass the material's yield point. For this reason, the following corrections according to the Johnson–Ostenfeld parabola (Hughes [14]) must be applied to the elastic stresses to calculate their critical values

$$\begin{aligned} \sigma_{cr} &= \sigma_{E,cr} \text{ for } \sigma_{E,cr} \leq \frac{\sigma_y}{2} \\ \sigma_{cr} &= \sigma_y\left(1 - \frac{\sigma_y}{4\sigma_{E,cr}}\right) \text{ for } \sigma_{E,cr} > \frac{\sigma_y}{2} \end{aligned} \tag{5}$$

$$\begin{aligned} \tau_{cr} &= \tau_{E,cr} \text{ for } \tau_{E,cr} \leq \frac{\tau_y}{2} \\ \tau_{cr} &= \tau_y\left(1 - \frac{\tau_y}{4\tau_{E,cr}}\right) \text{ for } \tau_{E,cr} > \frac{\tau_y}{2} \end{aligned} \tag{6}$$

In the above equations, the material's yield stress is denoted by the 'y' subscript. According to LR [11] the shear yield stress can be calculated from the material's yield stress as $\tau_y = \sigma_y / \sqrt{3}$.

A plate's behavior can be visualized by plotting the critical buckling values from Equations (5) and (6) with respect to its slenderness ratio β (Figure 8), which is defined as

$$\beta = \frac{b_m}{t_m}\sqrt{\frac{\sigma_y}{E_m}} \tag{7}$$

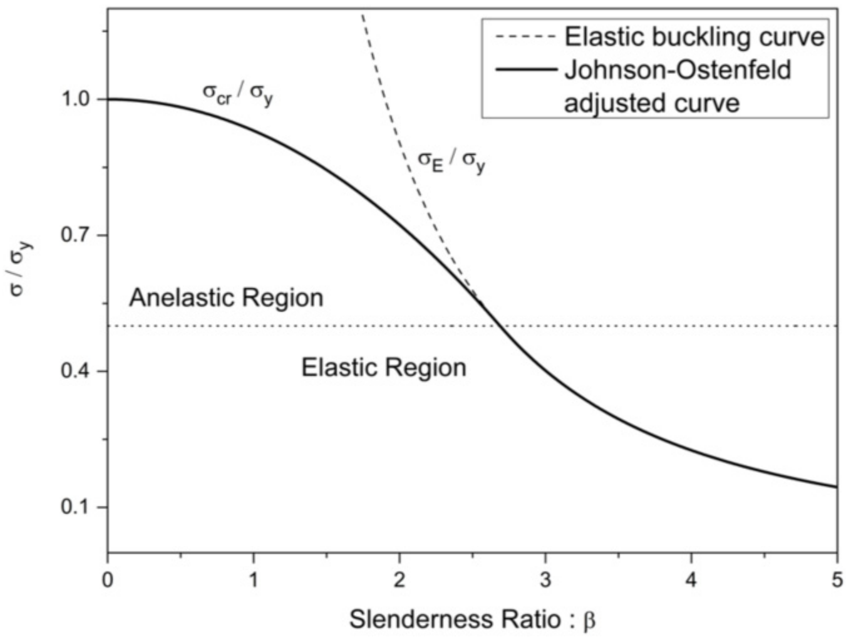

Figure 8. Anelastic buckling corrections for compressive buckling. The same curve applies to shear buckling.

The proposed method might be criticized for using elastic buckling theory and not introducing non-linearities to make the problem more realistic. However, the former allows for a safe preliminary assessment of the obtained FoS since it underestimates the critical buckling stress. This phenomenon is thoroughly explained by Hughes [14], where it is stated that the stresses do not distribute uniformly internally at a stiffened panel during compression. This occurs because the stiffened edges have higher rigidity than the unsupported center. Thus, the center is the first to buckle, while the former areas buckle at a higher value, demonstrating post-buckling capacity. Hence, by assuming elastic buckling, the proposed method's real-world application will exhibit a better structural response than the one obtained from numerical calculations.

An additional non-linearity is the existence of the adhesive bondline between the composite patch and the metal plate. According to Anyfantis et al. [15], the cohesive zone might be damaged, which could lead to crack initiation and propagation, resulting in debonding propagation. The latter may develop between the composite and the adhesive, the metal plate and the adhesive, or through a failure of the adhesive itself. In order to avoid non-linear solutions, the following method was proposed for developing an assessment method of the bondline fracture.

During loading, the stresses that develop on the bonded structure's cross-sections are transferred between the two substrates through the bondline. The latter's failure conditions can be evaluated using its fracture toughness G_C, which is its resistance to a defect's propagation. In order to evaluate if the bondline fails under a specific load, the acting strain energy release rate G must be known. This strain energy increases as the applied load also increases. According to the energy method, a bondline defect propagates if

$$G \geq G_c \tag{8}$$

The acting strain energy release rate G can be calculated using the steady state's release rate (SERR) debonding propagation formula

$$G = G_{SS} = \frac{1}{2\overline{E}_m}\left(\frac{P^2}{t_m} + \frac{P^2}{At_c} - \frac{M_b^2}{It_c^3}\right) \tag{9}$$

where:

- P is the axial acting force.

  $M_b = P(\delta - t_m/2)$ is the balance moment, with $\delta = \frac{1+2\Sigma\eta+\Sigma\eta^2}{2\eta(1+\Sigma\eta)}t_c$, $\Sigma = \overline{E}_c/\overline{E}_m$ and $\eta = t_c/t_m$.
- $A = 1/\eta + \Sigma$ and $I = \Sigma\left[\left(\Delta - \frac{1}{\eta}\right)^2 - \left(\Delta - \frac{1}{\eta}\right) + \frac{1}{3}\right] + \frac{\Delta}{\eta}\left(\Delta - \frac{1}{\eta}\right) + \frac{1}{3\eta^2}$.
- $\overline{E}_c = \frac{E_c}{1-\nu_c^2}$ and $\overline{E}_m = \frac{E_m}{1-\nu_m^2}$ are the effective plane stress Young's moduli of the composite and the plate respectively, while E_c and E_m are their Young's moduli of elasticity, and ν_c and ν_m their Poisson's ratio.

For the case being studied, P is replaced by $N_{x,cr}$ in order to determine whether the proposed patch repair could suffer from bondline fracture. Finally, the maximum stress developed within the metal plate and the composite patch must not exceed the respective material's yielding/fracture value.

4. Physics and Data-Based Models

4.1. FEA Model

The most efficient way of performing the buckling strength calculations and the statistical analysis is through the application of numerical methods. Thus, for the former case, FEA can be used to obtain accurate stress and displacement results. Furthermore, the problem being examined is a thin plate since $a_m/t_m >> 20$ is common in tankers and bulk carriers (Zhang [16]); hence, shell elements can be used for representing them in the numerical model. The same theory is valid for the composite patch. The shell elements used are the four-node and eight-node elements, which in ANSYS are represented by SHELL 181 and SHELL281, respectively. Their effectiveness is assessed through a mesh convergence test in order to find the optimal option. The metal's material is input as an isotropic material, while the composite is an orthotropic one. It should be noted that the analyses are based on a linear elastic foundation and the results are corrected according to Equations (5) and (6) for anelastic buckling.

An essential step to successfully model the problem's geometry is implementing the boundary conditions and loads. As pictured in Figure 9, the geometry is symmetrical to the center of the plate since the patch is centrally placed. This can be utilized for the compression model that can be reduced to its quarter model for the calculations, with symmetry boundary conditions at its edges (Figure 10). Thus, simply supported conditions, i.e., $U_Z = 0$, are applied to the external edges, while $U_X = ROT_Y = ROT_Z = 0$ and $U_Y = ROT_X = ROT_Z = 0$ are applied to the internal transverse and longitudinal symmetry edges, respectively. In order to obtain the critical buckling stress value, a distributed force is applied at the plate's short edges. By solving an eigenvalue buckling analysis, the critical buckling force $N_{x,cr}$ is acquired, and by using Equation (1), so is its equivalent stress.

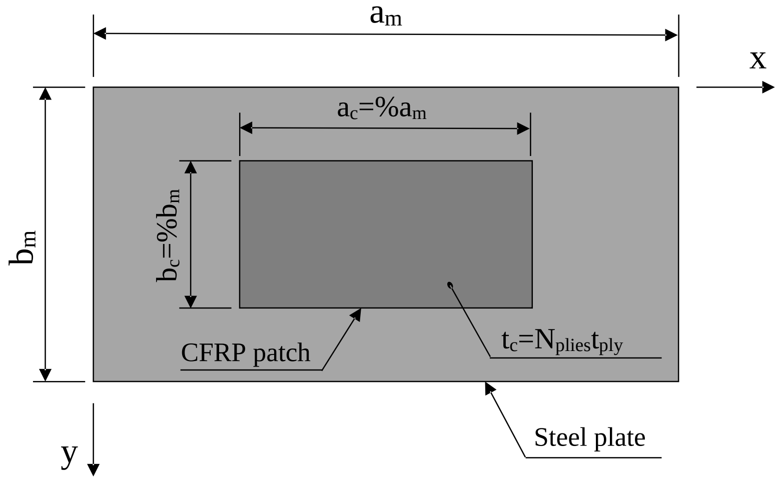

Figure 9. Design schematic of a rectangular composite patch applied to a metal plate.

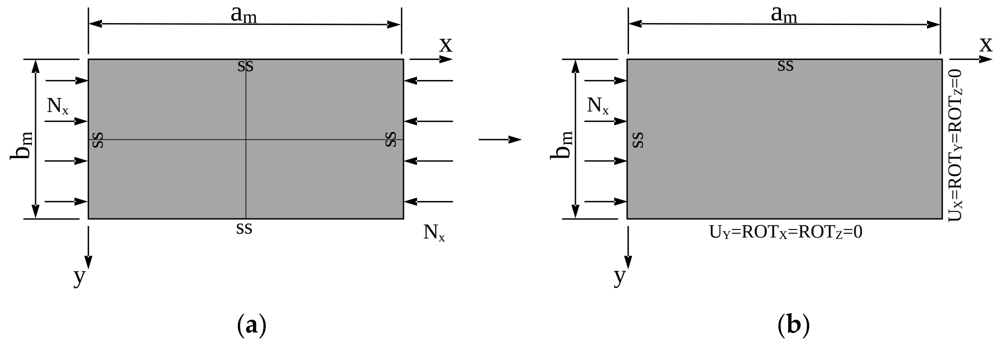

Figure 10. Two-dimensional sketch of the geometry's (**a**) full and (**b**) quarter model and its boundary conditions for the case of compressive buckling.

However, the same modeling cannot be applied to the shear buckling problem, since it utilizes a different approach to the problem with respect to the boundary and loading conditions that do not allow for symmetry to be used, hence the geometry is modeled in its entirety (Figure 11). The boundary condition in effect is the restriction of all degrees of freedom at one of the short edges, i.e., clamping conditions. In the rest of the edges, large beams are modeled with substantial stiffness that allows the geometry to be considered a cantilever, thus having low bending effects (Anyfantis [2]). This way, the shear buckling effect is acquired with a good approximation. The load is applied to a pilot node at the free short edge's center, with a direction parallel to it. Thus, the critical buckling force $N_{xy,cr}$ is acquired by dividing it by the plate's thickness (same principle as Equation (1)).

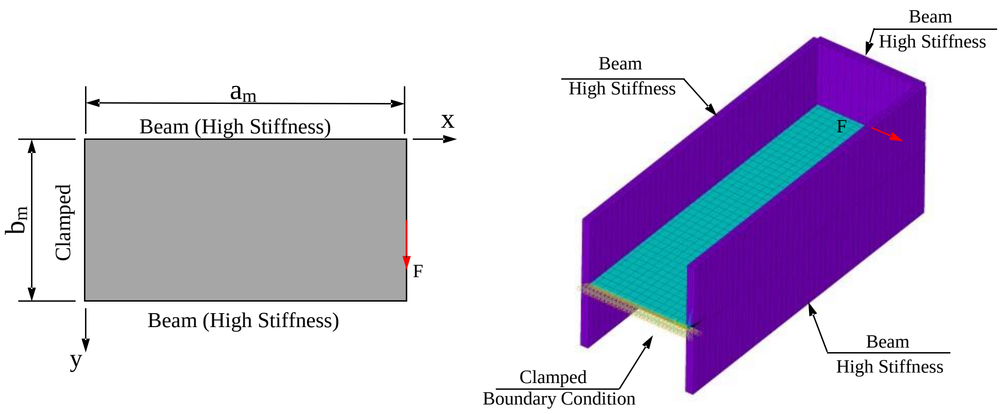

(**a**) (**b**)

Figure 11. (**a**) Two-dimensional sketch and (**b**) three-dimensional representation of the geometry's model and its boundary conditions for the case of shear buckling.

The values obtained from these analyses must be corrected according to Johnson–Ostenfeld's parabola for anelastic buckling (Hughes [14]). These calculations are performed at the data points specified by the DoE methodology.

4.2. DoE Analysis

DoE is the design of an experiment based on input parameters and using statistical tools to approximate the output as best as possible. One basic example of a DoE method is an OFAT analysis, in which the output of an experiment is based on one factor at a time (as indicated by the title itself) without implementing possible interactions between input parameters. Another method used for this study's purposes is an RSM, which is a two-level design. Specifically, two input design parameters are used to define the design space. A central composite design (CCD) then indicates the data points needed for the method to be performed. According to a face-centered CCD (CCF), three point types are used: factorial (shows two-factor interactions), center (shows curvature), and star (shows quadratic effects). At the points of the design space indicated by the CCD (Figure 12), the output is obtained from an experiment. Once these points are specified (known x_1, x_2, and y), a polynomial surface is best fit to them with the help of statistical tools for its lack-of-fit evaluation.

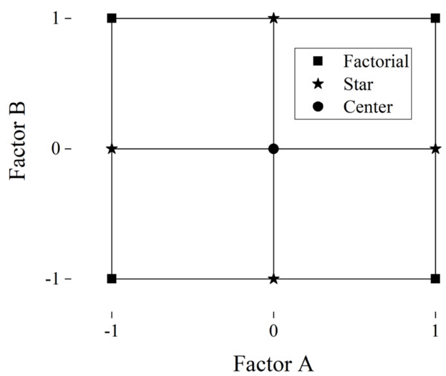

Figure 12. Design points indicated by a CCF.

In the case being studied, the design space consists of the patch's percentage coverage (denoted by c) and the number of plies (denoted by N_{plies}). After setting these values' range, their CCD points are configured at the three levels required, i.e., low level (−1), center (0), and high level (+1). Through numerical calculations using FEA, the experimental outputs for the data points are acquired. Then a quadratic polynomial equation of the form

$$y = a_0 + a_1x_1 + a_2x_2 + a_{11}x_1^2 + a_{12}x_1x_2 + a_{22}x_2^2 \quad (10)$$

is fit to these points to construct the response surface. In this case, x_1 is the percentage coverage c, x_2 is the number of plies N_{plies}, and y is the obtained FoS. This factor of safety is calculated as

$$FoS = \frac{\sigma_{repaired}}{\sigma_{intact}} \text{ or } FoS = \frac{\tau_{repaired}}{\tau_{intact}} \quad (11)$$

Using the combination of the above methods (FEA and RSM), a list of acceptable design configurations for the requirements set by FoS, bondline fracture, and material yield is created. A significant advantage of this technique is that it does not require lab experiments for this preliminary design as long as the model is as accurate as possible.

5. Case Study

In order to showcase the proposed methodology, a case study is conducted following the techniques mentioned in the previous paragraphs.

5.1. Problem Set-Up

Assume a survey is conducted on a commercial ship that is not newly built. During procedural visual inspections, corrosion is detected on a girder of the double bottom. The plate's thickness is then measured, indicating that the material wastage realized equals a 5% reduction of its initial thickness. After further assessing the defect and the damaged area according to the proposed flowchart in Figure 6, the Classification Society approves the application of a composite patch to rehabilitate the plate's initial buckling strength capabilities. The plate's dimensions and damage are listed in Table 2. After the repair, the plate shall have restored its buckling strength with a FoS equal to 1.0, i.e., its initial value.

Table 2. Metallic damaged plate's properties.

Plate's Property	Symbol	Value	Unit
Material	-	Grade 'AH32' Steel	-
Length	a_m	2250	mm
Width	b_m	900	mm
Intact thickness	$t_{m,intact}$	20	mm
Corrosion	-	5	%
Corroded thickness	$t_{m,corroded}$	19	mm
FoS requirement	FoS_{req}	1.0	-

The patch's properties under consideration are its material, its configuration, and its shape (as shown in the flowchart in Figure 6). In order to obtain the optimal combination, OFAT analyses are conducted. The parameters that are listed in Table 3 are examined against an increasing value of the number of plies and evaluated using the obtained FoS. However, before initiating any analysis, the element properties for the numerical calculations shall be defined. Specifically, mesh convergence tests for four- and eight-node elements were conducted for the compression and shear model containing only the intact metal plate. The results are illustrated in Figure 13 where the element size is plotted with respect to the percentage deviation of the obtained buckling stress from the one obtained by the minimum allowed size of 20 mm. The graphs indicate that the eight-node elements, combined with a mesh size of 100 mm, provide sufficient accuracy, with less than 0.2% deviation from the converged value.

Table 3. Patch's properties evaluated through OFAT analyses.

Patch's Property	Options	x	y
Material	CFRP/GFRP	No. Plies	FoS
Configuration	One-Sided/Two-Sided		
Shape	Rectangular/Ellipsoid/Octagonal		

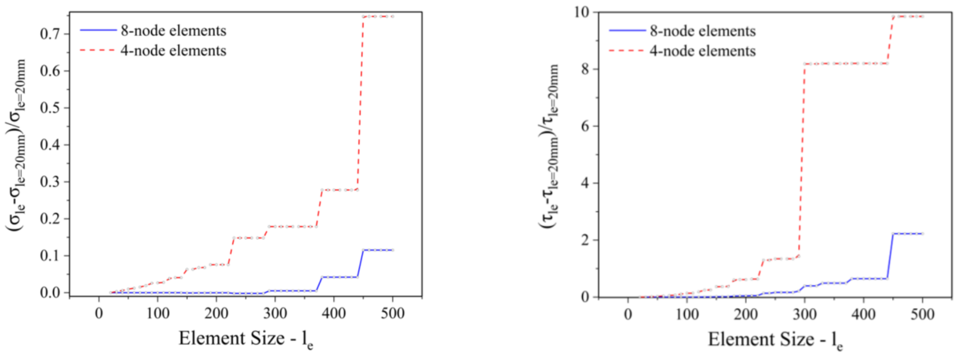

(**a**) (**b**)

Figure 13. Mesh convergence test for the (**a**) compression and (**b**) shear buckling model.

Two OFAT analyses were performed: one for defining the patch's material and configuration and another for the shape. The former analysis uses a rectangular patch as a typical shape, while the coverage percentage is 75%. The results are shown in Figure 14, where it can be concluded that the CFRP is a better acting material than the GFRP. Additionally, the one-sided patch has faster buckling restoration capabilities against compression, while the two-sided has a similar effect against shear. However, the one-sided CFRP patch is chosen as the most effective since it restores the buckling capacity for a similar number of plies in both compression and shear.

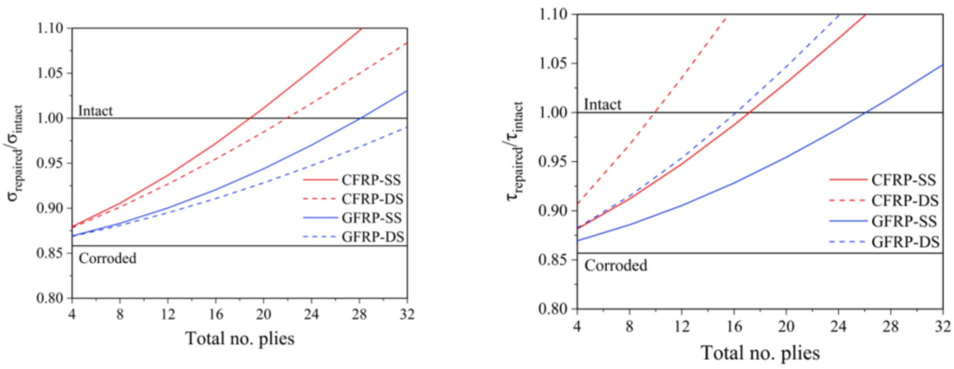

(**a**) (**b**)

Figure 14. OFAT analysis for determining the repair's optimal combination of material and configuration (SS: single strap, DS: double strap) for the (**a**) compression and (**b**) shear buckling model.

Afterward, using these findings, the possible shapes (Figure 3) were tested against each other. These analyses were carried out on the compression model, and similar results were assumed for the shear equivalent. The shape with the better rehabilitation performance is the rectangular patch (Figure 15). Thus, the optimal option for restoring the corroded plate's buckling capabilities is a one-sided CFRP rectangular patch.

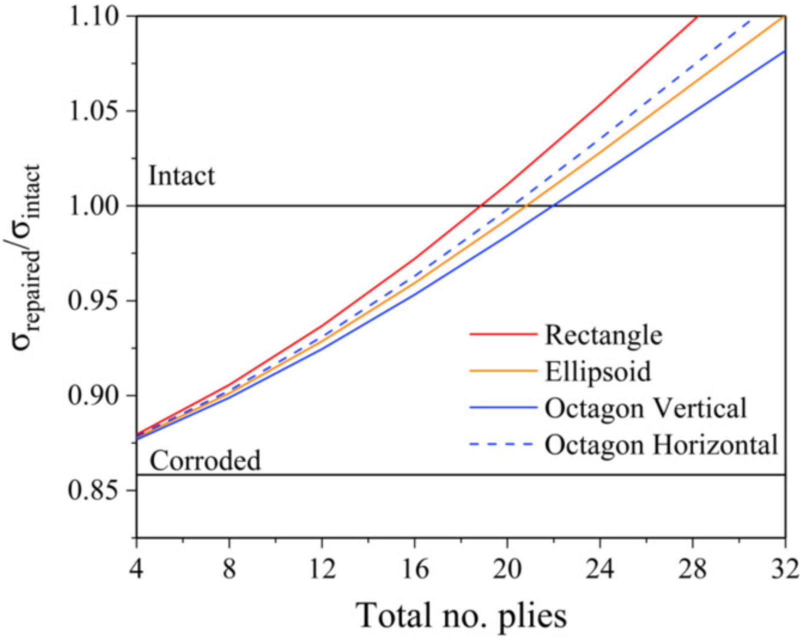

Figure 15. OFAT analysis for determining the repair's optimal shape (compression model).

5.2. Analysis Results

In order to perform the RSM, the CCD points, and consequently the design space, must be defined. The two design parameters, i.e., the patch's coverage c and the number of plies N_{plies}, are allowed to take values inside the range specified in Table 4 between the low and high-level indications. The same table specifies the design points using the CCD design space (Figure 12). It should be noted that each ply's thickness is equal to 0.33125 mm (Karatzas [3]).

Table 4. CCD design points.

Factor	Name	Low Level (−)	Center (0)	High Level (+)
x_1	Coverage (c)	40%	70%	100%
x_2	No. Plies (N_{plies})	4	18	32

Using the design points, numerical calculations were conducted, and the resultant stresses were corrected for anelastic buckling, if applicable. By fitting a polynomial as expressed in Equation (10), the resultant response surfaces for the compressive (Equation (12a)) and shear (Equation (12b)) buckling problem are defined by

$$FoS = 0.97689 - 0.01555c - 0.00138N_{plies} + 0.00752c^2 + 0.00454cN_{plies} + 5.46826e - 06\ N_{plies}{}^2 \quad (12a)$$

$$FoS = 0.99021 + 0.01289c - 3.39234e - 4N_{plies} - 0.0098c^2 + 0.00107cN_{plies} - 8.26793e - 07\ N_{plies}{}^2 \quad (12b)$$

These response surfaces are illustrated in Figure 16a,b, where both the experimental points obtained by the numerical calculations and the predicted points are plotted. Additionally, the FoS requirement is also visible on the surface as a curve. Any design parameters combination with a generated FoS below the indicated requirement curve is not acceptable. In Figure 17a,b, the same surfaces are plotted as a 2D contour for better visualizing the acceptable combinations.

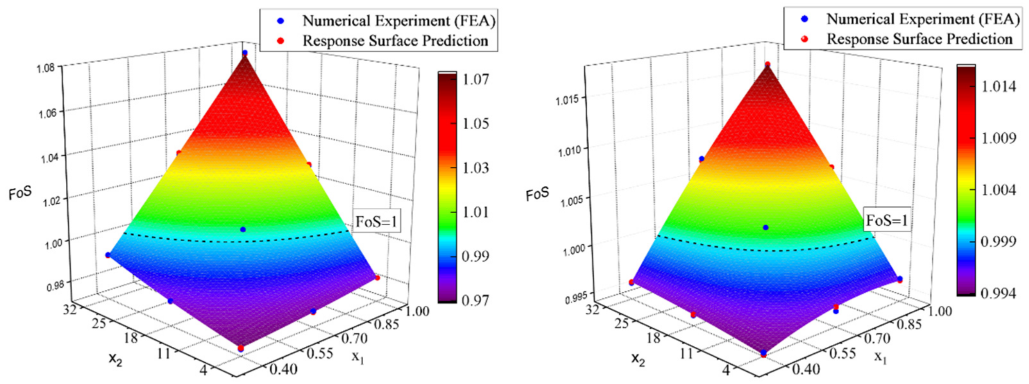

(**a**) (**b**)

Figure 16. Generated response surface from a polynomial fit to the CCD data points for (**a**) compressive and (**b**) shear buckling.

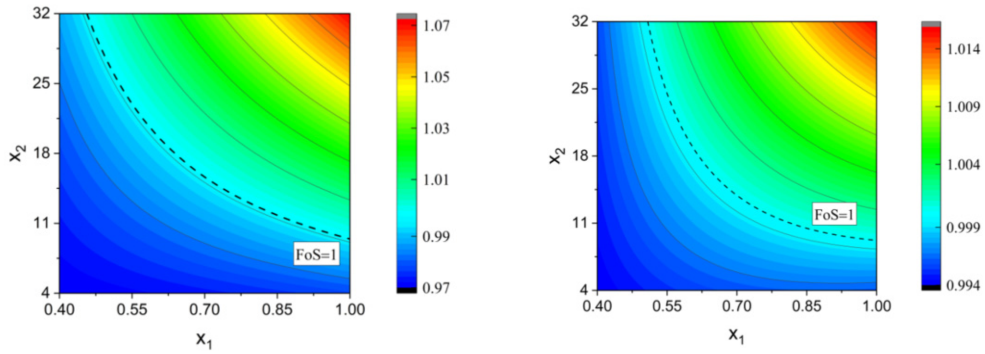

(**a**) (**b**)

Figure 17. 2D contour plot of the generated response surface for (**a**) compressive and (**b**) shear buckling.

The fitted surfaces are evaluated using statistical tools, such as a histogram and a normal probability plot, using the percentage deviation between calculated and predicted values as indicators. The data points used were the CCD design points with the addition of mid-points to further assess the surface's lack of fit (evaluation points). A list of all points used for the method's validation is shown in Table 5. The calculated R-squared value for both surfaces is greater than 0.99, which exhibits a 99% fit. The percentage deviations were plotted in histograms (Figure 18a,b) and normal probability plots (Figure 19a,b), concluding that the prediction model follows a normal distribution and lacks significant statistical noise.

Table 5. Design and evaluation points used in the response surface.

Factor	Name	D + E [1]	E [2]	D + E [1]	E [2]	D + E [1]
x_1	Coverage (c)	40%	55%	70%	85%	100%
x_2	No. Plies (N_{plies})	4	11	18	25	32

[1] Design and evaluation point, [2] Evaluation point.

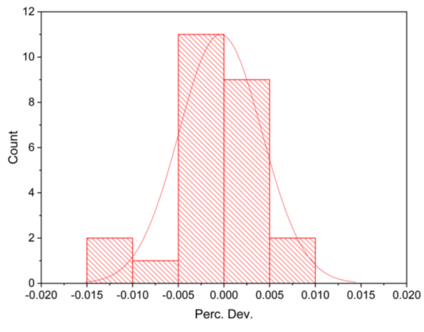

(**a**) (**b**)

Figure 18. Histogram of the percentage deviation between experimental and predicted values for (**a**) compressive and (**b**) shear buckling.

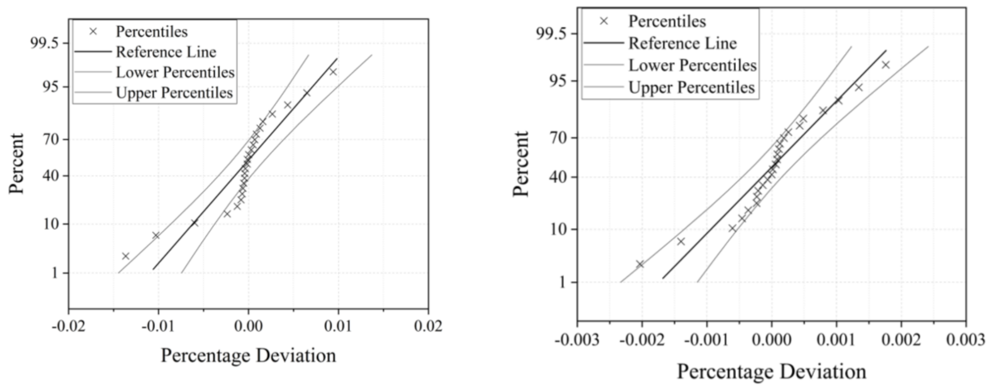

(**a**) (**b**)

Figure 19. Normal probability plot, with 95% confidence levels, of the percentage deviation between experimental and predicted values for (**a**) compressive and (**b**) shear buckling.

The acceptable design combinations are those that satisfy the FoS requirement for both compressive and shear buckling, as shown in Figure 17a,b respectively.

Having restricted the acceptable design combinations using the FoS requirements, the bondline is also checked. The maximum strain energy release rate from the surface's data points is equal to 0.185 N/mm and 0.085 N/mm for the compressive and shear problem respectively. The combination in which these values occur corresponds to [c, N_{plies}] = [1, 32] for both models, outputting FoS~1.08 and FoS~1.02 respectively. According to Lee [17], the resistance release rate for Mode-1 dominant conditions is equal to approximately 0.33 N/mm. Thus, since the acquired G is less than G_C, the bondline does not fail under Mode-1 failure conditions. It should be noted that Mode-1 dominant fracture was used since it is most probable of occurring than its Mode-2 equivalent, although further mixed-mode requirements could be used if requested.

Finally, the maximum normal stresses developed on the composite patch are equal to 297.6 MPa and 128 MPa for the compression and shear model respectively. Both values are less than the fracture stress and correspond to the combination [c, N_{plies}] = [0.7, 32] for both models, outputting FoS~1.03 and FoS~1.01 respectively.

It should be noted that partial safety factors for the assessment of the bondline and composite strength can be defined in addition to the primary FoS for the buckling restoration. These safety margins can be respectively defined as

$$\mathrm{FoS}_{\mathrm{bondline}} = \frac{G_C}{G_{\mathrm{acting,max}}} \tag{13}$$

$$FoS_{fracture} = \frac{\sigma_{fracture}}{\sigma_{acting,max}} \quad (14)$$

The safety factors obtained from this case study for the compressive buckling are $FoS_{bondline}$ = 1.78 and $FoS_{fracture}$ = 1.18, and for the shear buckling $FoS_{bondline}$ = 3.87 and $FoS_{fracture}$ = 2.75. If additional requirements for $FoS_{bondline}$ = 2 or $FoS_{fracture}$ = 1.4 were applied, then although the analysis showed adequate buckling restoration, some solutions would not be acceptable under the above evaluation criteria.

6. Concluding Remarks

This study examined the existing problem of material wastage due to corrosion and the risks of buckling it could potentially lead to in the case of a stiffened panel. In order to treat this damage, the alternative repair method of composite patches was proposed. The main goal was to present the theoretical background of the plate's and patch's mechanics that could restore the structure's initial buckling strength, and demonstrate its results through a numerical application. The results proved that such a repair practice is capable of rehabilitating the buckling capacity of a corroded marine plate against compressive and shear loads.

However, assumptions were made in order to minimize the problem's multi-parametrical nature. Thus, further studies should be made on the proposed methodology, introducing more parameters. For instance, the geometry and the adhesive could be modeled more accurately with solid elements to better capture the results of the applied buckling stress. Furthermore, since the linear analysis conducted over-engineered the problem, due to the post-buckling effect being ignored, a non-linear analysis should be performed to identify this effect. Thus, the proposed methodology would be enriched, and the model would more accurately represent reality.

Finally, it should be understood that even with the actions suggested for further improvement on the problem's analysis, real-world testing must be conducted. Installation and operating conditions should be accounted for since they also dictate the structural response of the repaired plate under examination. Hence, the next step after developing the analyses should be laboratory testing and then employing the method to existing damages dealt on marine structures. Only after years of monitoring the effects of the repair methodology will the concluding remarks be set, and perhaps will the technique be established as a proposed repair for primary and non-primary supporting members.

Author Contributions: Conceptualization, K.N.A.; Formal analysis, N.K.; Investigation, N.K.; Methodology, K.N.A. and N.K.; Supervision, K.N.A.; Writing–original draft, N.K.; Writing–review & editing, K.N.A. All authors have read and agreed to the published version of the manuscript.

Funding: This research received no external funding.

Conflicts of Interest: The authors declare no conflict of interest.

References

1. IACS. *Guidelines for Surveys, Assessment and Repair of Hull Structures—Container Ships, Rev.1*; Witherbys Publishing: Livingstone, UK, 2018.
2. Anyfantis, K.N. Preliminary design assessment of an alternative repair method for corroded shear panels in ship hull structures. *Ocean Eng.* **2019**, *188*, 106323. [CrossRef]
3. Karatzas, V.A. Assessment and Design of Composite Patch Repairing in Marine Applications. Ph.D. Thesis, National Technical University of Athens, Athens, Greece, 2016.
4. Karatzas, V.A.; Kotsidis, E.A.; Tsouvalis, N.G. Experimental fatigue study of composite patch repaired steel plates with cracks. *Appl. Compos. Mater.* **2015**, *22*, 507–523. [CrossRef]
5. BV. *Adhesive Joints and Patch Repair*; Guidance Note NI613DTR00E; BV: Paris, France, 2015.
6. DNV. *Design, Fabrication, Operation and Qualification of Bonded Repair of Steel Structures*; Recommended Practice DNVGL-RP-C301; DNV: Belum, Norwegen, 2015.
7. ASME. *Repair of Pressure Equipment and Piping*; ASME PCC-2-2011; The American Society of Mechanical Engineers: New York, NY, USA, 2011.

8. Hashim, S.; Berggreen, C.; Tsouvalis, N.; McGeorge, D.; Chirica, I.; Moore, P.; Boyd, S.; Nisar, J.; Anyfantis, K.; Misirlis, K.; et al. Fabrication, testing and analysis of steel/composite DLS adhesive joints. *Ships Offshore Struct.* **2011**, *6*, 115–126. [CrossRef]
9. Aabid, A.; Hrairi, M.; Mohamed Ali, J.S. Optimization of composite patch repair for center-cracked rectangular plate using design of experiments method. *Mater. Today Proc.* **2020**, *27*, 1713–1719. [CrossRef]
10. Turan, K. Buckling behavior of adhesively patch-repaired composite plates. *J. Compos. Mater.* **2013**, *48*, 3253–3261. [CrossRef]
11. Lloyd's Register. *Rules and Regulations for the Classification of Ships*; Lloyd's Register: London, UK, 2016.
12. Kollar, L.; Springer, G. *Mechanics of Composite Structures*; Cambridge University Press: Cambridge, UK, 2003.
13. Timoshenko, S.; Gere, J. *Theory of elastic stability, International Student Edition*, 2nd ed.; McGraw-Hill: New York, NY, USA, 1985.
14. Hughes, O.; Paik, J. *Ship Structural Analysis and Design*; SNAME: Jersey City, NJ, USA, 2010.
15. Anyfantis, K.; Stavropoulos, P.; Chryssolouris, G. *Fracture Mechanics Based Assessment of Manufacturing Defects Laying at the Edge of CFRP-Metal Bondlines*; CrossMark: Plano, TX, USA, 2018.
16. Zhang, S. A review and study on ultimate strength of steel plates and stiffened panels in axial compression. *Ships Offshore Struct.* **2016**, *11*, 81–91. [CrossRef]
17. Lee, M.J.; Kim, W.S.; Jang, C.J.; Kim, K.H.; Cho, T.M.; Lee, B.C.; Lee, J.J. Analysis and Simulation of the Failure Characteristic of a Single Leg Bending Joint with a Micro-Patterned Surface. *J. Adhes.* **2011**, *87*, 826–841. [CrossRef]